THESIS

CHARACTERISTICS OF ATMOSPHERIC ICE NUCLEATING PARTICLES ASSOCIATED WITH BIOMASS BURNING IN THE US: PRESCRIBED BURNS AND WILDFIRES

Submitted by

Christina S. McCluskey

Department of Atmospheric Science

In partial fulfillment of the requirements

For the Degree of Master of Science

Colorado State University

Fort Collins, Colorado

Fall 2013

Master's Committee:

Advisor: Sonia Kreidenweis
Co-Advisor: Paul DeMott

Jeffery Pierce
John Volckens

ABSTRACT

CHARACTERISTICS OF ATMOSPHERIC ICE NUCLEATING PARTICLES ASSOCIATED WITH BIOMASS BURNING IN THE US: PRESCRIBED BURNS AND WILDFIRES

Insufficient knowledge regarding the sources and number concentrations of atmospheric ice nucleating particles (INP) leads to large uncertainties in understanding the interaction of aerosols with cloud processes, such as cloud life time and precipitation rates. An increasingly important source of aerosol in the United States is biomass burning, particularly in the form of prescribed burns and wildfires in the southeastern and western U.S., respectively. Prior field and laboratory observations have suggested that biomass burning can be a source of INP. However, emissions from biomass burning are complex, varying with combustion efficiency, fuel type, plume age and dilution. Thus, this potentially important source of INP is poorly characterized. This study utilizes measurements of INP from a diverse set of biomass burning events to better understand INP associated with biomass burning in the U.S.

Prescribed burns in Georgia and Colorado, two Colorado wildfires and two laboratory burns were monitored for INP number concentrations (n_{INP}) using the Colorado State University continuous-flow diffusion chamber (CFDC) to activate INP in the condensation/immersion freezing nucleation mode. Additional measurements included total particle number concentrations, number concentrations of particles with diameters larger than 500 nm, aerosol mass concentrations, carbon monoxide concentrations and chemically-speciated bulk aerosol filter samples. Additionally, activated INP were collected onto TEM grids downstream of the CFDC, isolating INP for single particle chemical and morphological analyses. These fires varied

by fuel type, including wiregrass, longleaf pine and ponderosa pine, and also varied by combustion efficiency, ranging from highly flaming to a mixture of flaming and smoldering. Additionally, plume histories were different between the fires including aged plumes from the wildfires and freshly emitted smoke from the prescribed and laboratory burns.

The relationship between n_{INP} and total particle number concentrations, evident within prescribed burning plumes, was degraded within aged smoke plumes from the wildfires, limiting the utility of this relationship for comparing laboratory and field data. Larger particles, represented by n_{500nm}, are less vulnerable to plume processing and have previously been evaluated for their relation to n_{INP}. Our measurements indicated that for a given n_{500nm}, n_{INP} associated with the wildfires were nearly an order of magnitude higher than n_{INP} found in prescribed fire emissions. That is, n_{INP} represented a much larger fraction of n_{500nm} in wildfires as compared with prescribed fires. Further, an existing parameterization for "global" n_{INP} that relates INP abundance to n_{500nm} largely under-predicted and over-predicted n_{INP} emitted from wildfires and prescribed burns, respectively. Reasons for the differences between INP characteristics in these emissions were explored, including variations in combustion efficiency, fuel type, transport time and environmental conditions.

Combustion efficiency and fuel type were eliminated as controlling factors by comparing samples with contrasting combustion efficiencies and fuel types. Transport time was eliminated because the expected impact would be to reduce n_{500nm}, thus resulting in the opposite effect from the observed change. Bulk aerosol chemical composition analyses support the potential role of elevated soil dust particle concentrations during the fires, contributing to the population of INP, but the bulk analyses do not target INP composition directly. Predictions from the Naval Aerosol Analysis and Prediction System model further indicate elevated dust mass

concentrations during the wildfire periods, suggesting impact of mineral dust from long-range transport (LRT). It is hypothesized that both hardwood burning and soil lofting are responsible for the elevated production of INP in the Colorado wildfires in addition to LRT of mineral dust.

The chemical compositions of INP were probed directly via TEM imaging. Single particle analyses of residual INP showed that they comprised various C-containing particle types, but with a higher abundance of mineral and metal oxide containing INP in emissions from flaming phase combustion. Fractal soot was found as an INP type comprising up to 60% of collected INP in young smoke emissions from the Georgia prescribed burns. In a series of laboratory combustion experiments, the use of a new instrumental set up, pairing the CFDC with a single particle soot photometer, revealed up to a 60% decrease in active INP after the removal of refractory black carbon from smoke aerosol emitted from a highly flaming burn of wiregrass, supporting that soot particles serve as INP in fire emissions. The presence of soil minerals was clearly evident in TEM images of samples taken during the wildfires in addition to tarballs, carbon balls most commonly associated with aged smoke plumes. These results demonstrate that the ice nucleating particles observed in the wildfires were influenced by other factors not represented in the smoke emitted from the laboratory or prescribed burns.

Finally, an INP parameterization was developed based on the temperature dependent relationship between n_{INP} and n_{500nm}, following methods used by previous studies. This parameterization is likely only representative of the Hewlett and High Park wildfires due to the apparent impact of non-biomass-burning aerosol. However, all wildfires are typically associated with vigorous localized convection and arid soils, required for the lofting of the soils and dusts similar to these wildfires. It will be useful to compare future wildfires in various regions to the proposed parameterization.

ACKNOWLEDGEMENTS

I would like to first extend gratitude to Dr. Sonia Kreidenweis and Dr. Paul DeMott for their direction and motivating passion regarding this project, in addition to their inspiring example as world-class scientists. I would like to thank my committee members, Dr. Jeffery Pierce and Dr. John Volckens for their productive discussions and contributions to this work. Additionally, I would like to thank Dr. Ezra Levin, Dr. Gavin McMeeking, Dr. Anthony Prenni, Dr. Amy Sullivan and all members of the Kreidenweis research group for generously engaging in discussions that greatly benefited this project.

Many people were instrumental in the success of these field studies. Logistical support during the Georgia prescribed burns was given by the Joseph W. Jones Research Center of Ichauway, GA. I wish like to acknowledge Dr. Amy Sullivan for the aerosol composition data and both R.J. Lee Inc. and Norbert Swoboda-Colberg at the University of Wyoming High Resolution Electron Microscopy Facility for transmission electron microscopy analyses. Acknowledgement is also extended to Bob Yokelson's research group from the University of Montana for gas measurements during the FLAME IV study. Finally, I would like to thank Paul DeMott, Anthony Prenni, Ezra Levin, Amy Sullivan, Shunsuke Nakao, Gavin McMeeking, and Christian Carrico for their contributions to all aerosol measurements during these studies.

Funding for measurements made during the Georgia prescribed burns and both wildfires was provided by the National Oceanic and Atmospheric Administration Atmospheric Composition Program (NA10OAR4310103) and the National Aeronautics and Space Administration Earth Science Division grant NNX12AH17G provided support for the FLAME IV project.

TABLE OF CONTENTS

LIST OF TABLES

LIST OF FIGURES

1. Introduction

1.1. Motivation

Atmospheric aerosols play an important role in the phase, formation, lifetime, and precipitation rates of clouds, yet remain sources of uncertainties in determining the future state of the Earth's climate and hydrological cycle [Lohmann and Feichter, 2005]. Aerosols emitted into the atmosphere affect populations of cloud condensation nuclei (CCN) and ice nucleating particles (INP). INP have the potential to alter clouds via the "glaciation indirect effect", which suggests that enhanced populations of INP can increase the number of ice crystals in mixed phase clouds, thereby increasing precipitation rates and decreasing cloud lifetimes [Lohmann et al., 2002]. Cloud modeling results also provide evidence that the uncertainty in the competing effects of CCN and INP on cloud microphysics has important consequences when determining the net effect of aerosols on the microphysical and radiative properties of clouds [Levin et al., 2005, Twomey, 1977].

An improved understanding of atmospheric INP is needed in order to advance the representation of aerosols in numerical models, thus enhancing the ability to identify the effects of aerosol-cloud interactions on the Earth's radiative and hydrological budgets. Parameterizations do exist for predicting ambient concentrations of INP, but DeMott et al., (2010) suggest that unexplained shortcomings of the parameterizations are likely due to unclear variations in the chemical composition of INP found in regions dominated by specific aerosol sources, such as dust, biological aerosol, smoke, or oceanic aerosol.

A large source of atmospheric aerosol is biomass burning, a source that is expected to grow based on recent trends, particularly in the western United States [Spracklen et al., 2009, Westerling et al., 2006]. A majority of observations have confirmed that carbonaceous particles

from biomass burning are associated with increases in populations of INP [Sassen and Khvorostyanov, 2008; Petters et al., 2009; Twohy et al., 2010; Pratt et al., 2011; Prenni et al., 2012]. However, a study by Rosenfeld et al. (2011) reported that smoke emitted from Siberian wildfires were associated with the lowest glaciation temperatures in effected clouds, indicating smoke particles as poor source of INP. These studies have shown that emissions of INP from biomass burning are highly variable and poorly characterized. Accordingly, this study was motivated by a strong need for field observations of INP from biomass burning events in efforts to better understand the contribution of biomass burning to the atmospheric INP population.

1.2. Atmospheric ice nucleating particles

Ice nucleation is the primary mechanism for first ice particle formation in ice-phase and mixed-phase clouds in the atmosphere. Two pathways for ice nucleation exist: homogeneous and heterogeneous nucleation. Homogeneous nucleation occurs at temperatures below -36 $^{\circ}$C, with a prohibitively large energy barrier between pure supercooled water and ice crystal phases above this temperature [Lamb and Verlinde, 2011]. Ice formation can occur at temperatures warmer than -36 $^{\circ}$C via heterogeneous nucleation, where active sites on ice nucleating particles act to reduce the energy barrier required for ice to form [Cantrell and Heymsfield, 2005].

There are four conceptual modes of heterogeneous nucleation: deposition nucleation, contact nucleation, immersion freezing, and condensation freezing. The aim of this study is to measure INP active under conditions for the immersion and condensation freezing modes of heterogeneous nucleation. The immersion-freezing mode requires the INP to be immersed into a preexisting water droplet and initiate freezing, whereas the condensation-freezing mode occurs when the INP initially acts as a CCN and collects water, which eventually freezes [Pruppacher

and Klett, 1997]. The distinction between these two modes may be quite difficult in practice, but together they appear to represent the most important mechanism for ice crystal initiation in mixed-phase cloud conditions [Hoose and Möhler, 2012; de Boer et al., 2011]. Results presented herein support the same conclusion specifically for prescribed fire smokes.

Knowledge of the sources, concentrations, and special characteristics of INP remains poor in comparison to other cloud relevant aerosol types, such as CCN. Typically, INP make up less than 1 in 10^5 particles in a given environment [Rogers et al., 2001; DeMott et al., 2011]. Known sources of INP include mineral dust [DeMott et al., 2003; Richardson et al., 2007], biological particles [Pratt et al., 2009; Prenni et al., 2013] and biomass burning [Petters et al., 2009, Prenni et al., 2012, Pratt et al., 2011, Stith et al., 2011].

In efforts to describe the interaction of INP with clouds, parameterizations have been developed and implemented in cloud resolving models [e.g., Seigel et al., 2013]. The D10 (DeMott et al., 2010) parameterization was developed based on a multi-study n_{INP} data set and predicts n_{INP} as a function of the number concentrations of particles with diameters greater than 500 nm and of temperature. D10 is intended to capture a representation of the average "global" INP population, encompassing dust, biological, and urban emissions of INP. However, in reality, the abundance of INP likely changes depending on the dominant source of aerosol at a given location. Thus, regions dominated by mineral dust particles may have differing concentrations of INP in comparison to regions dominated by biological INP, even when INP are normalized in some way to account for variations in total aerosol loading. Since regions of varied particle sources do exist, the most basic need is to predict n_{INP} as a function of temperature, ideally including co-relation to the type and abundance of available aerosol.

1.3. Biomass burning

A study by Westerling et al., (2006) examined the impact of climate change on wildfires in the western US and found that 66% of the variance in annual wildfire frequency from 1970 to 2004 was explained by regional temperature trends. They suggest an increase in wildfire frequency is expected with the future warmer temperatures evident in climate model projections [Westerling et al., 2006]. A study by Park et al. (2007) showed that biomass burning accounts for approximately 50% of the annual mean total carbon aerosol mass concentration. Park et al. (2007) also examined the spatial contributions of biomass burning in the US by pairing observations of total carbon and non-soil potassium aerosol mass concentrations from the Interagency Monitoring of Protected Visual Environments (IMPROVE) network with satellite fire data during the years 2001 to 2004 (Figure 1.1). They concluded that wildfires contributed up to 80% of the annual total carbon aerosol mass concentration in western US and that the eastern US was strongly influenced by prescribed burning, a technique used for forest medication.

With several reports of INP measured from biomass burning sources in the laboratory (Petters et al., 2009) and in the field (Prenni et al., 2012, Twohy et al., 2010, and Pratt et al., 2011), it appears that wildfires and prescribed burns may have an important contribution to the INP populations in the western and southeastern US, respectively. However, many obstacles exist in evaluating the emission of INP from biomass burning.

Many years of effort have been put forth to gain understating of the characteristics of smoke from biomass burning. Studies have shown that 80-90% of fresh smoke particle volume concentrations occur in the accumulation mode (particle diameters less than 1 μm) [Liousse et al., 1995]. In addition to highly variable inorganic aerosol components, the composition of the

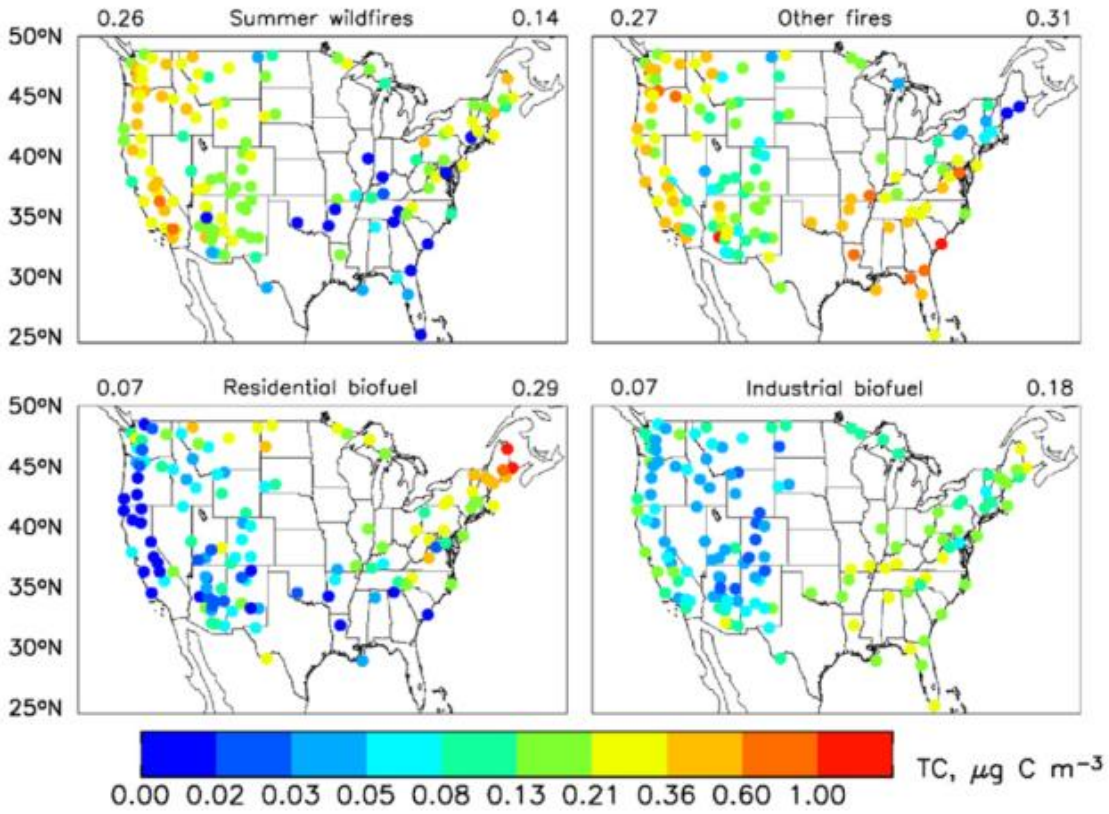

Figure 1.1. Contribution of different biomass burning types to annual mean total carbon aerosol concentrations in the US from Park et al., (2007).

emitted aerosol contains organic and black carbon and the mass ratio of OC and BC is variable [Levin et al., 2010]. Smoke particles have been found to effectively scatter and absorb incident solar radiation [Levin et al., 2010] and impact visibility. Smoke particles have also been observed to act as CCN [e.g. Eagan et al., 1974] and INP [e.g. Petters et al., 2009]. However, the emissions rates and characteristics of particles and gases released during biomass burning are strongly dependent on several parameters, including modified combustion efficiency, fuel type, impacts of transport and environmental conditions.

Complete combustion of a fuel yeilds CO_2 and H_2O, shown in Eq. 1.1.

$$\text{Fuel} + O_2 \rightarrow CO_2 + H_2O \qquad \text{(Eq. 1.1)}$$

Often times, fuel is not completely oxidized and the right side of Eq. 1.1 will include carbon monoxide (CO), particulate matter (PM), volatile organic compounds (VOCs) and nitrogen oxides (NOx) in addition to CO_2 and H_2O. Further, biomass contains species other than C and H, such as N and K, which can appear in the particle phase of emissions. Modified combustion efficiency (MCE) is a variable used to describe the "completeness" of the combustion process and is defined in Eq. 1.2,

$$MCE = \frac{\Delta[CO_2]}{\Delta[CO_2]+\Delta[CO]} \qquad \text{(Eq. 1.2)}$$

where $\Delta[CO_2]$and $\Delta[CO]$ are the increases in concentrations of carbon dioxide and carbon monoxide, respectively, emitted from the fire [Ward and Radke, 1993]. In the field, MCE typically ranges from 0.8 to 0.99 for predominantly smoldering to predominantly flaming phase combustion [Yokelson et al., 1996]. Laboratory studies have found MCE is variable between fires of the same fuel due to differences in water content and the portion of the fuel that burns (e.g., leaves vs woody material) [McMeeking et al., 2009]. The production of CO, VOCs, NOx, CO_2 and H_2O from combustion is highly variable with differences in MCE.

Relevant to ice nucleating particle emissions and properties, the number of particles and particulate mass emitted from fires is also dependent on MCE, where smoldering combustion typically produces higher particle number and aerosol mass concentrations [Ward and Radke, 1993; Janhäll et al., 2010]. Additionally, the composition and morphology of particles changes with combustion phase and between biomass burning events. A study by Pósfai et al. (2003) determined aerosol particle types as a function of plume age measured from the same fire and as a function of fire conditions. From measurements of a smoldering fire, they found aged smoke had a greater abundance of tarballs, small carbonaceous spherical particles, and fresh smoke had the largest abundance of organics, as shown in Figure 1.2. They also observed higher

abundance of soot, fractal-like carbonaceous particles, released from fresh flaming phase combustion than from fresh smoldering fires. Their findings indicate that the chemical properties are variable between fires and also change during aging processes, which may have implications on the properties of INP.

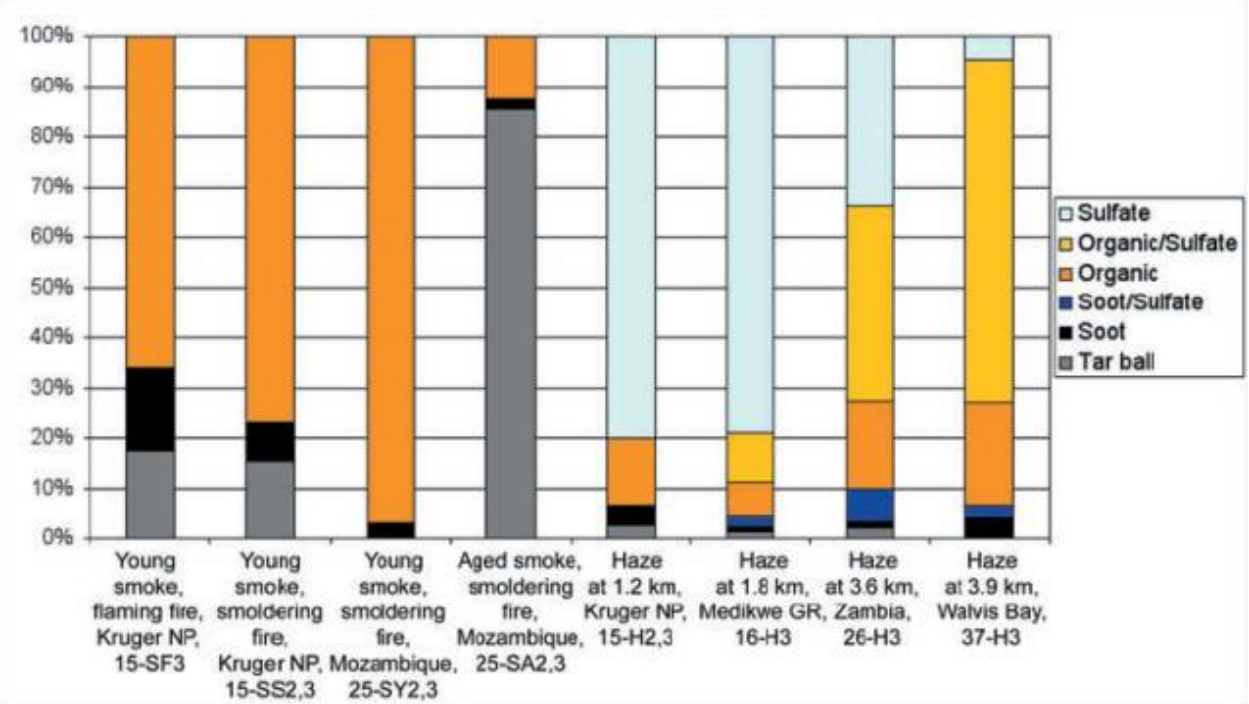

Figure 1.2. Posfai et al., 2003 study evaluating the aerosol chemical composition of smoke from fires with different phases and plumes of various ages (labeled above)

In addition to MCE and plume aging, the type of fuel that is burning also controls the chemical composition of the aerosol emitted from a fire. A laboratory study conducted by Levin et al., 2010 investigated $PM_{2.5}$ aerosol composition emitted from several different combustion events of various fuel types, shown in Figure 1.3. It is clear from their results that the composition between different fuel types is highly variable, with some smoke containing mostly organic matter and some containing more inorganics.

These previous studies show the complexity of smoke aerosol and how MCE, transport and fuel type control the amount and chemical composition of emitted aerosol, both of which are potentially relevant to the abundance of INP. Thus, it is important to consider these burning properties when evaluating biomass burning as a source of INP.

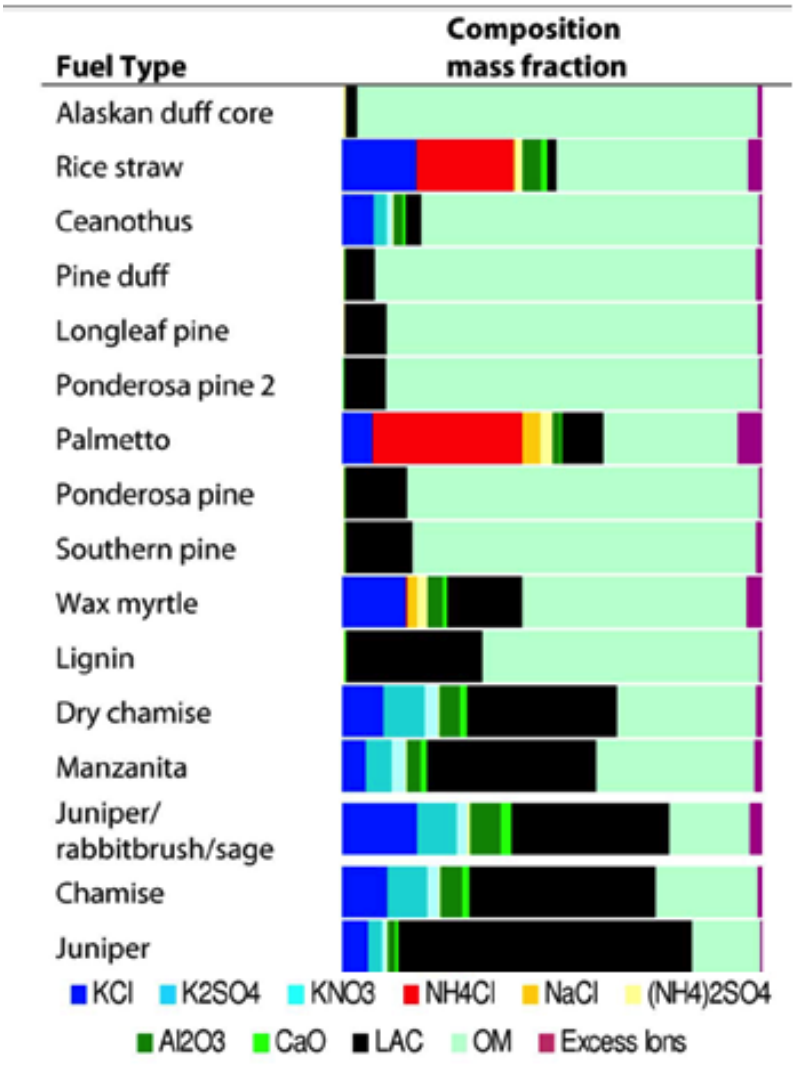

Figure 1.3. $PM_{2.5}$ aerosol composition of smoke from laboratory burns of several different fuel types during FLAME I. Figure modified from Levin et al., 2010.

1.4. Previous observations of INP from biomass burning

Laboratory studies were conducted by Petters et al. (2009) during the Fire Laboratory at Missoula Experiments (FLAME) II to investigate biomass burning as a source of INP. Multiple burns were performed of several fuel types, where smoke from a single combustion event filled a large room and was measured for an extended period of time. They used INP efficiency, defined as the log of the ratio of INP active at -30°C to total particles, to describe the emission rate of INP from each fire, shown in Figure 1.4. Ponderosa pine, a fuel type commonly found in the western US, was associated with a broad range of INP efficiencies: a few relatively high values and a majority of the cases below experimental detection limits. Longleaf pine and wiregrass, often found the southeastern US, had highly variable INP emission factors as well.

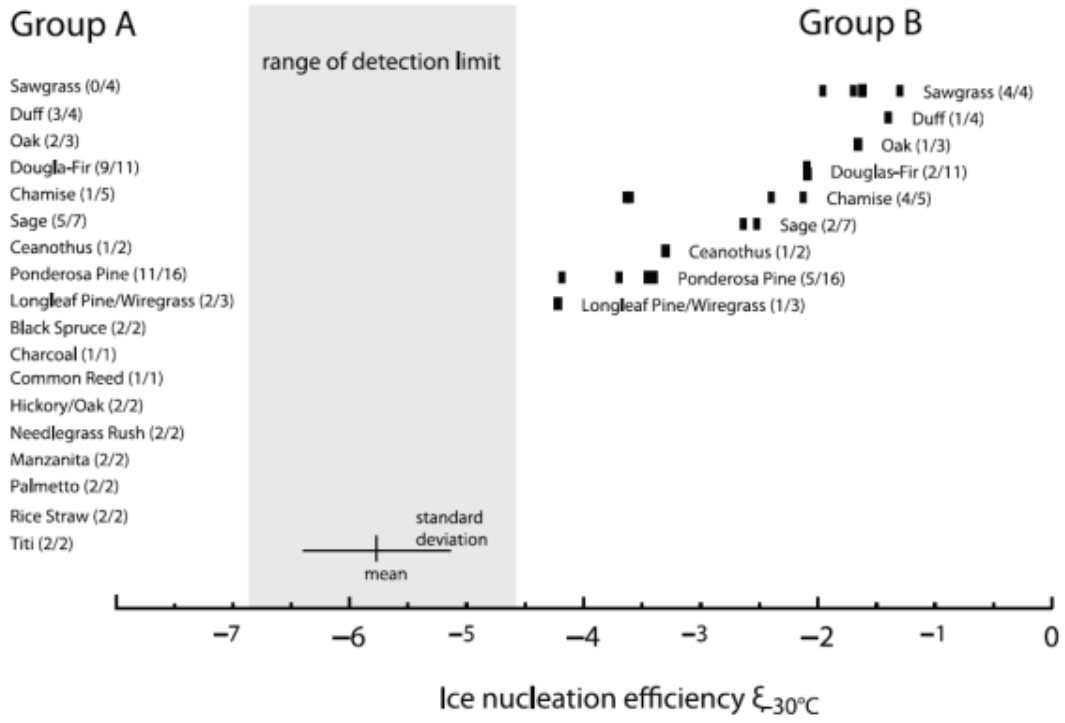

Figure 1.4. IN efficiencies for all the fuels burned during the FLAME II experiments. Group A is below detection limit and Group B is above. Figure is from Petters et al. (2009)

Many fire-related variables were also monitored in the experiments of Petters et al., (2009) and used to explain variability of INP production between fires, shown in Figure 1.5. They found INP concentrations were significantly positively correlated with modified combustion efficiency, aerosol inorganic, nitrite and potassium fractions, and aerosol hygroscopicity. They also found aerosol organic carbon fraction was anti-correlated with the production of INP. Other parameters, including fuel mass and moisture content, were not significantly correlated with INP. It is also clear from their results the fraction of INP emitted from the fires were variable between different fuel types (Figure 1.4).

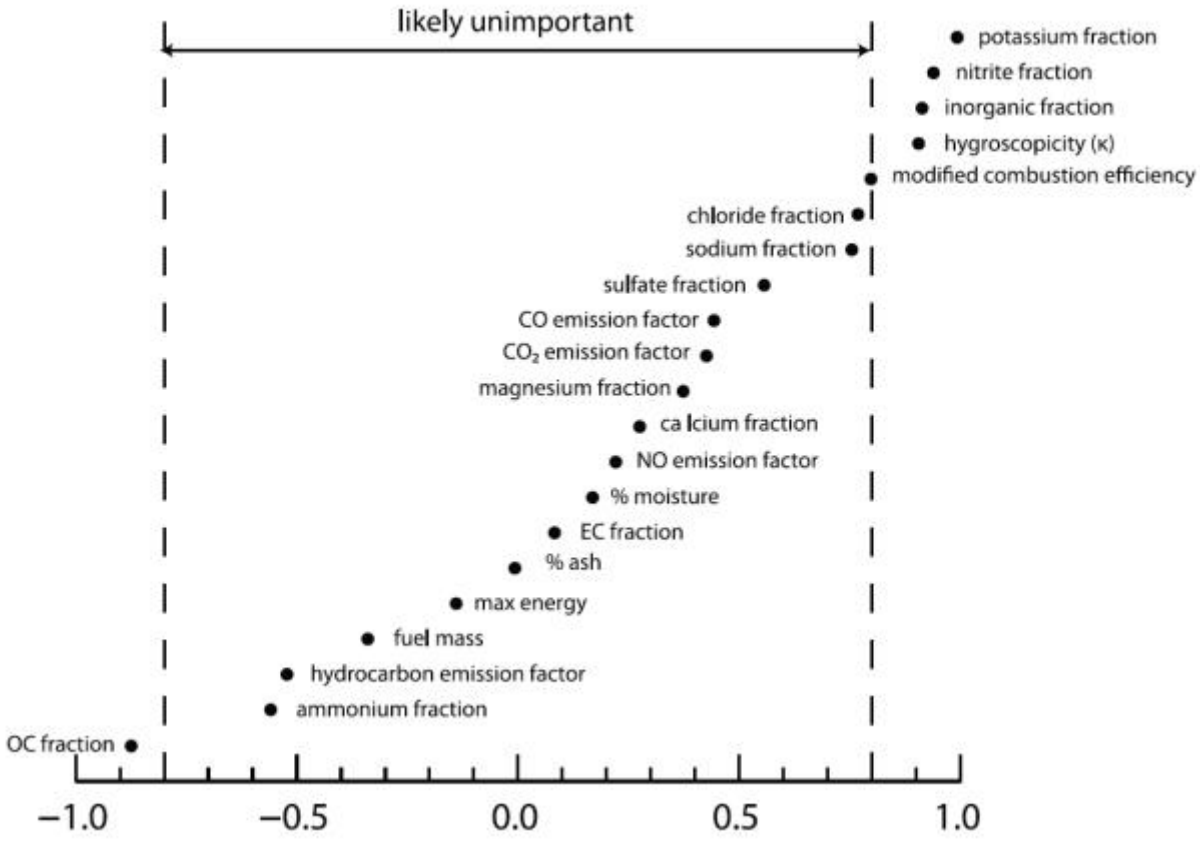

Figure 1.5. Correlation coefficients for INP efficiency versus smoke characteristics. Values above 0.8 were strongly positively correlated with increases in INP; points less than -0.8 correspond to variables with strong negative correlation. Figure is from Petters et al., 2009

Petters et al., (2009) also estimated the relevance of INP emissions from biomass burning on cloud processes using results from the controlled lab experiments. They concluded that fractions of INP to total CN greater than $1:10^4$ are required to perturb regional populations of INP. Many burns did not produce sufficient concentrations of INP for implied regional importance. However, these laboratory studies do not fully reflect what would happen in nature, where fires are often much larger and burn at higher temperatures. Additionally, these results assume plume aging and/or coagulation do not alter INP activity. Regardless, the findings of Petters et al. (2009) support the importance of fuel type and combustion efficiency on the concentrations of INP produced from different fires.

Field measurements of INP at -30°C from wildfires and prescribed fires in the western United States were reported by Prenni et al (2012). Their study observed higher concentrations of INP from the wildfires compared to the prescribed fires, most likely associated with differences in the intensity of the fire. The prescribed burns they studied produced number concentrations of INP elevated by a factor of 2 to 3 above background concentrations in the immediate area of the fires. However, the observed INP concentrations were below that which is considered capable of impacting the population of INP on a regionally relevant scale, based on estimates by Petters et al. (2009). Their study also examined concentrations of INP in aged smoke plume from a flaming-phase wildfire, located approximately 1600 km away, and found elevated number concentrations of INP. Their finding suggests a wildfire can serve as a means for increasing atmospheric INP on a large spatial scale. As in Petters et al., (2009), Prenni et al., (2012) based their studies and conclusions only on data collected at -30°C.

This study utilizes a unique and diverse collection of data from biomass burning events with contrasting burning conditions, fuel types and environments to assess their impacts on the

emissions of INP from biomass burning. A broader range of temperatures (-12 to -33°C) were explored, relevant to mixed-phase clouds and precipitation. Methods for describing the number concentrations of INP relative to other aerosol properties are explored and challenges pertaining to this complex aerosol system are discussed. Additionally, the single particle analyses performed in this study provide information on the types of particles that serve as condensation/immersion freezing INP during biomass burning influenced periods.

2. Experimental methods

The goal of this study was to evaluate aerosol samples obtained in plumes from various biomass burning events for differences in i) the emission of INP, ii) the relationship between INP and number concentrations of total and larger (diameter, d_p>500nm) particles and iii) the chemical and morphological properties of individual INP associated with biomass burning.

2.1. Sampling locations and conditions

Two prescribed burns, located in Colorado and Georgia, two Colorado wildfires and laboratory burns conducted during FLAME IV were evaluated in this study. Data from the Colorado prescribed burns were previously reported by Prenni et al., 2012. Table 2.1 is a summary of sampling dates, fuel types, distance between the fire and measurement and burn amount for each fire.

Table 2.1. Summary of measurement period, fuel type, distance of measurement from the fire, and the burn amount for fires in this study.

	Sampling location	Dates	Fuel type	Distance from fire	Burn amount
Colorado Prescribed*	Fort Collins, Colorado	July 2009	Ponderosa pine, aspen, Douglas fir, grasses	<3 km	~120 acres/day
Georgia Prescribed	Newton, Georgia	March 2011	Wiregrass/longleaf pine underbrush	<100-800 m	250-470 acres/day
Hewlett Wildfire	Fort Collins, Colorado	May 2012	Ponderosa pine timber and underbrush	30 km	7,700 acres total
High Park Wildfire	Fort Collins, Colorado	June 2012	Ponderosa pine timber and underbrush	30 km	87,000 acres total
Laboratory room burns	Missoula, Montana	Fall 2012	1)Wiregrass 2)Longleaf pine	<10 m	>1.5 kg

**Previously reported by Prenni et al., 2012*

2.1.1. Colorado prescribed burns

Measurements of ice nucleating particles were conducted during the Sheep Creek prescribed burns, published by Prenni et al., 2012, and are referred to here as the Colorado prescribed burns. These burns were located in the Roosevelt National Forest and measurements were made approximately 3 km or less from the fire using instruments installed within the CSU Mobile Lab (Brown Specialty Vehicles, Inc.) on July 23 and 24, 2009. Prenni et al.,(2012) report that ~ 125 acres were burned each day and a mixture of smoldering and flaming phase fire was observed at ground level. Number concentrations of INP (n_{INP}), particles with diameters greater than 500 nm (n_{500nm}) and condensation nuclei (n_{CN}) were monitored during this biomass burning event.

2.1.2. Georgia prescribed burns

Five days of sampling took place in March of 2011 at the Joseph W. Jones Ecological Research Center (JERC), located in rural southwestern Georgia, USA (map shown in Figure 2.1a). Prescribed burns of 250 – 470 acres took place on four of the sampling days (March 08, 11, 14 and 15) and March 09 was a background day with no known nearby active fires. Sampling duration, burn area, and ambient conditions are summarized in Table 2.2.

Ambient temperature and relative humidity measurements were made at the Ichauway weather station located at the JERC. Average ambient temperatures during the study ranged from 60 to 75 °F and average relative humidity ranged from 34 to 72%, with the exception of the background day where relative humidity was 100% during the sampling period. During the last 45 minutes of sampling on March 09, a total of 2 mm of rainfall was recorded.

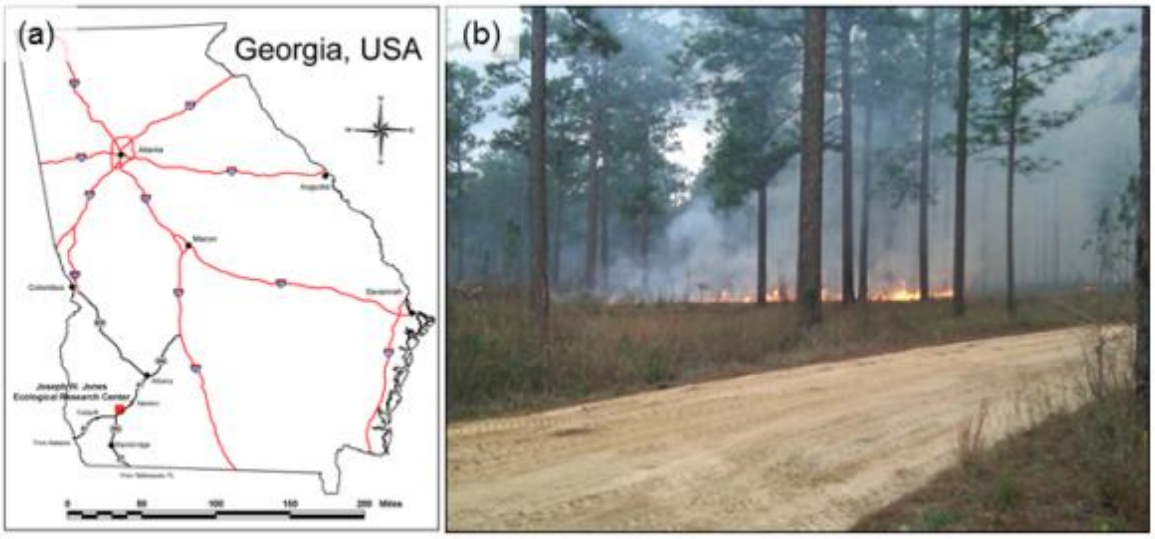

Figure 2.1. (a) Map of Georgia, USA with the location of the prescribed burns in southwestern GA (red square). (b) Photo of prescribed burn taken from the sampling site on March 15, 2011 (Photo credit: Paul DeMott)

Table 2.2. Summary of burn area, ambient temperature and relative humidity for each sampling period.

Sample period (EDT)	Acres burned	Temp (°F)	RH (%)
03/08/11 10:45 – 14:30*	468.2	74 (±2)	34 (±6)
03/09/11 10:30 – 12:30**	0	66 (±7)	100 (±0)
03/11/11 10:00 – 14:30**	451.8	60 (±3)	72 (±37)
03/14/11 09:46 – 14:00**	278.0	72 (±1)	47 (±2)
03/15/11 10:50 – 14:30**	249.4	75 (±2)	57 (±5)

**measured >50 meters from fire leading edge*
***measured less than 50 meters from fire leading edge*

Aerosol measurements were made onboard the CSU Mobile Lab, which was parked more than 50 meters from the nearest edge of the fire on March 08 and within 50 meters of the fire on March 11, 14 and 15. Figure 2.1b is a photo of the burn taken near the sampling site on March

15. Instruments for monitoring n_{INP}, n_{500nm} and n_{CN} were deployed for periods of 2-4.5 hours and bulk aerosol chemical composition was obtained each day.

A summary of the overstory land cover and soils burned during each burn day is provided in Figure 2.2 and Figure 2.3, respectively. In general, a mixture of wiregrass and longleaf pine shrubs and underbrush was burned, but a few differences exist between the burn area on March 08 compared to other days. A majority of the burn area forest overstory types had highest contributions from longleaf forest land cover type (defined by over 80% of longleaf), whereas the largest contribution to the land cover type burned on March 08 was longleaf/hardwood forest (defined as 50-80% longleaf and 20-50% hardwood forest). Additionally, the soils in the burn area of March 08 had greater contributions from sand rather than the loamy sand that dominated on the other days. Sands are dryer and contain less organic material than loamy sands.

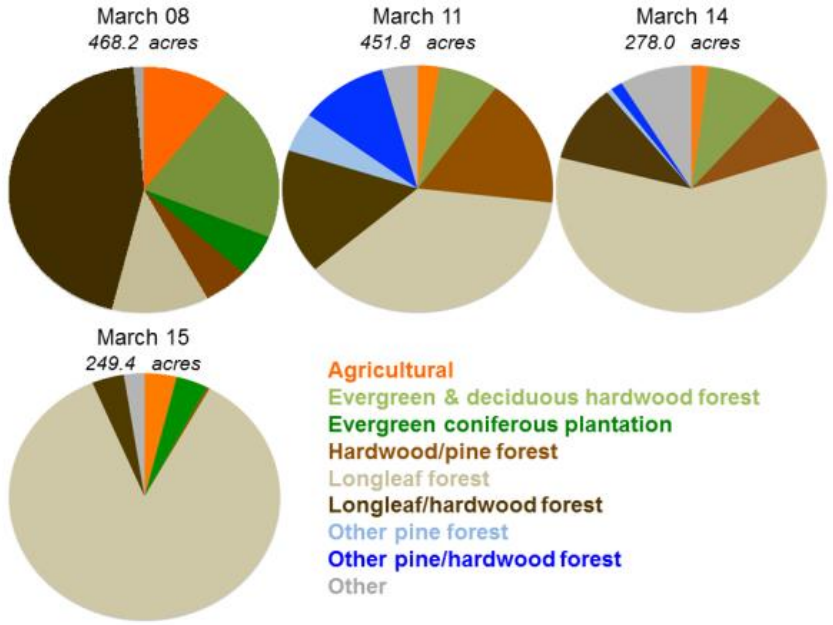

Figure 2.2 Contribution of different land cover types to the total area burned during each prescribed burn. Land cover surfaces included agricultural (orange), evergreen and deciduous hardwood forest (light green), evergreen coniferous plantation (green), hardwood/pine forest (brown), longleaf forest (light brown), longleaf/hardwood forest (dark brown), other pine forest (light blue), other pine/hardwood forest (blue), and other (grey)

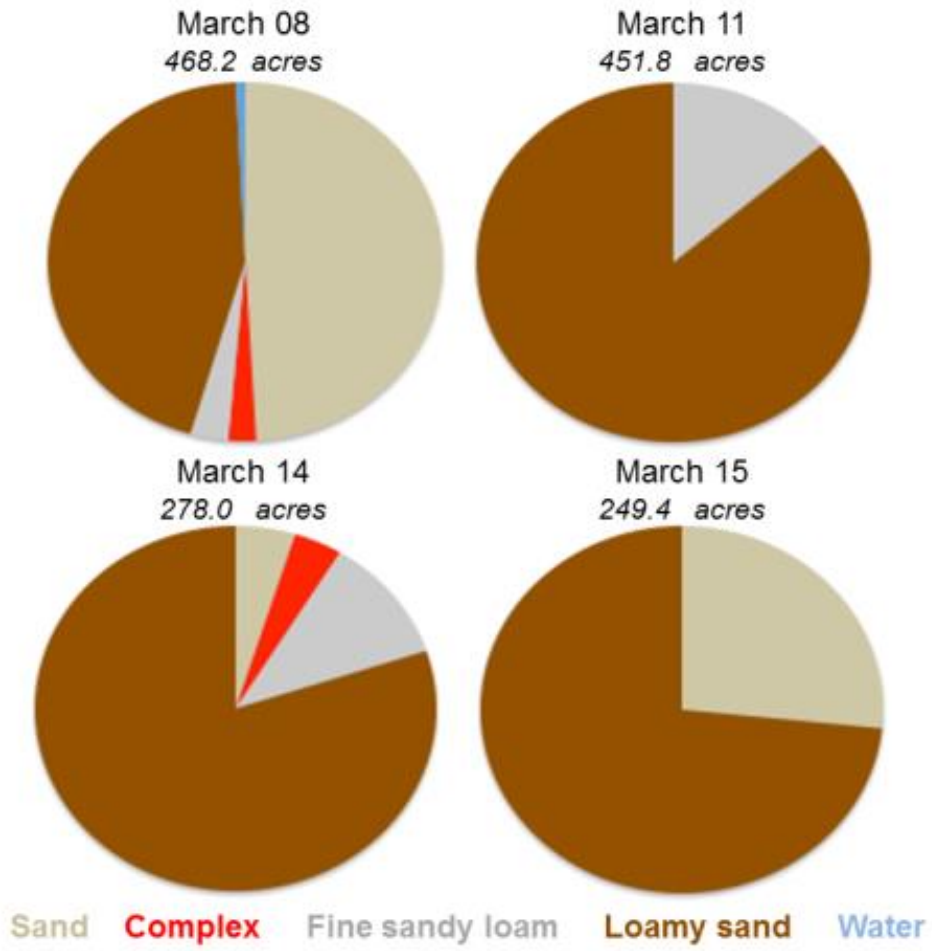

Figure 2.3 Contribution of different soil types in the total area burned during each prescribed burn. Soil types included sand (light brown), complex (red), fine sandy loam (grey), Loamy sand (brown), and water (light blue)

2.1.2. Colorado wildfires

The High Park and Hewlett Gulch wildfires occurred less than 30 km from Fort Collins, Colorado, USA. The Hewlett fire was 7,865 acres and started on May 14, 2012, reaching full containment on May 22, 2012. The High Park fire started on June 09, 2012 and the 87,284 acre fire was fully contained on July 01, 2012. A map of the final burn areas for these two wildfires is shown in Figure 2.4. [www.inciweb.org]. Measurements were made from the aerosol lab located at the CSU Foothills Campus; its location is also shown in Figure 2.4.

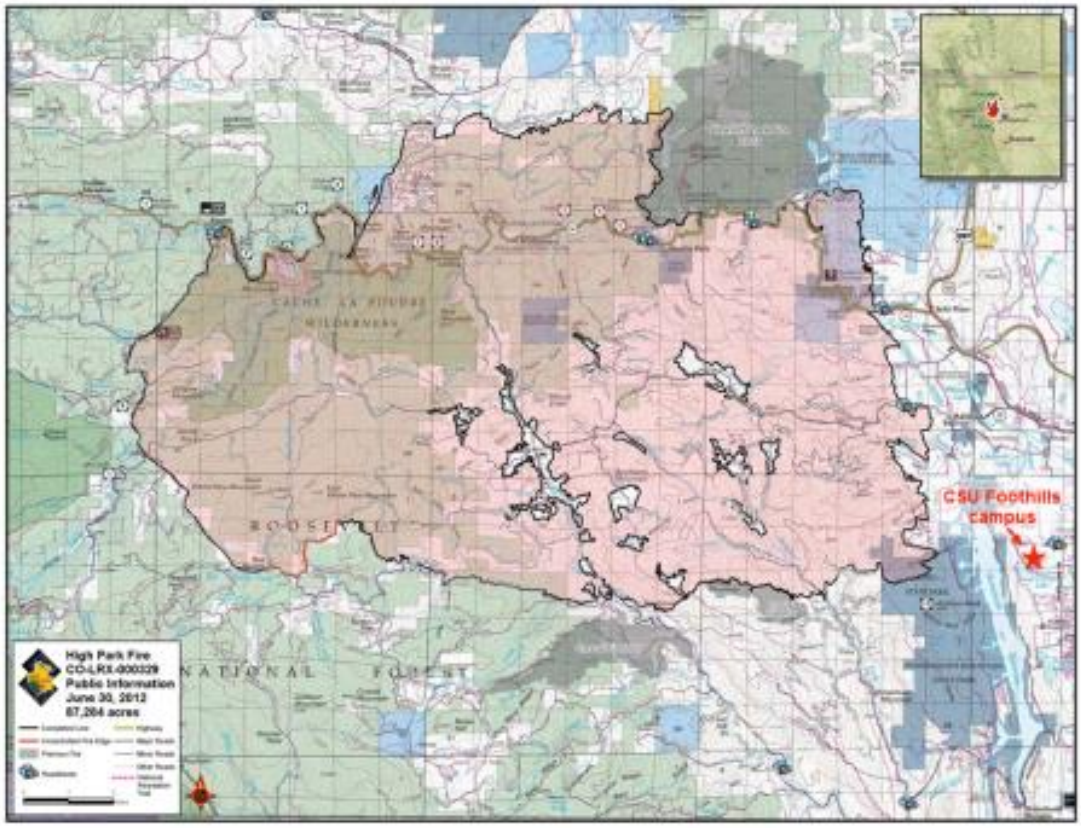

Figure 2.4. Map of the final burn areas for the CO wildfires: Hewlett Gulch (grey) and High Park (pink) wildfires. Red star indicates the location of the CSU Foothills campus.

Daily areas consumed by each wildfire, summarized in Table 2.3, were determined from progression maps [www.inciweb.org]. At least 900 acres were burned each day, with exception of May 15th, and exceeded the areas consumed by the Georgia and Colorado prescribed fires. Ambient temperature and relative humidity, measured at the Christman Field weather station located near the CSU Foothills Campus are also summarized in Table 2.3. Compared to the Georgia prescribed burns, the wildfires occurred in warmer and dryer ambient conditions.

Fuels burned during both wildfires consisted mostly of ponderosa pine timber, shrubs, and underbrush. Measurements made during these fires included n_{INP}, n_{500nm}, n_{CN}, bulk aerosol chemical composition and aerosol mass concentrations. Carbon monoxide (CO) measurements

were used as a conservative indicator for smoke due to the long atmospheric lifetime of CO, which is reported to be at minimum 2 months [Seinfeld and Pandis 2006].

Table 2.3. Summary of burn area, ambient temperature and relative humidity for each sampling period during the wildfires. Burn area is given as the total area consumed by the fire on each day and the number of acres burned in the previous 24 hours are listed in parentheses.

Sample period, MDT	Total (progressed) acres burned	Temp, °F	RH, %
Hewlett Gulch Wildfire			
05/15/12 12:45 - 17:15	400 (+140)	76 (±2)	12 (±1)
05/16/12 16:45 – 18:45	982 (+582)	73 (±2)	20 (±4)
05/17/12 11:00 – 16:30	5090 (+4108)	76 (±3)	18 (±3)
05/18/12 06:00 – 10:30 13:00 – 17:00	7673 (+2583)	68 (±9) 79 (±1)	26 (±7) 14 (±3)
05/21/12 13:00 – 15:00	7685 (+0)*	80 (±1)	13 (±1)
High Park wildfire			
06/11/12 06:30 – 14:30	36,930 (+29,470)	64 (±8)	21 (±7)
06/12/12 08:30 – 12:15	43,785 (+6,855)	70 (±7)	23 (±7)
06/13/12 05:45 – 08:30	46,823 (+3,338)*	64 (±9)	32 (±9)

** 87% contained*
***Measured at 02:20 MST*

2.1.3. Fire Laboratory at Missoula Experiments IV (FLAME IV)

The Fire Laboratory at Missoula Experiments (FLAME) IV project took place at the U.S. Forest Service Fire Sciences Laboratory in Missoula, Montana, USA from October 16 to November 08, 2012. Room experiments, where fuels were loaded onto a platform and ignited in a large enclosed room, were beneficial for this study because measurements could be made from a smoke sample for a longer period of time than what is feasible in the field. Measurements of n_{INP}, n_{500nm}, n_{CN}, CO and aerosol mass concentrations began soon after the room became well

mixed, as determined by stabilized n_{CN}. A new instrumental setup was also used to explore the role of refractory black carbon on INP concentrations.

Two room burns were of particular relevance to this study, for their similarity to fuel burned during the field burns. A total of 1.5 kg of wiregrass branches and needles were ignited during the wiregrass room burn and the modified combustion efficiency was 0.98 (±0.0003), as determined from CO and CO_2 gas measurements using Eq. 1.3.2, indicating mostly flaming phase combustion [Yokelson et al., 1996]. Approximately 1.7 kg of ponderosa pine branches and greens were burned during the ponderosa pine room burn and the fire was less flaming with a MCE of 0.93 (±0.002).

2.2. Instrumentation

Instruments deployed during each field project, summarized in Table 2.4, are explained in more detail in the following sections. Individual biomass burning events utilized different combinations of various aerosol size, mass, compositional, and cloud activation property measurement methods. Ambient number concentrations of ice nucleating particles and particles with diameters d_p>500nm, hereafter referred to as "larger particles" with number concentrations indicated as n_{500nm}, were determined using the CSU continuous flow diffusion chamber (CFDC) [Rogers et al., 2001]. Transmission electron microscopy (TEM) was used to analyze residual INP collected on TEM grids downstream of the CFDC: the collection was done via impaction that selects only supermicron ice crystals, containing INP, and passes through unactivated, non-INP particles. Total condensation nuclei number concentrations were determined using an ultrafine condensation particle counter (TSI, Model 3776) or integrated size distributions from a fast mobility particle sizer (TSI, Model 3091). A tapered element oscillating microbalance

(TEOM, TSI, Model 1505-DF) was used to measure mass concentrations of particles smaller than 2.5 μm and smaller than 10 μm. HiVol filters were collected over 3-24 hour periods and analyzed to determine bulk daily aerosol chemical composition. Carbon monoxide measurements were also made to distinguish in-plume sampling. Finally, a single particle soot photometer (Droplet Measurement Technologies) was used to determine mass concentrations of refractory black carbon.

Table 2.4. Summary of instruments deployed during each biomass burning event, "YES" indicates the instrument was deployed, "NO" indicates the instrument was not deployed, and "NA" means the instrument was deployed but the data were not available due to instrument malfunction.

Instrument Summary	Georgia Prescribed	Colorado Prescribed	Hewlett/High Park Wildfires	FLAME IV
CFDC (n_{INP}, n_{500nm})	YES	YES	YES	YES
CPC or FMPS (condensation nuclei, n_{CN})	YES	YES	YES	YES
TEOM (aerosol mass conc, $PM_{2.5}$, PM_{10})	NA	NO	YES	NA
TEM (single particle analysis)	YES	NO	YES	YES
HiVol filters (bulk aerosol chem)	YES	YES	YES	NO
CO (Teledyne, [CO])	NO	NO	YES	YES
SP2 (refractory black carbon)	NO	NO	NO	YES

2.2.1. Ice nucleating particle and larger particle measurements

The Colorado State University continuous flow diffusion chamber (CFDC, Rogers et al., 2001; Petters et al., 2009) was operated in the humidity regime favoring condensation and immersion freezing nucleation to measure ambient INP number concentrations (schematic shown in Figure 2.5). The chamber contains two temperature controlled cylindrical columns, which comprise the inner and outer walls. Prior to measurements, these walls are coated in ice at

-27 °C. A total flow of 10 vlpm travels between the vertically oriented columns in the form of a laminar aerosol flow (1.5 lpm) surrounded by recycled, filtered and dried sheath flow (8.5 lpm).

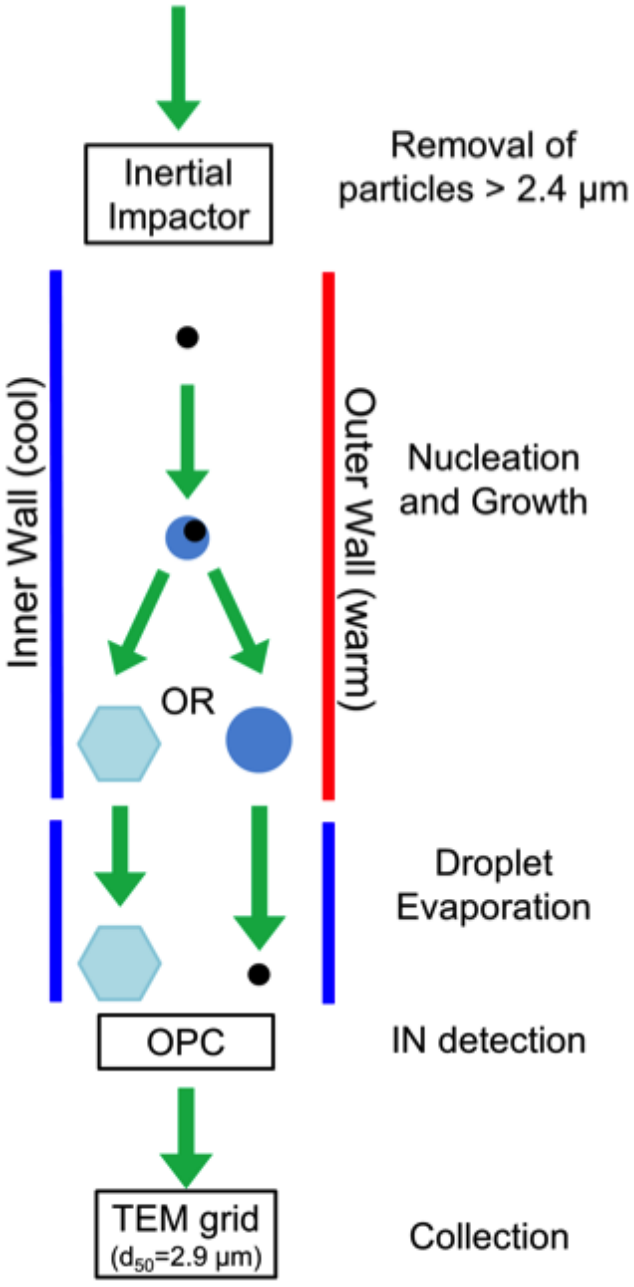

Figure 2.5. Schematic of the Colorado State University continuous-flow diffusion chamber.

Two regions are utilized in the CFDC to activate and detect INP: the nucleation/growth region and the evaporation region. In the nucleation/growth region, the inner wall is set to a

lower temperature than the outer wall, creating a water supersaturation (SS_w) region for particles to nucleate and grow into large droplets. Particles that act as ice nuclei at the CFDC operating temperature and SS_W will activate and grow as ice crystals. Residence time in this region is about 5 seconds for the flow rates used in this study. Activated droplets and ice crystals then enter the evaporation region where both walls are the same temperature and the saturation state changes to water subsaturation and ice saturation. Here, droplets will evaporate, while the nucleated ice crystals will remain.

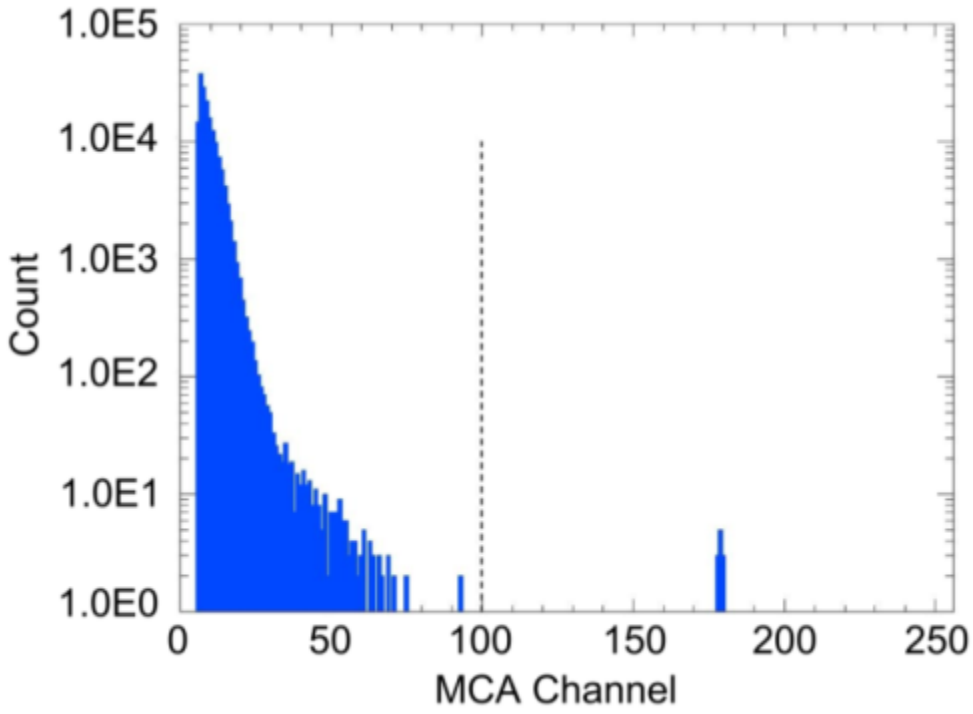

Figure 2.6. Example of MCA channel spectrum (function of particle size) measured by the CFDC OPC at the base of the CFDC chamber. The dashed line represents the cut off MCA channel used to distinguish ice crystals from unactivated particles.

Following the evaporation region, particles with optical diameters greater than 300 nm are detected using an optical particle counter (OPC, CLiMET 3100), which counts particles exiting the CFDC on the basis of scattered light collected from a diode laser. Sizing is

accomplished by accumulating voltage pulses from individual particles that are proportional to particle size using a multi-channel analyzer (MCA). The MCA accumulates data as a pulse height spectrum each second and these pulse heights are translated into sizes on the basis of calibration studies. An example of a MCA spectrum is shown in Figure 2.6. The largest detected particles, which are ice crystals, are easily distinguishable as the separate peak at highest MCA channels. To ensure larger non-IN active particles do not influence INP number concentrations, an inertial impactor is used upstream of the CFDC inlet to remove particles with aerodynamic diameters larger than 2.4 μm.

Number concentrations of INP (n_{INP}, cm^{-3}) at standard temperature and pressure (STP) were determined based on the total number of particles (ν_{INP}) above a threshold MCA channel representative of 2 μm (typically channel 100) integrated over the sample period, following Eq 2.1.

$$n_{INP} = \frac{\left(\nu_{500nm} \times 980ms \times 60\frac{sec}{min}\right)}{\left(1000\,\frac{cm^{-3}}{L} \times Q_{samp} \times t_{MCA}\right)} \qquad \text{Eq. 2.1}$$

Where, Q_{samp} is the sample flow rate in L/min (reported at STP) and the MCA live time, t_{MCA}, is a time between 0 and 980 ms that accounts for the time the MCA is counting versus transferring data. At high particle rates into the OPC, the live time is lower than the maximum values of 980 ms. Number concentrations of particles with diameter greater than 500 nm, n_{500nm}, are calculated similarly following Eq 2.2.

$$n_{500nm} = \frac{\left(\nu_{500nm} \times 980ms \times 60\frac{sec}{min}\right)}{\left(1000\,\frac{cm^{-3}}{L} \times Q_{samp} \times t_{MCA}\right)} \qquad \text{Eq. 2.1}$$

Here, the ν_{500nm} is the integrated number of particles in MCA channel bins greater than channel 6, as determined by sizing calibrations of the OPC (Appendix A). The concentrations of INP and >500 nm particles reported herein are at STP. Concentrations determined using the CFDC OPC were compared to measurements made using a CFDC independent OPC and were strongly correlated. The CFDC OPC is thus considered the best means for comparing n_{INP} with n_{500nm}. Uncertainties associated with measurements using the CFDC are discussed in Section 2.3.2.

The processing temperature of the CFDC, T_{CFDC}, also governs the number of activated INP, in that more INP are expected to be active at colder temperatures. The effect of temperature on n_{INP} during these studies is shown in Figure 2.7, clearly illustrating the increased INP activity at lower T_{CFDC} and the high variability of n_{INP} at any particular temperature that reflects diverse aerosol and INP sources. For the purposes of this study, samples are reported as a function of temperature and the primary temperature regimes used in the following analyses are those with the largest number of points: -22 ±1, -26 ±1, and -30 ±1 °C.

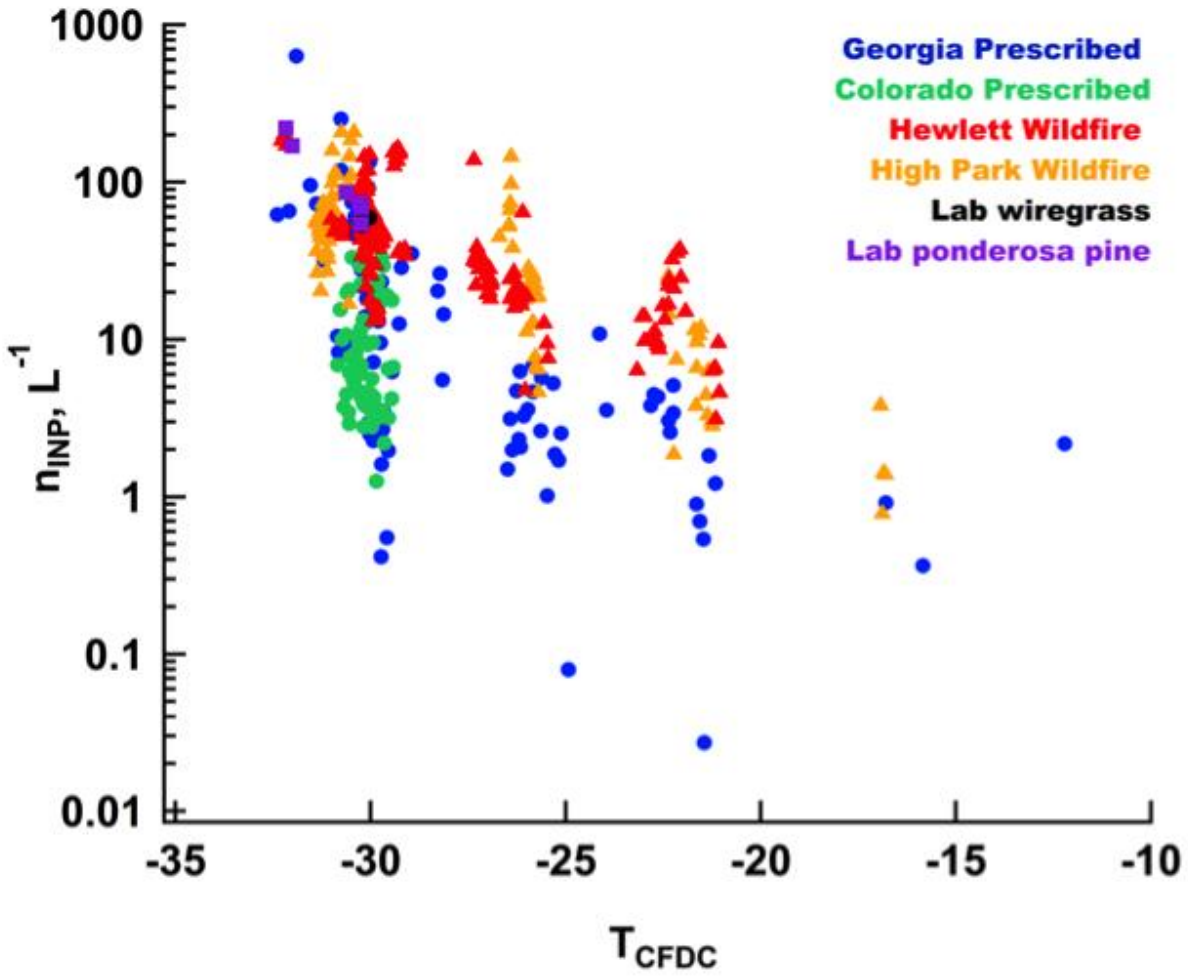

Figure 2.7. Dependence of n_{IN} on T_{CFDC} for the Georgia Prescribed (blue), Colorado prescribed (green), Hewlett wildfire (red), High Park wildfire (orange) and the FLAME IV wiregrass room burn (black). Values are 3-5 minute averages during sampling periods.

2.2.2. Single particle chemical and morphological analysis

In efforts to classify the types of particles active as INP, ice crystals were collected onto grids at the base of the CFDC via impaction during the Georgia prescribed burns and Colorado wildfires. At minimum, 5,000 ice crystals were collected onto each grid and at least 50 particles were individually analyzed using transmission electron microscopy (TEM), providing single particle imagery and energy dispersive x-ray (EDX) chemical spectra. Background spectra were collected at clean areas surrounding particles to account for additional noise associated with the

grid, coating, or EDX detector and revealed trace amounts of oxygen, carbon, copper and silicon were present in spectra from the particle-free regions. Thus, the elemental composition of each particle was determined based on spectral peaks that were elevated relative to the background spectrum. Additionally, the walls of the CFDC are made wettable through a chemical ebonization process that creates copper sulfide crystals on the copper surface. Over time, these crystals may release from the walls when frost particles break of, so care was taken to only record Cu peaks that were clearly above those found on the particle free regions.

For grids from the Georgia prescribed burns, initial collection of imagery and elemental chemical spectra were made by R.J. Lee Incorporation (Monroeville, PA), using a Hitachie HD-2300 scanning transmission electron microscope (STEM) and energy dispersive x-ray (200 kV). Imagery (200 kV FEI Tecnai G2 F20 (S)TEM) and compositional (Oxford Inca X-Stream EDX Spectrometer) analyses were performed at the University of Wyoming (Laramie, WY) at the High Resolution Transmission Electron Microscopy Facility for grids collected during the wildfires.

Particles were categorized into six types based on physical and chemical properties: soot, tarballs, carbonaceous other (C-other), carbonaceous-mineral mixture (C/Min-mix), mineral/metal oxide mixture (Min/Ox mix), and other. Carbon (C) dominated particles include soot, tarballs, C/Min-mix, and C-other. Soot particles were composed mostly of C with trace amounts of oxygen (O), silicon (Si), and/or potassium (K) and were easily identified by their fractal-like morphology, comprised of many small spheres [Pösfai et al., 2003]. Tarballs were perfectly spherical with typical diameters of 100 - 400 nm and were also comprised of mostly carbon with trace amounts of S, K, Cl and Si [Pösfai et al., 2004]. Carbon dominated particles with inclusions made up of inorganics, such as aluminum (Al), calcium (Ca), manganese (Mn),

silicon (Si), iron (Fe), copper (Cu) and magnesium (Mg), were referred to as C/Min-mix particles. Particles with mostly C and trace amounts of O, Si, and/or K without an easily recognizable shape were placed into the C-other category. Min/Ox mix particles were dominated by non-carbonaceous elements, including Ca, Al, Si, Mn, O, Fe, and Cu, and typically resembled crystalline structures. Finally, particles that did not discernibly fall in any of these particle types based on their chemical spectrum and morphology were categorized as other. One example of each of these categories are shown in Figure 2.8. The color of the backgrounds in each category will be used in figures to follow.

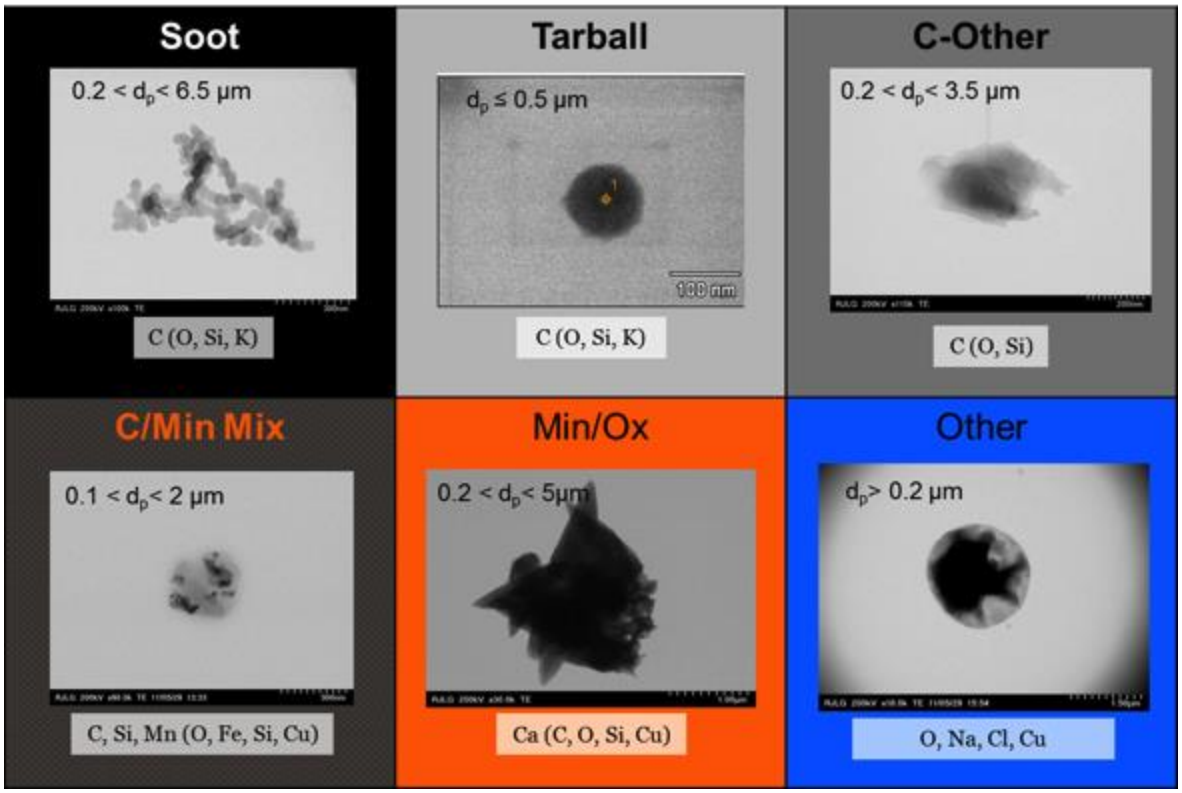

Figure 2.8. Example particles for each category used to describe ice nucleating particles based on chemical and morphological information from TEM analyses.

2.2.3. Total particle number concentrations

An ultrafine condensation particle counter (CPC, TSI Model 3776) was used to measure n_{CN} during the prescribed burns and wildfires. The Model 3776 CPC operates at a total flow rate of 0.3 (± 0.015) L/min with an aerosol flow rate of 0.05 (+/- 0.005) L/min. Aerosol flows through a heated saturator, where alcohol vapor diffuses into the sample stream. As the aerosol proceeds through a cooled supersaturated region, particles act as condensation nuclei and alcohol vapor condenses onto the particles. Particles continue to grow into sizes measureable with an optical detector. The Model 3776 CPC can detect particles with diameters greater than 2.5 nm (upper limit of >3µm) at number concentrations up to 3.0×10^5 cm^{-3} with +/- 10% accuracy. The response time of this instrument is less than 0.8 seconds.

During the FLAME IV laboratory study, a Fast Mobility Particle Sizer (FMPS) Spectrometer (TSI, Model 3091) was used to measure size distributions of submicron particles. The total flow rate of the FMPS is 40 lpm, with an aerosol flow rate of 10 lpm. A corona charger is used to positively charge particles prior to entering a chamber that contains a large high voltage electrode at its center. A strong positive charge on the electrode acts to force the positively charged particles away from the electrode towards highly sensitive electrometers. These electrometers are distributed vertically, such that particles will collect onto different electrometers based on their electric mobility, thereby providing an aerosol size distribution. Particles with diameters between 5.6 and 560 nm are detected by the FMPS based on size at a resolution of 1Hz into 32 size bins. Bins were integrated to determine conservative n_{CN} for comparison to CPC measurements from the other burning events.

Total number concentrations obtained from the CPC and integrated size distributions from the FMPS were averaged over sampling periods, determined by the CFDC data processing described in Section 2.3.1.

2.2.4. Aerosol mass concentrations

A tapered element oscillating microbalance (TEOM) was used during the Colorado wildfires to determine the mass concentrations of coarse particulate matter (PM_{coarse}, 2.5 μm < d_p < 10 μm) and particles having diameters less than 2.5 μm and 10 μm ($PM_{2.5}$ and PM_{10}, respectively). The TEOM can quantify mass concentrations from 5 $\mu g/m^3$ to several g/m^3. An air sample travels through the TEOM, at a total flow rate of 16.7 lpm and is separated into two flows; 1.7 lpm for PM_{coarse} and 15.0 lpm for $PM_{2.5}$. The $PM_{2.5}$ flow is further separated to 3 lpm sample and 12 lpm by-pass flows. Particulate matter from the $PM_{2.5}$ and PM_{coarse} sample flows are collected on a $PM_{2.5}$ filter and a PM_{coarse} filter, respectively. These filters are continuously weighed and provide mass concentrations of $PM_{2.5}$ and PM_{coarse} every 6 minutes. PM_{10} was calculated as the arithmetic sum of $PM_{2.5}$ and PM_{coarse}. No averaging was performed on the TEOM data for the analyses of this study.

The TEOM instrument was also deployed during the Georgia prescribed burns, however an adequate amount of time was not allotted for the instrument to warm up before the burns and thus uncertainty exists in using the data from those burns. Also, the TEOM was deployed during the FLAME IV study; however data acquisition stopped in the middle of the burn for unknown reasons.

2.2.5. Carbon monoxide concentration

A carbon monoxide (CO) analyzer (Teledyne, Model 300EU) was used to measure CO during the Colorado wildfires, with the exception of two days. A high energy infrared source is targeted through two chambers: one with no CO and one filled with the sample air (1800 cm^3/min flow rate). The differences in energy absorption between the two chambers are then used to determine the concentration of CO in the sample air. The lower detection limit for the Model 300EU CO analyzer is < 20ppb with a precision of 0.5%. Carbon dioxide (CO_2) was not monitored and therefore MCE was not calculated for the biomass burning events. CO_2 measurements should strongly be considered for future studies of INP from biomass burning.

Carbon monoxide was monitored at the Foothills Campus during a period between the two wildfires (May 29 through June 3) to characterize background CO concentrations. The average background CO concentration was found to be 136 (±20) ppb. Thus, excursions of CO concentrations above 176 ppb (two standard deviations above the mean) are taken to be clearly influenced by local and/or regional smoke.

2.2.6. Bulk aerosol chemistry

Bulk aerosol water soluble chemical composition was determined from aerosol collected onto quartz filters using Thermo Anderson Hi-Volume (HiVol) Air Sampler collection systems. Filter collected was collocated with the CFDC during the Georgia prescribed burn and both wildfires. The Georgia prescribed burn filters were collected over periods of approximately 3 hours whereas the wildfire filters were collected over 24 hour periods. The HiVol sampler operates at a flow rate of 1.13 m^3/min and collects PM_{coarse} and $PM_{2.5}$ on two separate filters. $PM_{2.5}$ samples were analyzed for chemical composition and used in this study. Blank filters,

ones which were handled and placed in the HiVol sampler for 2 minutes without airflow, were also analyzed to account for contamination associated with filter installation.

Extracts of the filters were prepared with two 25 mm diameter punches in 2 ml of deionized water. Concentrations of carbohydrates, such as levoglucosan, were measured using a high-performance anion-exchange chromatography system with pulsed amperometric detection [Sullivan et al., 2011]. Ion chromatography (IC, Dionex DX-500) was used to measure major water soluble cations and anions, including Na^+, NH_4^+, K^+, Mg^{2+}, Ca^{2+}, Cl^-, NO_3^-, and SO_4^{2-}. A Dionex IonPac CS12A analytical separation column was used for cation detection and a Dionex IonPac AS14A column was used to separate anions. Water soluble organic carbon and total organic carbon concentrations were determined using a Sievers Model 800 Turbo TOC Analyzer and organic carbon and elemental carbon concentrations were determined for filter punches using a Sunset Labs EC/OC analyzer with the standard Sunset protocol for splitting between elemental carbon and organic carbon. Concentrations are reported as ambient $\mu g/m^3$ of air.

2.2.7. Online detection of refractory black carbon

During the FLAME IV laboratory study, a single particle soot photometer (SP2, Droplet Measurement Technologies) was used in series with the CFDC. This method is a new procedure used to evaluate the ice nucleating ability of black carbon. The SP2 directs a 1046 nm laser towards a thin aerosol stream and the beam is absorbed or reflected by the aerosol based on its composition. Substances reflect radiation at 1046 nm unless refractory black carbon (rBC) is present, which will efficiently absorb the beam and incandesce. Two sensors are used to measure light that is scattered by each particle and two sensors are used to measure the radiation

emitted by the incandescent rBC. From these two sensors, the rBC mass distribution is determined as a function of particle size.

The SP2 operates at a flow rate of ~120 cm^3/min at a data acquisition rate of 0-25,000 particles/second, or until particles become coincident. The minimum detection limit of BC is 10 ng/m^3 and the detectable size range for the scatter signal is particles with diameters ranging from 200-430 nm and the size range for the absorption signal is 70-500nm mass-equivalent diameter assuming a black carbon density of 1.8g/cm^3.

During this FLAME IV room burns, the SP2 was essentially used as an rBC filter upstream of the CFDC. The CFDC measured n_{INP} with the SP2 laser on and off, providing information on the the effect of removing rBC on n_{INP} and n_{500nm}. There are uncertainties associated with this novel method, including the fate of the rBC after interaction with the laser, the impact the laser has on non-rBC containing INP and the selectivity of the SP2 to rBC. Laboratory experiments were performed to evaluate these potential interferences.

Two SP2 instruments in series revealed that rBC detected by the first SP2 was essentially transformed into smaller rBC particles, which were large enough and contained enough mass to be detected by the second SP2. Tests using this set up with calibration aerosol also revealed a 94-95% reduction in rBC mass concentration from the first SP2 to the second SP2 for sizes ranging from 150 nm to 500 nm. Since the INP population is typically dominated by larger particles [DeMott et al., 2010], the small secondary rBC particles are likely unimportant to the INP detected by the CFDC. The mechanism for which these small rBC particles are formed remains uncertain, whether rBC particles are fragmented into tiny particles or if rBC particles are evaporated during/after incandescence and re-condensed into small rBC particles.

Laboratory tests have been conducted to evaluate the effect of the laser on known INP, specifically organic alfalfa soil and kaolinite, and no apparent change in the INP concentration was observed between laser on and laser off samples. These results indicate that the SP2 laser does not change the nucleating ability of kaolinite or alfalfa soil. Studies on a mixture of rBC and kaolinite were also performed to evaluate the impact of the laser on a known-IN active particle that is attached to incandescing rBC. During a period when the mixture had more rBC-containing particles than purely scattering particles, a reduction in n_{INP} was observed after turning the laser on. When the mixture was about half rBC-containing and half purely scattering particles, a lesser reduction in INP was observed after the laser was turned on. These results suggest the nucleating ability of rBC-kaolinite particles was compromised after they interacted with the SP2 laser.

These laboratory tests confirm the SP2 removes rBC from the aerosol stream in the form of secondary small rBC particles, which are likely unimportant to INP measurements. Results indicated that known non-rBC containing INP are unaffected by the laser and the SP2 is selective to rBC such that even INP containing only a fraction of rBC are compromised by the laser. Uncertainties associated with the applicability of this method to more complex aerosol, such as those containing organics, are yet to be explored.

2.2.8. Navy aerosol analysis and prediction system (NAAPS) model

The Navy Aerosol Analysis and Prediction System (NAAPS), a model for predicting tropospheric aerosol distributions, was used in this study for evaluating regional dust influences. Meteorology in the model is driven by the Navy Operations Global Atmospheric Prediction System, which has a horizontal spatial resolution of a 1x1 degree, a 6 hour temporal resolution

and 24 vertical levels reaching 100 mb. Dust emissions are determined based on frictional velocity, landuse type, snow depth and surface moisture. Dust fluxes are determined for particles with radii smaller than 5 μm and injected into the two lowest layers. Predictions for the Western United States region were used in this study and specifically a grid box located over the fire and sampling sites (40.5 ºN, 104.5 ºW).

2.3. Data processing

2.3.1. Sample period criteria

With INP as the primary focus, valid measurements made by the CFDC were used to identify the sampling periods for data averaging in this study. In order to isolate valid CFDC sample periods, filtered air measurements and changes in INP activity due to fluctuations in water supersaturation (SS_w) and temperature (T_{CFDC}) were identified and used to flag the data meeting specific criteria during those periods.

CFDC measurements of ambient air were 3-15 minutes long and were further divided into 3-5 minutes sampling periods, after the exclusion of 30 seconds of sampling after any transitions in operating conditions, to account for residence time in the chamber. Since INP activity is sensitive to changes in T_{CFDC} and SS_w, periods where SS_w and T_{CFDC} deviated by more than 2% or 1°C, respectively, over the 3-5 minute periods were removed. The remaining time periods in each 3-5 minute sampling period were then used to calculate average n_{INP}, n_{500nm}, T_{CFDC}, SS_w, n_{CN} and CO concentrations.

Measurements of filtered air were made between ambient air samples in order to monitor and correct for CFDC background frost particle formation [Rogers et al., 1994]. Background INP number concentrations were averaged over filtered air periods of constant T_{CFDC} (± 1 °C) and

SS_w (± 2%), with the omission of transition air (30 seconds). Linearly interpolated background n_{INP} and n_{500nm} were subtracted from ambient n_{INP} and n_{500nm} to correct for frost background. If background n_{INP} or n_{500nm} was greater than the sample concentrations, the sample was removed. An example of processed data is shown in Figure 2.9.

2.3.2. Measurement uncertainties

Uncertainties in number concentrations measured with the CFDC were determined using the Square-Root Rule for Counting Experiments, which is based on counting statistics and the Poisson distribution [Taylor, 1997]. The uncertainty of each average number concentration (σ_x) is dependent on the volume of sample air (V_{samp}) and the average count of x (ν_X),

$$\sigma_x = \frac{2\times\sqrt{\nu_X}}{V_{samp}} \qquad \text{Eq 2.3.}$$

where x is the variable counted (INP or particles larger than 500nm). All uncertainties for n_{INP} and n_{500nm} presented here were determined using this method. Uncertainties associated with all other measurements are reported as the standard deviation of the mean.

Previous studies by Petters et al., 2009 and DeMott et al., 2011 have revealed high SS_w (110% or higher) is required to access measurements of the full expressions of condensation/immersion freezing INP in the CFDC. That is, only at these high SSw can it be guaranteed that all of the particles in the sample stream have been immersed in water droplets and thus have been prepared to permit expression of INP activity via one of these modes. At these high SS_w, for the sizes and hygroscopicities of aerosol sampled in the field, the residence time in the evaporation region of the CFDC is inadequate for removing enough water mass from the droplets to reduce them to sizes that appear below the ice crystal cutoff channel (Figure 2.6). As a result, some droplets that do not contain INP and have not formed ice exit the. As a result,

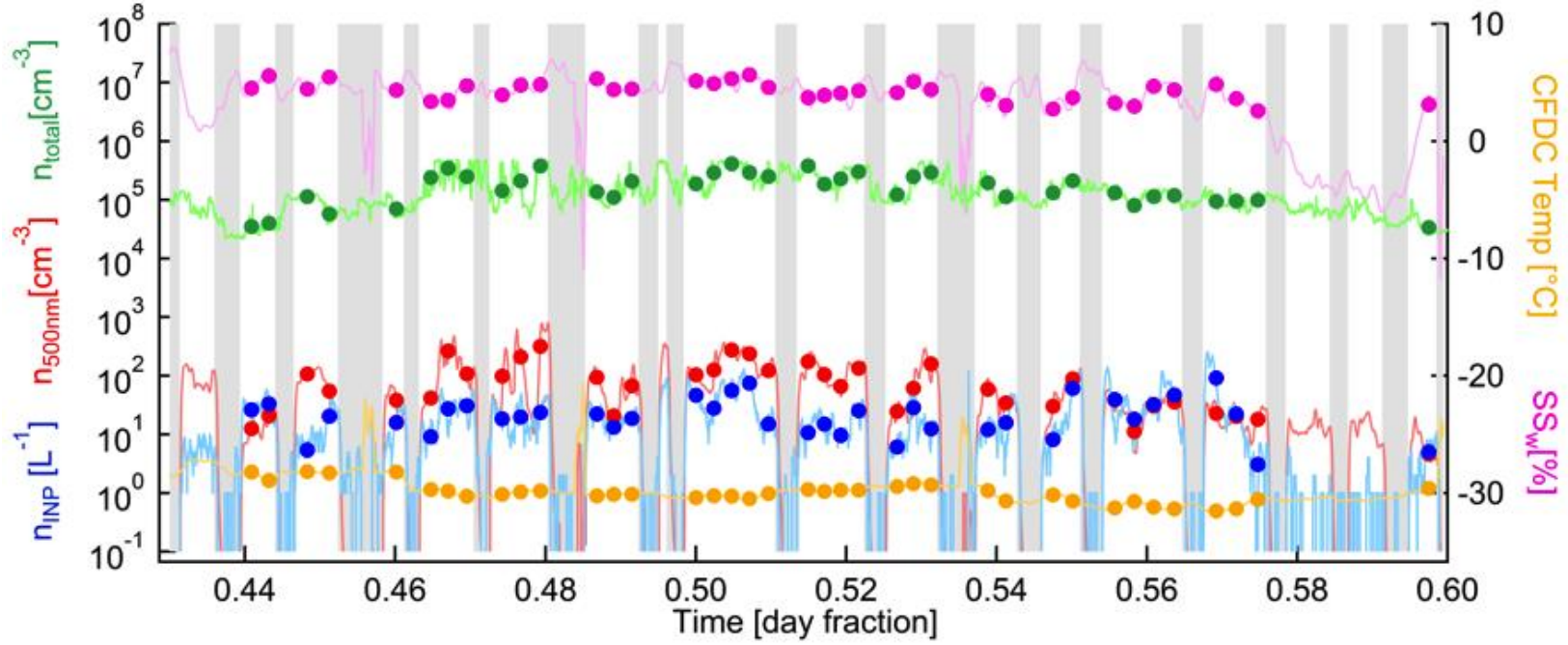

Figure 2.9. Running mean (30 seconds) (line) and sampled averaged of ambient (dots) n_{INP} (blue), n_{500nm} (red), n_{CN} (green), SS_w (pink), T_{CFDC} (orange).

some droplets that do not contain INP and have not formed ice exit the evaporation section large enough that they are erroneously detected as INP. To avoid these invalid counts, a narrow range of SS_w from 102.5 to 107% was used during these studies and n_{INP} were expected to be underestimated by a factor of 3 to 4 [DeMott et al., 2013].

2.3. Power law regression method

Power law regression analysis was performed for several variables in this study using R statistical software. The power law equation is

$$Y=bX^m$$

where b is the y-intercept and m describes the slope of the relationship between X and Y. This analysis was used for the relationship between different number concentrations of total particles, INP, and particles with diameters greater than 500nm. To determine b and m, a linear fit was calculated for the logarithmically transformed X and Y values.

The R statistical software provides information on the statistical significance of the fit by estimating the probability that the slope between X and Y is non-zero. This probability is described by the p-value, where a smaller p-value indicates greater probability that the slope is non-zero. For each of the Power law regressions reported herein, a p-value is provided.

3. Results and discussions

Particle number concentrations, carbon monoxide concentrations, and bulk aerosol chemical composition of the biomass burning events are described in Section 3.1. Multiple approaches are then explored in Section 3.2 in efforts to describe the emissions of INP from these plumes in relation to n_{CN} and n_{500nm}. Finally, Section 3.3 is focused on identifying chemical and physical properties of residual INP associated with biomass burning and how they change with burning conditions.

3.1 Overview of field study measurements

Identifying the presence of smoke emitted from fires using total particle and carbon monoxide concentrations is discussed in Section 3.1.1. Timelines of bulk aerosol chemical composition are also presented in Section 3.1.2. to provide an overall description of the biomass burning events and how they may differ from one another.

3.1.1. Total particle number and carbon monoxide concentrations as indicators for smoke

Timelines of n_{CN} measured during the Georgia prescribed burns and the Colorado wildfires are provided in Appendix B. Median n_{CN} were used as a measure for background conditions rather than average n_{CN} because sporadic excursions in n_{CN} often occurred during non-smoky periods from local non-biomass burning emissions (e.g., vehicles). Background number concentrations were determined on days with no apparent smoke influence or burns near the sampling location: March 09 for the Georgia prescribed burns and May 29 through June 03 for the Colorado wildfires. The median background n_{CN} during the Georgia prescribed burns and Colorado wildfires were 2370 and 4570 cm^{-3}, respectively.

During the burns on March 11, 14, and 15, n_{CN} were well above median background conditions during the whole sampling period, with highest n_{CN} observed on March 14 and 15. On some days, especially March 15, the n_{CN} were at or above the upper limit of the CPC (3.0 x 10^5 cm^{-3}). Measurements of the March 08 burn were made from a further distance and sampling took place during both low and high n_{CN}, shown in Figure B.1. Measurements from the Georgia prescribed burns covered a wide range of n_{CN}, due to the migration of the smoke plumes around the fixed sampling site, similar to the data collected during the Colorado prescribed burns presented by Prenni et al., (2012).

The Hewlett and High Park wildfires differed from both prescribed burns in that they burned continuously for many days and measurements were made from over 30 km from the burn area. For the Hewlett wildfire measurement period, May 16 and 17 had only a few periods of n_{CN} higher than background median concentrations, despite the activity of the nearby wildfire (Table 2.3). The amount of smoke that reached the sampling location was more dependent on wind direction during the wildfires compared to the prescribed burns because the larger distance between the fires and sampling site. Wind observations, also shown in Appendix B, provide evidence that there were many sampling periods during the wildfires without favorable wind conditions for smoke transport to the sampling location, consistent with sporadically high CN concentrations. However, the majority of measurements made on May 15, 18 and 21 had total particle number concentrations higher than the median background, as did each day of the High Park wildfire measurements. The sampling periods during these wildfires provide a large range of smoke conditions, from heavy smoke to none.

Total particle number concentrations observed during the Georgia prescribed burns exceeded those observed during the wildfires by an order of magnitude. Two important aerosol-related differences between the smoke measured during the wildfires and prescribed fires were

plume age and the effects of terrain. The distance between the wildfires and the measurement site was greater by a factor of 10 or more than the distance between the prescribed burns and sampling location, and thus emissions reaching the sampling site in the wildfire events were more aged than the prescribed burns. Transport of smoke permits dilution, coagulation, and gas-to-particle conversion mechanisms to change total particle concentrations.

For example, Hobbs et al. (2003) followed a smoke plume emitted from a savanna fire while measuring the number concentrations of accumulation-mode particles (0.1 μm $<d_p<$ 3 μm). During the first 10 minutes of aging, n_{CN} decreased by an order of magnitude. After accounting for dilution, they concluded coagulation and gas-to-particle conversions were additional effective mechanism for changing n_{CN}. Another potentially important mechanism for altering n_{CN} during transport is volatilization of organic aerosol species in smoke emissions, which has been demonstrated in the laboratory (e.g. Hennigan et al., 2011). The loss of aerosol mass may be large enough that some particles are completely evaporated, and n_{CN} decreases in the diluting plume. However, to our knowledge, this effect has not been conclusively demonstrated in the field.

Further, the wildfires were located at elevations above the sampling site and produced plumes that were often transported aloft with minimal mixing to the surface during the day. Mixing to the surface would not occur until the evening with the collapsing of the boundary layer. Smoke density at the surface would remain high until the deepening of the boundary layer, which diluted the smoke in the morning. This terrain effect has implications for changes in the smoke due to night time processing and uncertainties associated with the extent of dilution and plume processing that occurred between the emission and sampling points.

Although elevated n_{CN} are a good indicator of smoke near the emission point, such as the measurements made during the prescribed fires, the variability in plume age, transport, and

dilution, and therefore n_{CN}, during the wildfires suggests that there is uncertainty associated with assuming that smoke-free conditions are defined by low n_{CN} for measurements during the wildfires.

Carbon monoxide was monitored during most of the sampling periods of the Colorado wildfires and used as an indicator for the presence of smoke. CO measurements were not made during the Georgia prescribed burns or on May 15 and 16. Also, about an hour of data was not recorded on May 21 due to instrument malfunction. Timelines of CO concentrations are shown in Appendix B for each day of measurements. The mean background CO concentration was determined over the smoke-free period between the wildfires (May 29 to June 03) and was approximately 136 (±20) ppb. The measurements during the Hewlett wildfire had elevated CO concentrations up to 500 ppb and CO measurements at our sampling site during the High Park fire reached nearly 3000 ppb. The effect of dilution and plume processing is unknown in addition to uncertain burn conditions of the wildfires, all of which can alter CO concentrations. Thus, although CO was much higher during the High Park wildfire, high CO can only be interpreted as plume presence. CO is not impacted by plume processing mechanisms, such as coagulation or volatilization, and therefore serves as a better indicator of plume presence in comparison to n_{CN}. For sampling days with CO measurements available, periods with CO concentrations greater than 2 standard deviations above the mean (176 ppb) were considered to be in-plume measurements and hereafter referred to as "smoke-impacted" (versus "non-impacted") samples.

Since CO data were not available for May 15 and 16 during the Hewlett wildfire period, identifying smoke-impacted periods was not as trivial. n_{CN} observed during smoke-impacted samples, those with > 176 ppb CO, were examined in efforts to determine a threshold n_{CN} for smoke-impacted periods. A clear distinction was not found between n_{CN} values during measurements made in smoke-impacted and non-impacted periods. For example, CO

concentrations were well above 176 ppb on May 18, especially in the morning, and did not exceed 180 ppb during measurements made on May 12. Yet, total particle concentrations were similar on both days. This ambiguity is further depicted by the relationship between CO and n_{CN}, shown in Figure 3.1, where high n_{CN} are associated with both smoke-impacted and non-impacted periods. Consequently, an explicit filtering of smoke-impacted sampling was not possible using n_{CN} for periods without CO measurements during the Hewlett wildfire.

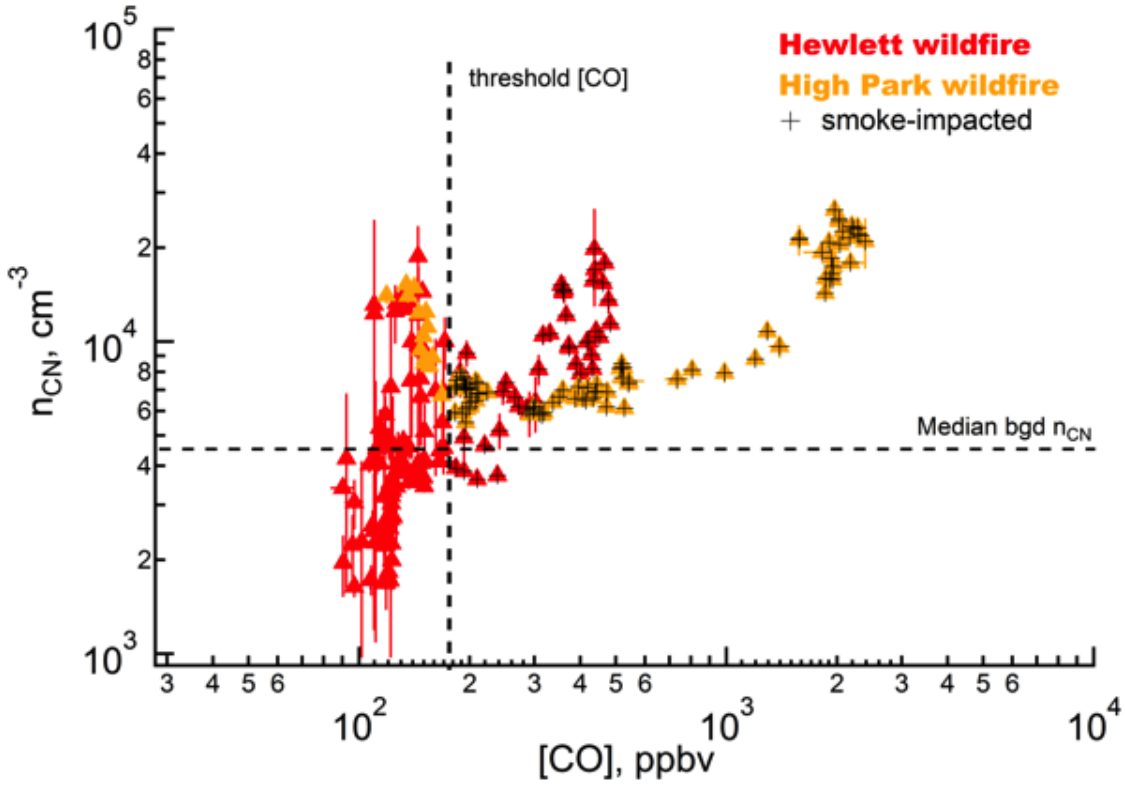

Figure 3.1. Relationship between n_{CN} and CO during the Hewlett (red) and High Park (orange) wildfires. Background concentrations are shown by the dashed lines. Error bars show 1 standard deviation of the average n_{CN} and [CO]. Black crosses indicate smoke-impacted (CO > 176 ppb) samples.

Wind speed and direction were monitored at the Christman field site, located near the CSU foothills campus, and provided some additional insight on whether smoke was being transported to the sampling location. During the measurement periods on May 15 and 16, winds were from the S and SE, whereas the Hewlett wildfire was located WNW from the sampling site,

suggesting little transport of the smoke from the fire directly on these days. Additionally, photos taken at the CSU Foothills Campus throughout these days indicate the plume was not transported to the sample location during the measurement periods on May 15 and 16. Therefore, data collected on May 15 and May 16 during the Hewlett wildfire period appear to have not been directly influenced by smoke and are non-impacted samples.

For the following analyses performed on these data, the wildfires are examined as "smoke-impacted" and "non-impacted" samples, as defined by CO concentrations and wind direction. This is to determine the influence of smoke on various aerosol properties because n_{CN} provides little indication of smoke presence when measured at such a far distance. However, n_{CN} was directly related to the amount of smoke in the sampling area when measurements were made near the fire, such that relatively high n_{CN} was indicative of smoke presence. Therefore, all data collected during the prescribed and laboratory fires are evaluated as burning days, providing a dynamic range of smoke concentrations, similar to analyses performed by Prenni et al., (2012)

3.1.2. Bulk aerosol chemical composition

Timelines of total carbon (TC) aerosol mass concentrations during each biomass burning event are shown in Figure 3.2. These data give an indication of how the aerosol emissions measured during each biomass burning event differed from each other. TC mass concentrations were variable from day to day, especially during the Georgia prescribed burns, which had concentrations ranging from 20 to 750 $\mu g/m^3$. The filter collected during the background period (collected from March 09-March 11, hereafter referred to as March 09), had a low TC mass concentration (1.48 $\mu g/m^3$) compared to the other days, supporting classification of March 09 as

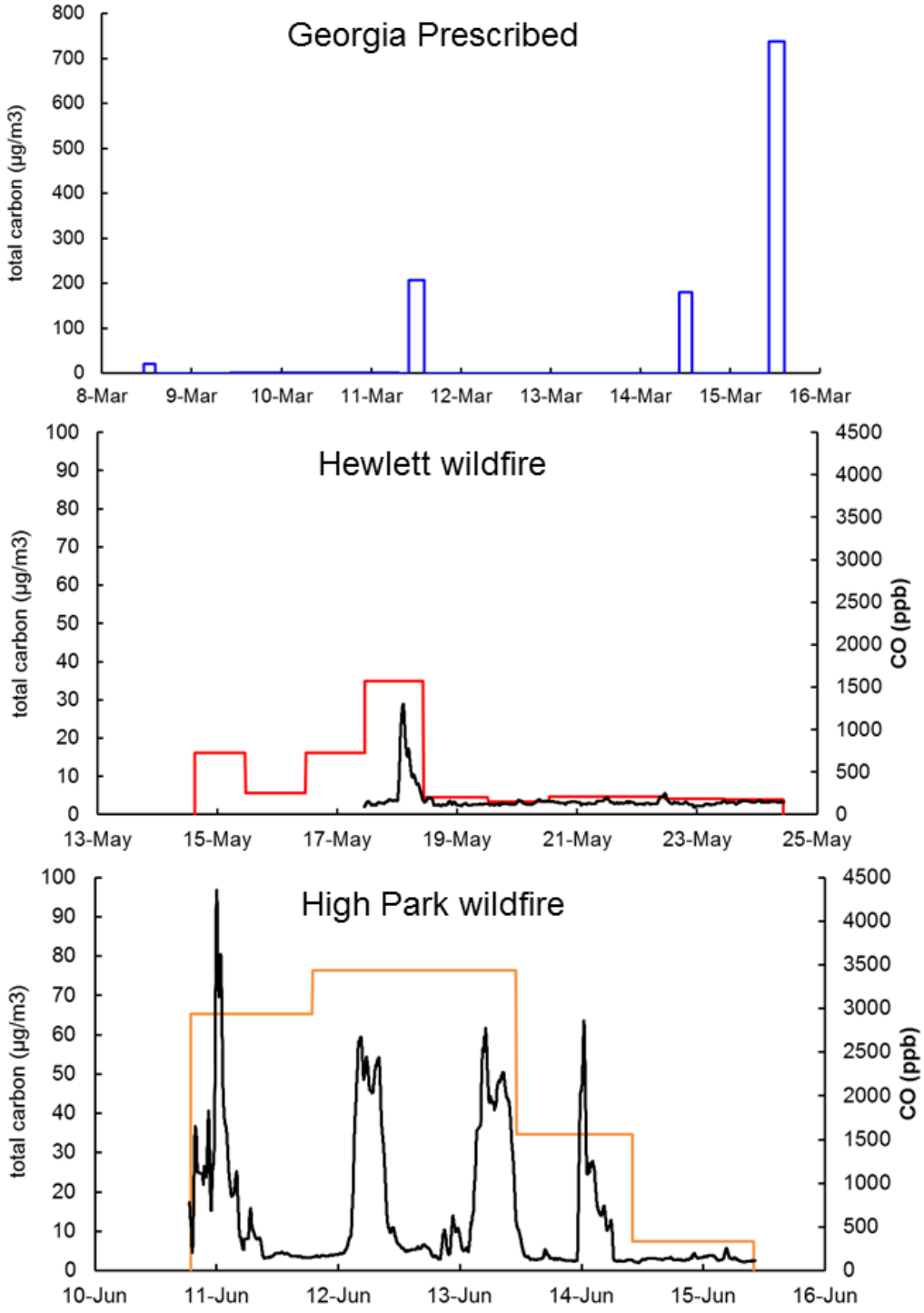

Figure 3.2. Mass concentration of total carbon collected onto HiVol filters during the Georgia prescribed burns (top), Hewlett wildfire (middle), and High Park wildfire (bottom). Timelines of carbon monoxide (CO) during both wildfires are also presented (black). Note that the scales differ between plots.

a "background" sample. The highest concentrations of TC were observed on March 15 of the Georgia prescribed burns, corresponding with the highest sustained n_{CN} as mentioned in Section 3.1.1. TC concentrations during the Georgia prescribed burns surpassed those of the wildfires (note scale change), consistent with the higher n_{CN} observed with the Georgia prescribed fires, likely due to the proximity of the measurements to the burns. Higher concentrations of TC were observed during the High Park fire than the Hewlett fire.

Levoglucosan is often used as a biomass burning aerosol-phase chemical tracer [Simoneit et al., 1999] and was therefore assessed in each filter sample. Levoglucosan concentrations were normalized by TC mass concentration, shown in Figure 3.3. During the Georgia prescribed fires, the Lev:TC ratios were generally the same with the exception of the lower Lev:TC ratio measured in the background sample (March 09). Furthermore, elevated Lev:TC ratios in filter samples collected during the wildfires were observed on days with elevated CO concentrations and the ratios were similar for both Hewlett and High Park wildfires. These Lev:TC ratios appear to track the TC mass concentrations and suggest that the associated detected carbon originated from biomass burning sources.

Potassium (K) has also been commonly used as an aerosol-phase chemical tracer for flaming phase combustion (Andreae et al., 1983). Although the HiVol filters represent bulk aerosol chemical composition associated with fires that are likely changing combustion phase on short time scales, K:TC ratios may provide an indication of the averaged combustion phase of each measurement day. Here, K^+ from ionic species quantification is used to form the K:TC ratio. The K:TC ratios, shown in Figure 3.4, did not vary greatly between burn days or between fire events, typically ranging from 0.010 to 0.025. K:TC was highest on March 9th of the Georgia prescribed burns, but this high ratio was likely skewed by the low TC mass concentrations on that day. During the Hewlett wildfire, a peak in the K:TC ratio occurred on

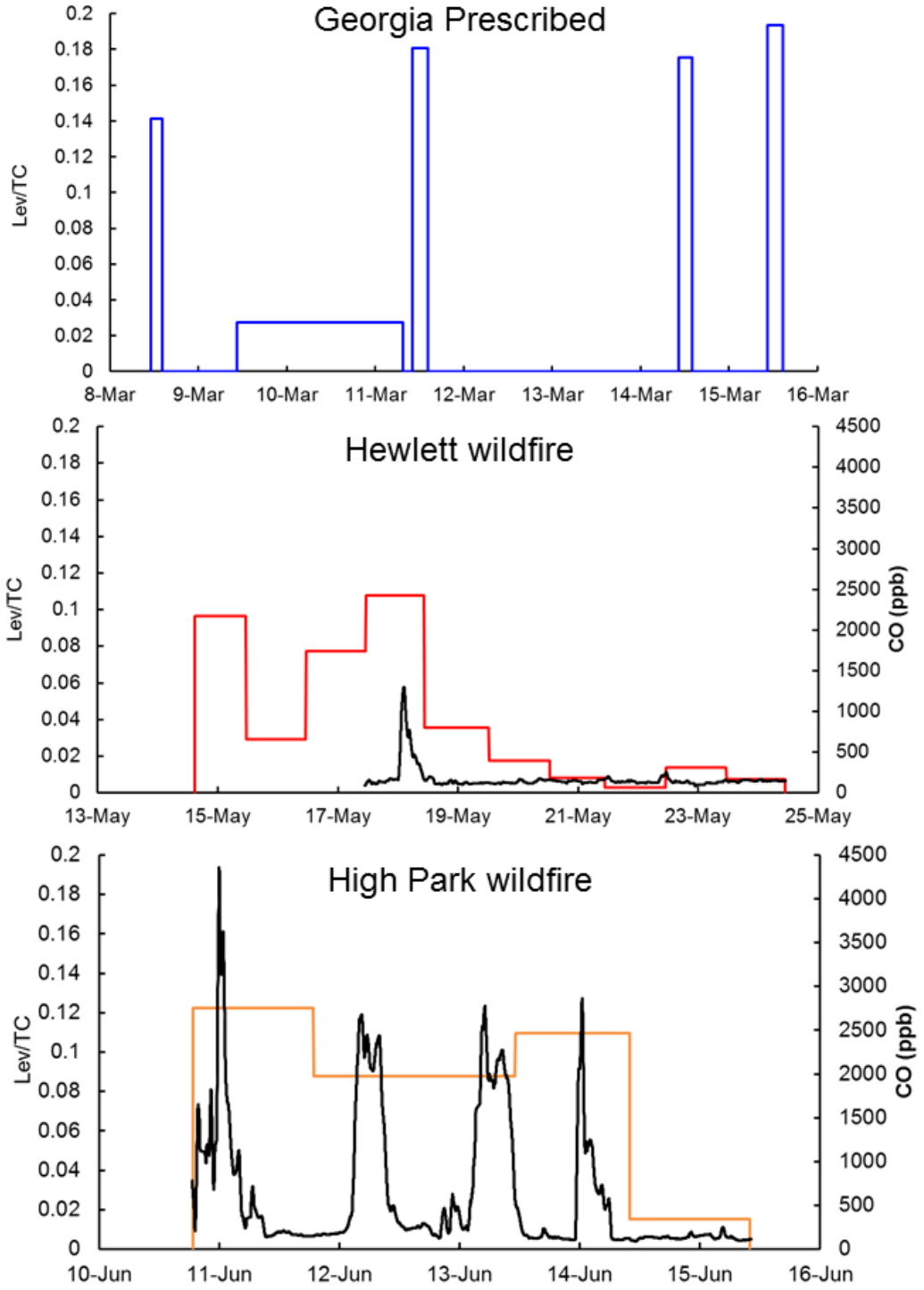

Figure 3.3. Timelines of the bulk levoglucosan to TC (Lev/TC) ratios for the Georgia prescribed burns (top), Hewlett wildfire (middle) and High Park wildfire (bottom). Measurements of carbon monoxide (CO) are also presented for the wildfires (black). Note that the scales differ between plots.

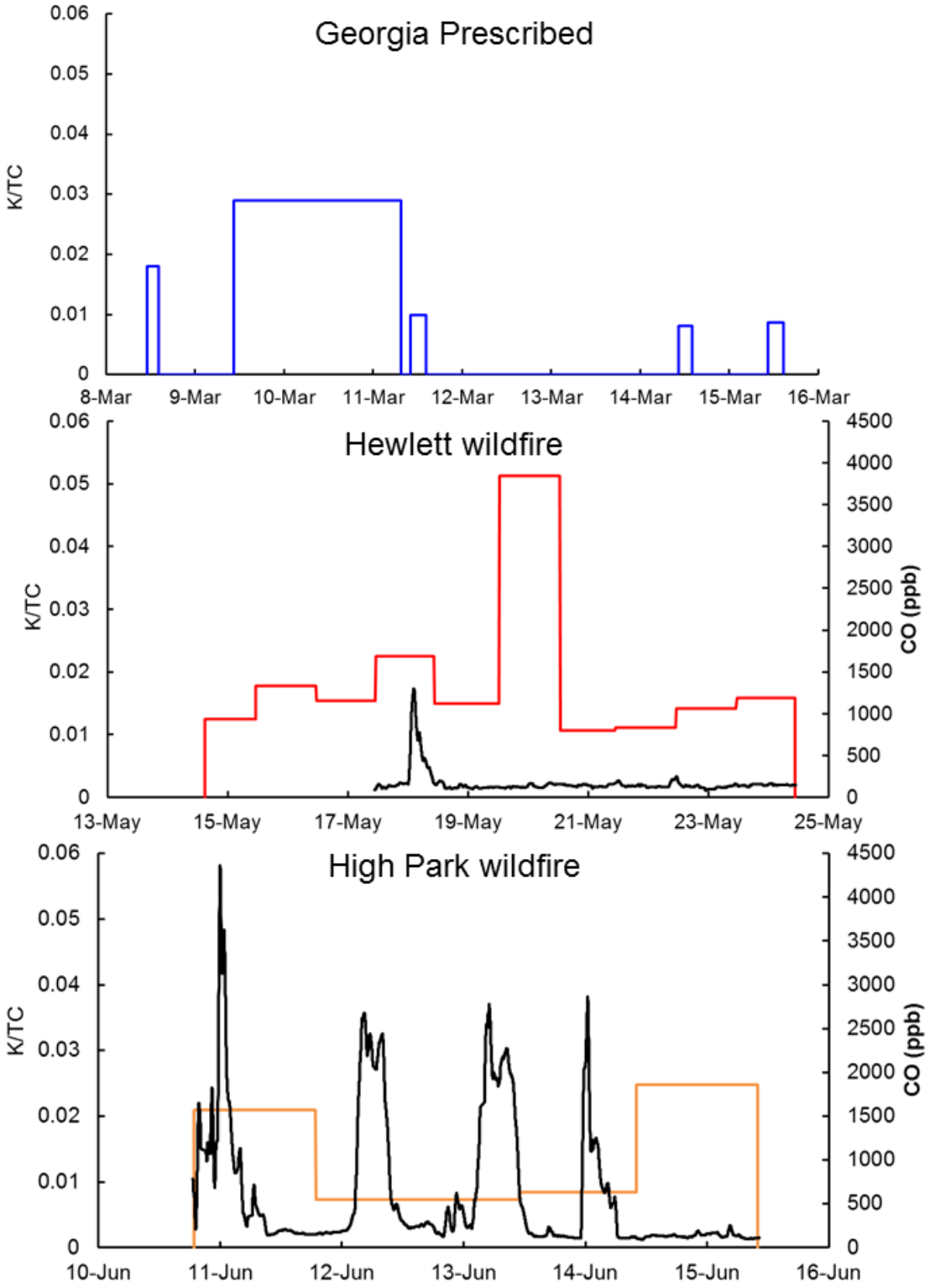

Figure 3.4. Timelines of the bulk potassium to TC ratios (K/TC) for the Georgia prescribed burns (top), Hewlett wildfire (middle) and High Park wildfire (bottom). Measurements of carbon monoxide (CO) are also presented for the wildfires (black).

May 20 and was not associated with a corresponding increase in CO or Lev:TC; the origin of this peak has yet to be determined. Overall, these data were unable to detect variability in combustion phase between measurement days.

Finally, the presence of dust or soils was of interest due to their potential effect on INP. Dust and/or soils may have originated from long-range transport and could have also been lofted in winds generated by the fires, as suggested by Clements et al., (2008). As a potential indicator of the presence of dust/soils, the ratios of water soluble calcium (Ca^{+2}) to TC for the Georgia prescribed and Colorado wildfires were determined, shown in Figure 3.5. Ca:TC ratios observed during the Georgia prescribed burns were much lower than those in the wildfires, suggesting soils and/or dust represented higher mass fractions of the aerosol during the wildfire measurements. Some of the elevated Ca:TC ratios occurred during periods of elevated CO, but there were also elevated Ca:TC ratios during lower CO concentrations. These data indicate the measurements made during the wildfires were potentially influenced by dust and soil emissions. More discussion on the possible impact of long-range transport of mineral dust and emissions of soils and dusts from the fires is given in Section 3.2.5.

3.2. Describing INP associated with biomass burning

Relationships between smoke markers (n_{CN} and CO) and INP are described in Section 3.2.1. Different approaches are used to compare INP emitted from these biomass burning events, including n_{INP} relation to n_{CN} (Section 3.2.2), and n_{INP} relation to n_{500nm} (Section 3.2.3). Finally, the possible influence of additional non-carbonaceous coarse aerosol on n_{INP} is investigated in Section 3.2.4.

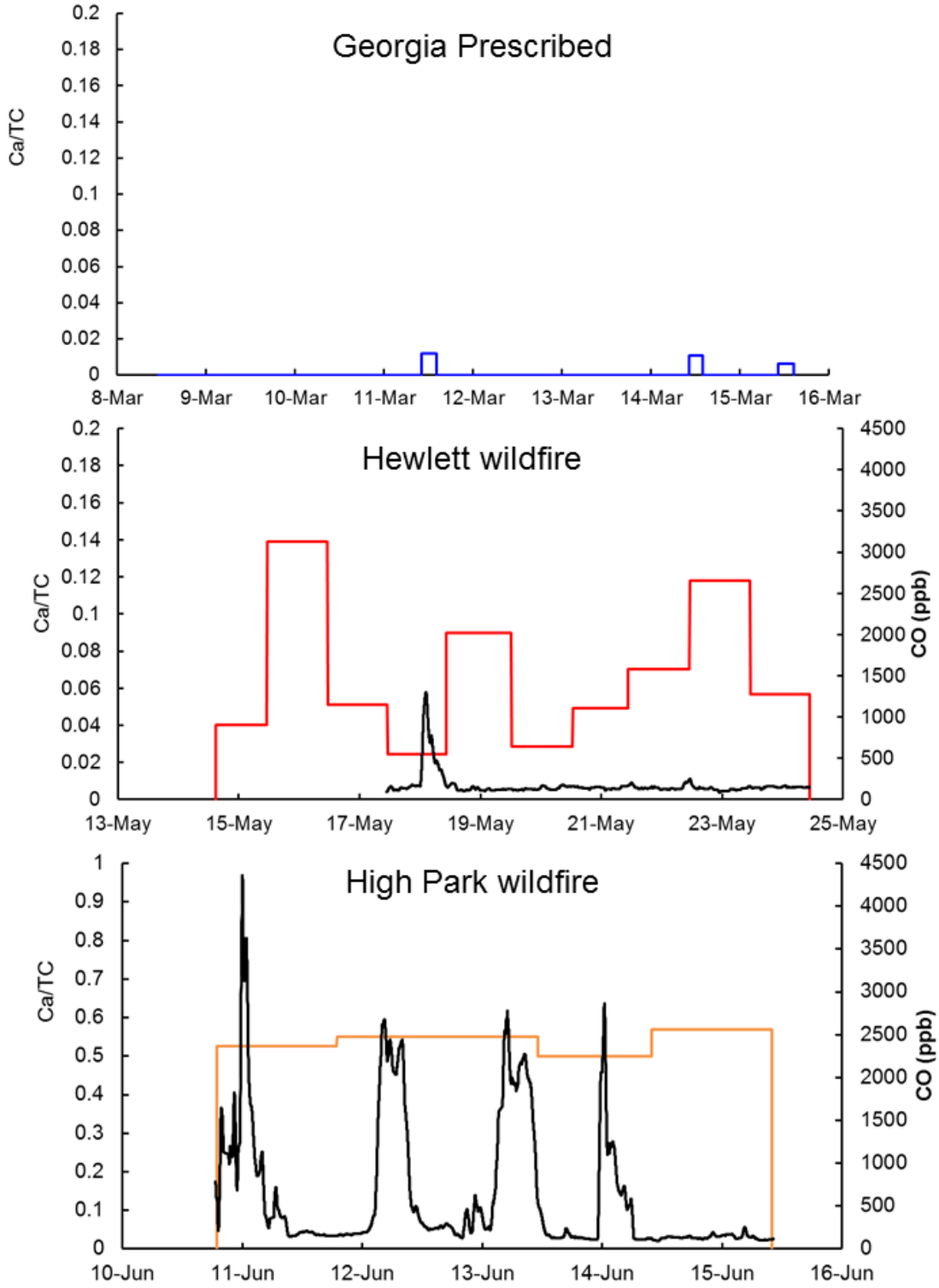

Figure 3.5. Timelines of the bulk calcium to TC (Ca/TC) ratios for the Georgia prescribed burns (top), Hewlett wildfire (middle) and High Park wildfire (bottom). Measurements of carbon monoxide (CO) are also presented for the wildfires (black). Note that the scales differ between plots.

3.2.1. Relation of INP with smoke markers

The relationship between n_{INP} and CO measured at -30°C is shown in Figure 3.6 for the smoke-impacted and non-impacted Colorado wildfire samples. n_{INP} were above the upper end of literature ambient background concentrations ($10L^{-1}$, DeMott et al., 2010) for all data collected at -30°C during the wildfires, including non-impacted periods. A power law regression, revealed a statistically significant relationship ($m=0.389$, $p<0.001$) between n_{INP} and CO. However, n_{INP} excursions of an order of magnitude were observed for Hewlett fire samples during periods of CO concentrations lower than the smoke-impacted threshold concentration. The elevated concentrations of INP during non-impacted periods are indicative of the presence of INP that originated from non-biomass-burning sources.

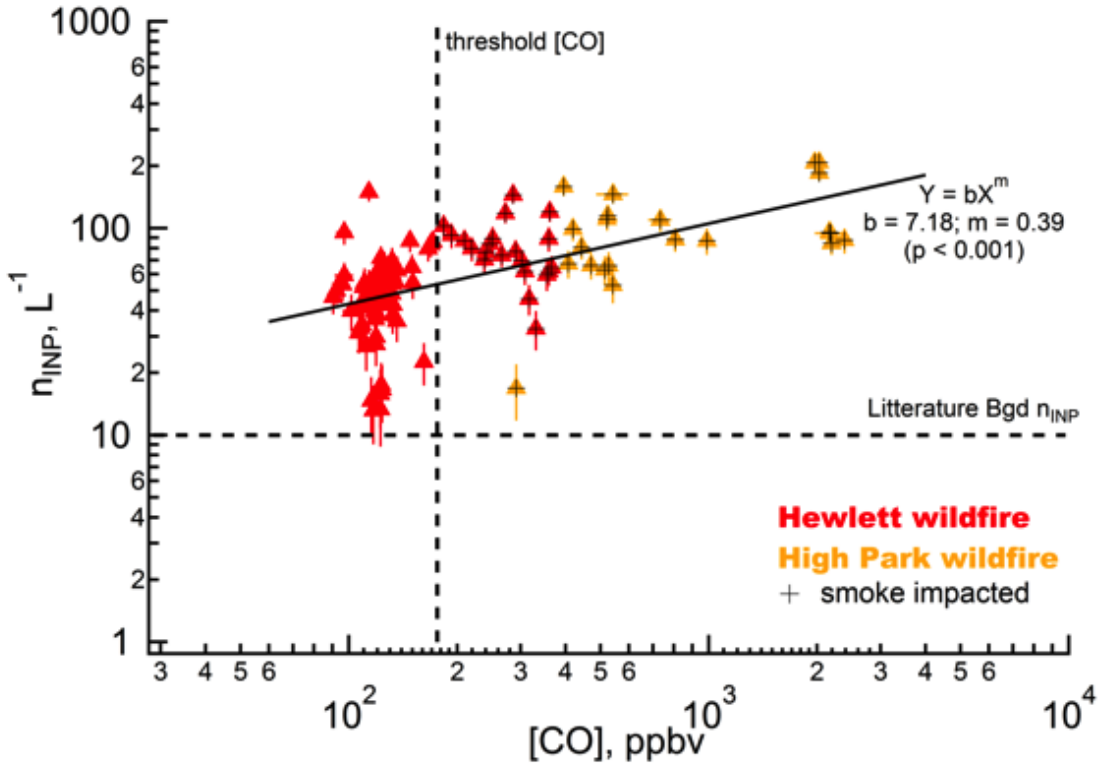

Figure 3.6. Relationship between CO and n_{INP} measured at -30 °C for the Hewlett (red) and High Park (orange) wildfire periods. Background concentrations are outlined by dashed lines and error bars show the Poisson counting error and standard deviation for n_{INP} and [CO], respectively. Black crosses indicated smoke-impacted samples.

Based on the discussion in Section 3.1.1, n_{CN} serves as a valid tracer for smoke measured near the source, such as the measurements made during the prescribed and laboratory burns. A positive statistically significant ($p < 0.001$) power law relationship between n_{INP} and n_{CN} was observed during the Georgia prescribed ($m = 0.43$; $b = 0.10$) and Colorado prescribed burns ($m = 0.44$; $b = 0.13$; $p<0.001$), shown in Figure 3.7. The likeness in the slope and intercept of these fits suggests the aerosol emitted from both prescribed burns contributed to the INP population and in a similar manner. Measurements made during laboratory burns of wiregrass and ponderosa pine are also presented and closely fall within the n_{INP} to n_{CN} relationship observed during the prescribed fires.

The n_{INP} to n_{CN} relationship for the smoke-impacted wildfire measurements had a smaller slope ($m = 0.18$), higher y-intercept ($b = 17$) and higher p-value ($p < 0.1$) compared to the prescribed burns. The weaker correlation (higher p-value) is most likely due to the narrow dynamic range of the n_{CN} observed during the wildfires, due to the plume being subject to transport impacts on total particle counts, as discussed in Section 3.1.1. The slope of the n_{INP} to n_{CN} relationship of the smoke-impacted wildfires data suggests that the production of INP from the wildfires was different compared to the prescribed fires and the higher intercept suggest there was a greater concentration of INP for a given concentration of CN, even during periods with little smoke presence. This is the first indication that the INP emitted from the wildfires was much different than the prescribed fires.

The difference in the INP to CN relationship between the wildfires and prescribed fires is likely due to the transport distance of the smoke between the wildfires and the sampling location. Based on observations reported by Hobbs et al., 2003, CN is expected to decrease due to dilution and coagulation. Dilution would change n_{INP} at the same rate as n_{CN}, such that dilution would not alter the INP to CN relationship. However, assuming the activity of INP endures after

collisions and collection of small particles and that the probability of two INP colliding to form one INP is extremely low, n_{INP} is likely unchanged due to coagulation. The INP to CN relationship was likely altered due to coagulation during transport and was therefore evidently differently between the wildfires and prescribed fires. In any case, it is not possible from these data alone to quantify the impact of plume transport on the relationship between n_{INP} and n_{CN}, and this important relationship remains to be explained in future studies.

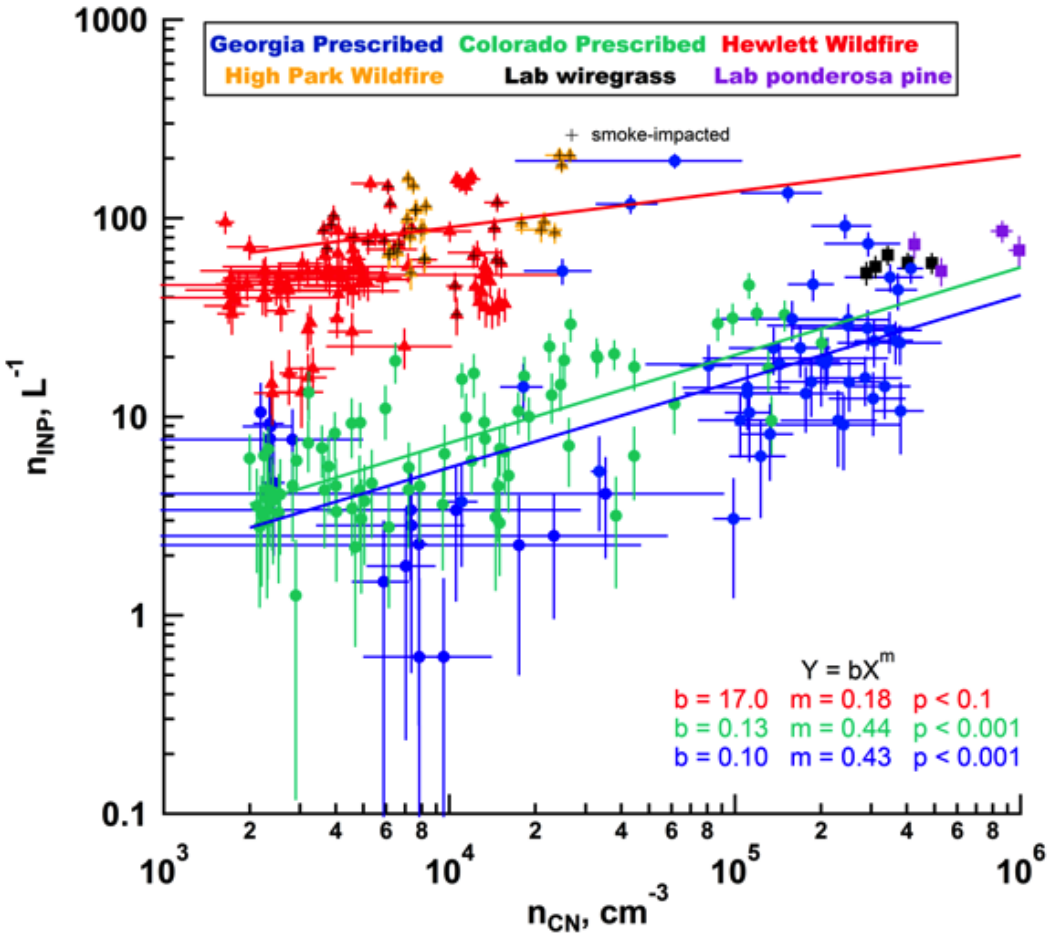

Figure 3.7. n_{CN} versus n_{INP} measured at -30°C during the Georgia (blue) and Colorado (green) prescribed fires, FLAME IV wiregrass (black) and ponderosa pine (purple) room burns, and the Hewlett (red) and High Park (orange) wildfires. Values are averaged over sampling periods (3-5 minutes). Smoke-impacted samples during the wildfire periods are indicated by black crosses. Solid lines indicate power law regression fits of the smoke-impacted wildfire, Colorado and Georgia (blue) prescribed burn points, with the parameters summarized in text in the lower right corner of the figure.

3.2.2. INP efficiency

INP efficiency, ξ_{-30}, has been used to quantify the INP fraction at -30°C and is defined according to Petters et al., 2009, by Eq. 3.1. Less negative ξ_{-30} indicates higher INP fraction.

$$\xi_{-30} = \log_{10} m\,; \quad m = \frac{n_{INP}\ (cm^{-3})}{n_{CN}(cm^{-3})} \qquad \text{Eq 3. 1}$$

Normalized distributions of ξ_{-30} for the Georgia and Colorado prescribed burns, smoke-impacted samples from the Colorado wildfires, and laboratory wiregrass and ponderosa pine burns are shown in Figure 3.8. INP efficiencies ranged from -7.5 to -4.5 and highest observed INP efficiencies were during the Colorado wildfires. Samples from the Colorado prescribed burns had higher INP efficiencies than those from the Georgia prescribed burns.

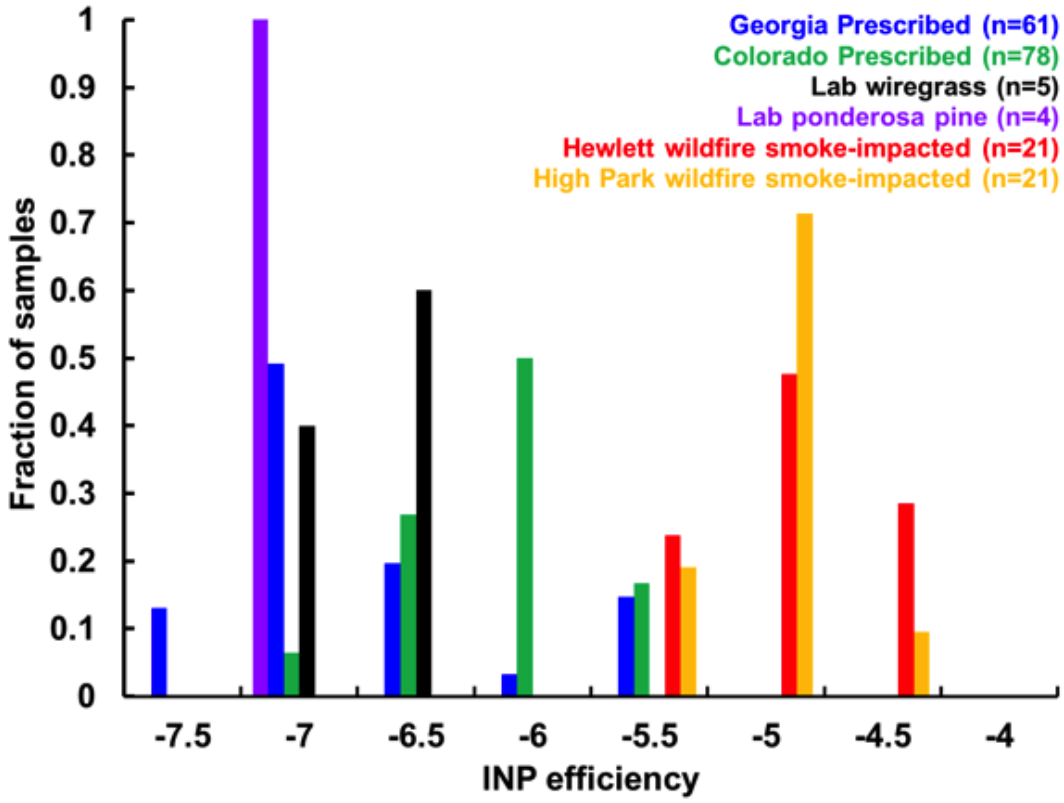

Figure 3.8. Normalized distribution of ξ_{-30} for each biomass burning event. Wildfire periods only include smoke-impacted samples. Number of samples for each event is indicated in parentheses.

INP efficiencies from the Georgia prescribed fires and laboratory wiregrass burn were within the range reported for burns of similar fuels from the FLAME II study by Petters et al. (2009). In that study, two of three longleaf pine/wiregrass FLAME II burns were below detection limit ($\xi_{-30} < -4.6$) and one was approximately -4.3, as shown in Figure 3.9. Ponderosa pine dominated fires, namely the Colorado prescribed, laboratory ponderosa pine burn, and wildfires, had a large spread of ξ_{-30} ranging from -7 to -4.4. During FLAME II, 5/16 ponderosa pine burns had ξ_{-30} above the experimental detection limit and ranged from approximately -4.2 to -3.3. All of the lab and field observations of ξ_{-30} presented here are within range of the FLAME II results, but this range remains very large even for a single fuel.

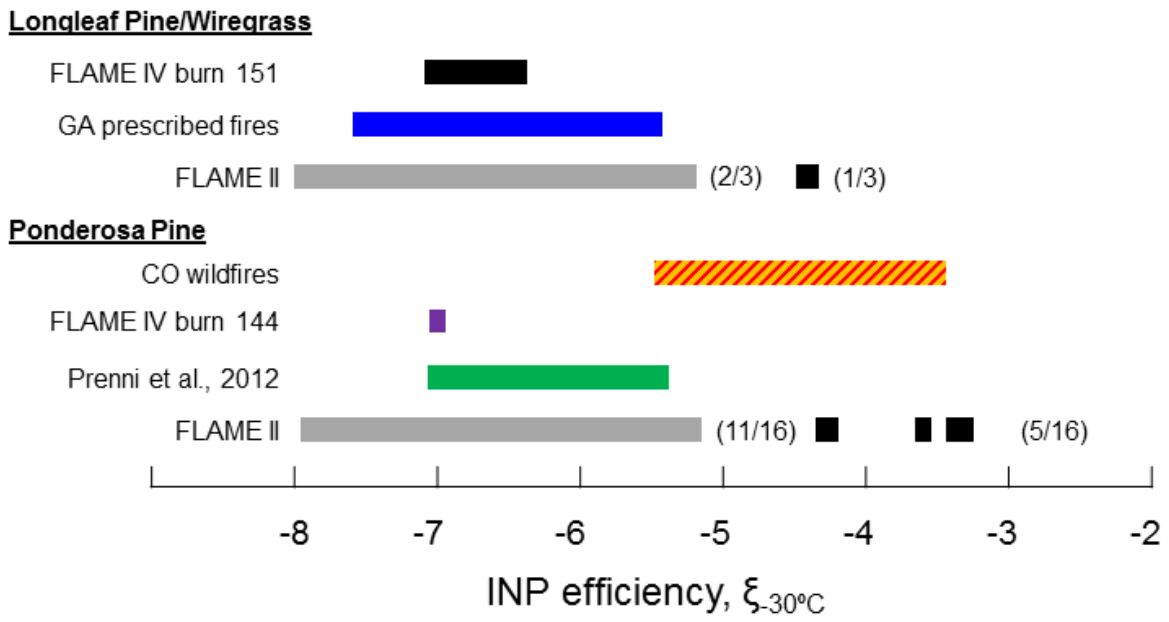

Figure 3.9. IN efficiencies from the Colorado wildfires, Georgia and Colorado prescribed fires, FLAME IV room burn and the FLAME II studies. Grey bars indicate the range of the FLAME II experimental limit of detection.

Since calculated ξ_{-30} is dependent on n_{CN}, it is important to consider the impact of variations in n_{CN} due to transport, as discussed in preceding sections. Figure 3.10 shows ξ_{-30} as a

function of n_{CN} for each biomass burning event, demonstrating that samples with highest ξ_{-30} were associated with lower values of n_{CN}. For the wildfires, this relationship reveals that for a given n_{CN}, the fraction of particles detected as INP was greater for nearly all smoke-impacted samples.

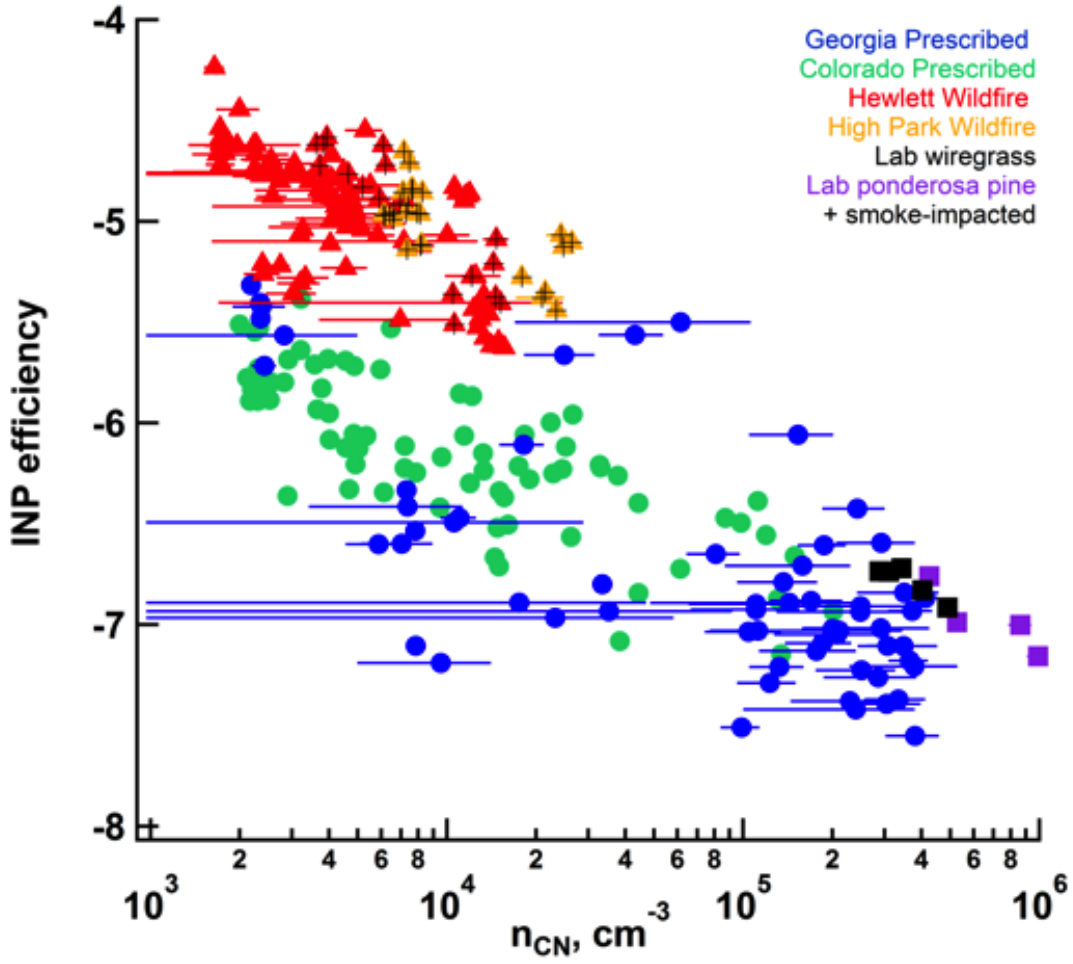

Figure 3.10. Relationship between IN efficiency and number concentration of condensation nuclei n_{CN} for all biomass burning events. Error bars indicate one standard deviation of the average n_{CN} and black crosses indicate smoke-impacted samples.

The number of INP per number of total particles emitted from wildfires may, in fact, have been greater than that of prescribed fires at the point of emission. However, the applicability of ξ_{-30} for comparing INP emitted from different fire types, particularly with

contrasting plume histories, is hindered by its strong dependence on n_{CN}. Therefore, the usefulness of ξ_{-30} appears to be limited to comparisons of INP detected at the near emission stage, something that is difficult to achieve in wildfire situations. Because n_{CN} is so strongly influenced by plume processing, INP are poorly described by n_{CN}, directing focus towards particles with less dramatic changes associated with transport as more appropriate descriptors of INP emitted from biomass burning.

3.2.3. Relation of INP to larger particles in biomass burning

Relating n_{INP} emitted from biomass burning to particles with diameters greater than 500nm is useful because these particles are less vulnerable to plume aging processes compared to condensation nuclei and because this relationship has been explored in previous studies. Specifically, an INP parameterization was developed by DeMott et al., 2010, which describes the temperature dependent relationship between n_{500nm} and n_{INP} using a multi-study aerosol database (Eq 3.2).

$$n_{INP} = a(273.16 - T_K)^b (n_{500nm})^{(c(273.16-T_K)+d)} \quad \text{Eq. 3.2}$$

where a = 0.0000594, b = 3.33, c = 0.0264, and d = 0.0033. The 500nm cutoff is motivated by observations that revealed the mode diameter of collected residual INP was 500nm, as reported by Richardson et al. (2007). Since this parameterization is useful for describing the "global", or well-mixed, INP populations without consideration of source, it is useful to compare these predicted INP number concentrations to observed n_{INP} associated with biomass burning sources.

Predicted n_{INP} using the D10 parameterization for the biomass burning plumes evaluated in this study are shown in Figure 3.11. D10 over-predicts by a factor of 2 or more for 68% and 46% of the Georgia prescribed and Colorado prescribed burning events, respectively. The majority (92%) of the laboratory measurements are also over-predicted by D10. The wildfires

are mostly under-predicted by D10, with 75% and 56% of the smoke-impacted Hewlett and High Park wildfire periods underestimated by more than a factor of 2. The wildfire measurements during non-impacted periods were also under-predicted by D10; 98% and 100% of non-impacted Hewlett and High Park wildfire measurements were underestimated by more than a factor of 2.

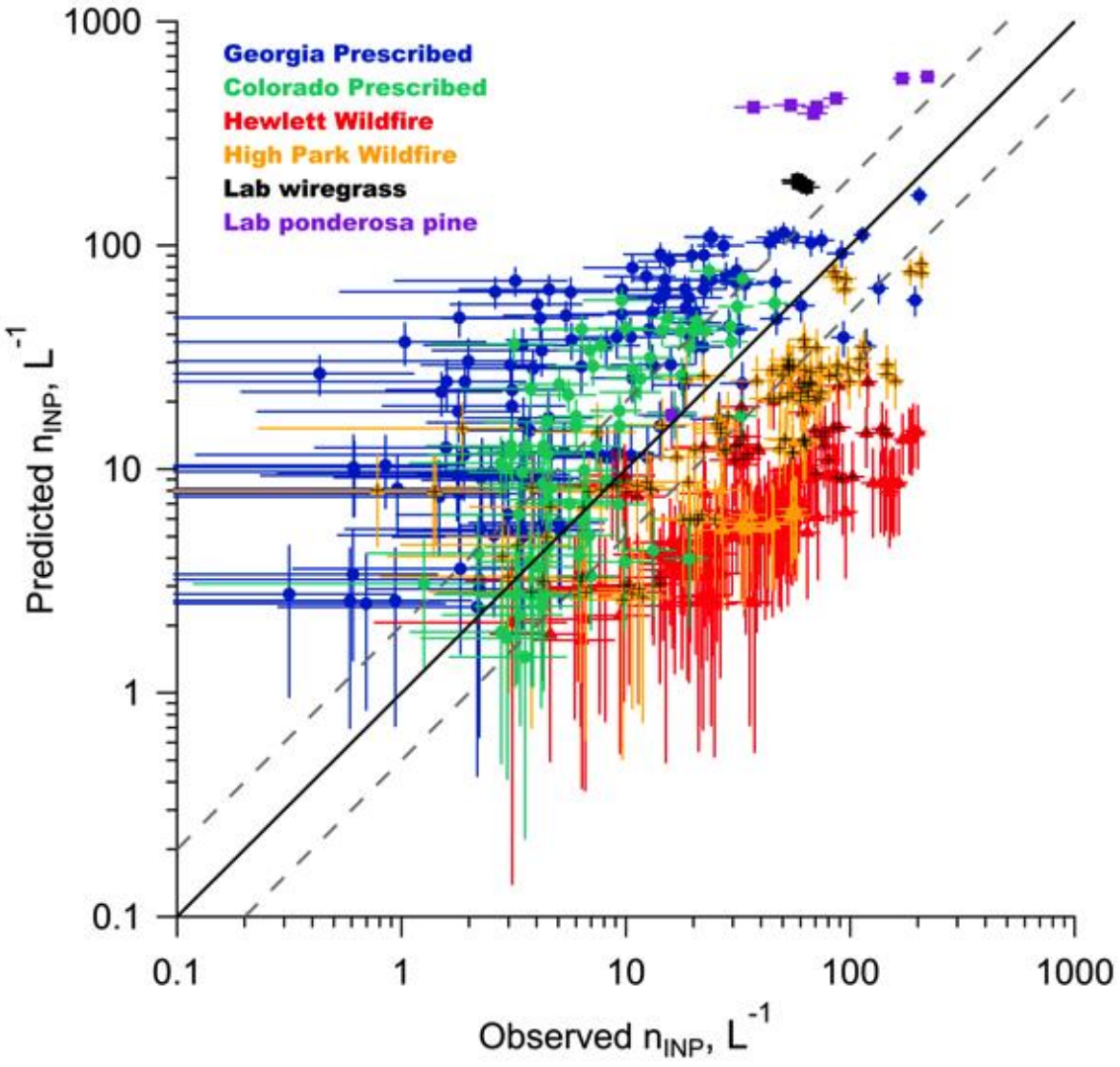

Figure 3.11. Correlation between observed and predicted n_{INP} for the Georgia prescribed (blue), Colorado prescribed (green), Hewlett wildfire (red), High Park Wildfire (orange), and the FLAME IV wiregrass room burn (black). Solid line is the 1:1 line with a factor of 2 outlined with dashed lines. Black crosses indicate smoke-impacted periods.

This dissimilarity in the bias of D10 between the prescribed/laboratory burns and wildfires is mirrored by the different n_{INP} to n_{500nm} relationships for measurements made at -30°C, shown in Figure 3.12. A power law regression on the prescribed fires (Colorado and Georgia) showed a statistically significant relationship between n_{INP} and n_{500nm} ($m=0.32$; $p<0.001$). The n_{INP} to n_{500nm} relationship was also statistically significant on a 99% confidence level for the smoke-impacted periods of the wildfires ($m=0.15$; $p<0.01$). The difference in the y-intercept between the smoke-impacted wildfires ($b=57.5$) and prescribed burns ($b=4.57$) measurements demonstrate that the wildfire periods had up to an order of magnitude more INP for a given n_{500} than the prescribed/laboratory fires. The power law regression was also calculated for the non-impacted wildfire periods, revealing a statistically significant relationship between n_{INP} and n_{500nm} ($m=0.774$, $b=42.15$, $p<0.001$). The high y-intercept is similar to the smoke-impacted periods, but the steeper slope suggests the non-impacted samples were of a different aerosol type. Dissimilarities in fuel type, combustion efficiency, transport time, and the potential influence of mineral dust are all possible explanations for these differences between biomass burning events.

Laboratory results from Petters et al., (2009) indicate that the combustion of some fuel types were associated with higher INP emissions than others (e.g., INP efficiencies of smoke emitted from the combustion of sawgrass were consistently higher than those for smoke emitted from black spruce combustion). However, Figure 3.12 shows that the relationship between n_{500nm} and n_{INP} was similar for both prescribed burns, which were of different fuel types. The similarity in INP production is also evident in the calculated INP efficiencies (Figure 3.8). The wildfires were of the same fuel type as the Colorado prescribed burns (ponderosa pine) and yet had different n_{500nm} to n_{INP} relationships. Although the fuel type may not be an important parameter for INP variability based on these data, dissimilarities in the section of fuel being

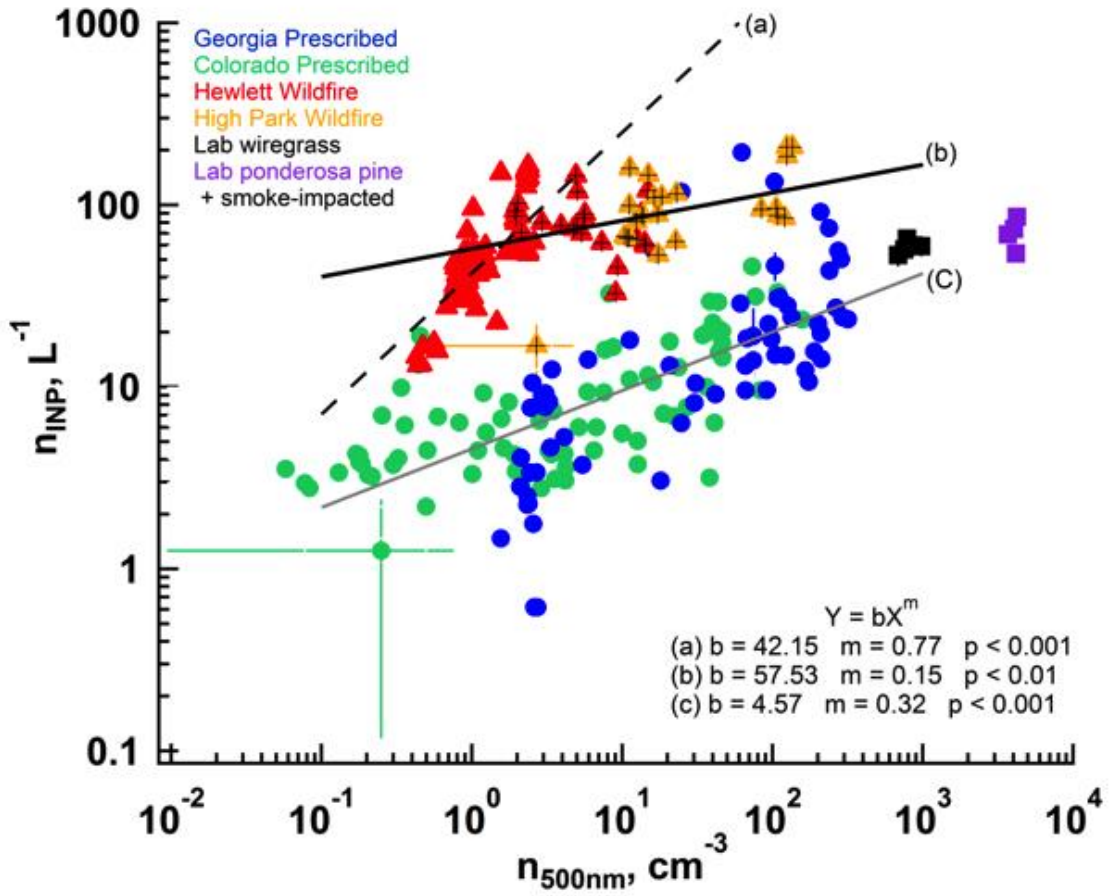

Figure 3.12. Relationship between n_{500nm} and n_{INP}, measured at -30°C for the Georgia prescribed (blue), Colorado prescribed (green), Hewlett wildfire (red), High Park wildfire (yellow) and lab burns of wiregrass (black) and ponderosa pine (purple). Black crosses indicate smoke-impacted samples. Power law fit lines are shown for the prescribed burns (grey line), smoke-impacted wildfire samples (black line) and non-impacted wildfire samples (dashed line).

burned may also be important to consider; prescribed fires typically burn understory shrubs, grasses, litter and smaller dead branches, whereas wildfires burn shrubs and large amounts of timber. These data suggest that burning timber may produce aerosol that contains particles more likely to serve as INP. However, this remains to be explored through future studies.

The studies by Petters et al., (2009) also provide evidence for a statistically significant positive correlation between the abundance of INP and the modified combustion efficiency (MCE), suggesting that flaming fires are associated with higher emissions of INP. However, the

relationship between n_{INP} and n_{500nm} was similar for measurements during the FLAME IV wiregrass room burn, which was flaming-dominated (MCE=0.97), and during the Georgia prescribed fires, which were a mixture of smoldering and flaming phases according to ground observations. The same is true for burns of ponderosa pine, where the MCE in the ponderosa pine room burn was 0.93 and the Colorado prescribed burn was a mixture of flaming and smoldering. These data do not provide conclusive evidence for MCE as the driving factor for the difference in n_{INP} emitted from these biomass burning events. However, the range of MCE measured here was limited and did not include a smoldering-dominated fire.

Another difference between the measurements made during the wildfires versus the prescribed/laboratory fires was transport distance. The prescribed and laboratory fires were measured within 3 km from the fire source, whereas the wildfires traveled at minimum 30 km before reaching the sampling location, and the wildfire plumes were subjected to additional overnight aging in the collapsed boundary layer. Transport has implications on smoke aerosol due to coagulation, dilution, and chemical processing, all of which could alter the relationship depicted in Figure 3.12.

Hobbs et al. (2003) evaluated transformations in aerosol distributions ($0.5\mu m < d_p < 3\mu m$) before and after plume aging. Coagulation acted to decrease number concentrations of smaller sized particles ($d_p < 1.5\ \mu m$) and increase number concentrations of particles with diameters greater than 1.5 μm. However, the integrated distribution of particles with diameters greater than 0.5 μm did not change significantly. If coagulation did act to increase n_{500nm}, the relationship depicted in Figure 3.12 would have shifted up the n_{500nm} axis for the smoke-impacted wildfire samples, opposite of what was observed. In essence, coagulation alone does not explain an order of magnitude shift in the n_{INP} to n_{500nm} relationship. Dilution is also expected to have occurred during plume transport, but likely influenced both n_{INP} and n_{500nm} in a similar manner with little

effect on their relation to each other. Finally, chemical processing and coagulation during the aging process could act to coat the active sites on the INP and essentially inhibit their ice nucleating ability, as suggested by Georgii et al., 1963. However, this hypothesis has never been validated in the field, and this process would act to decrease observed INP activity in the wildfire plumes and n_{INP} would be more over-predicted by D10. The impact of transport on smoke emissions does not appear to be responsible for the order of magnitude enhancement of INP concentrations observed from the Colorado wildfires.

Some unique characteristics of wildfires may have implications on the abundance of INP. Wildfires are often associated with vigorous winds and convection at the surface, which can loft soils and plant materials, as demonstrated by measurements of grass fires by Clements et al., (2008). A recent study by Chalbot et al. (2013) reports that soils lofted by a prescribed burn contributed up to 27% of the PM_{10} water soluble organic carbon detected in the smoke. In fact, it is hypothesized that the lofting of soils would be enhanced during wildfires compared to prescribed burns, because wildfires are often associated with stronger winds and arid land conditions (Chalbot et al., 2013). These soil particles potentially emitted from the wildfires are expected to be highly IN active if they are dusts or biological materials, based on measurements of INP associated with these particle types [e.g., DeMott et al., 2003 and Prenni et al., 2013]; their presence may greatly enhance INP concentrations during wildfire studies.

The Colorado wildfires were also located in a region often influenced by long-range transport of Asian mineral dust. Asian mineral dust is highly, and predictably, active as INP [Richardson et al., 2007, Archuleta et al., 2005]. Since the presence of dust is expected to enhance concentrations of INP per number concentration of particles greater than 500nm, D10 would under-predict n_{INP} for wildfires and during the presence of desert dust, consistent with

these data. Evidence for regional dust influence and non-carbonaceous coarse aerosol emitted from wildfires is discussed in Section 3.2.5.

The implication of the preceding discussion is that the prescribed/laboratory burns and wildfires cannot be treated as the same type of INP source, despite both being biomass burning. The data also demonstrate the difficulty in clearly isolating smoke impacts during wildfire periods with possibly high natural n_{INP} present at times.

3.2.4. Parameterization for INP from smoke sources

Although most of this chapter has focused on INP data obtained at -30 ºC, other temperature regimes were investigated using the CFDC, motivated by the need for INP measurements at warmer temperatures, which have not previously been reported for biomass burning emissions. Data collected at -22 and -26 ºC, shown in Figure 3.13, indicate a temperature dependent relationship between n_{INP} and n_{500nm} does exist for these smokes, where the number concentration of active INP at warmer temperatures is less than what is detected at colder temperatures. Additionally, differences in the n_{INP} to n_{500nm} relationship between the wildfires and prescribed/laboratory fires, evident in measurements conducted at -30 ºC (Section 3.2.3), are preserved at warmer temperatures. To develop parameterizations for predicting INP from these data, it is apparent the wildfires and prescribed/laboratory fires must be evaluated separately.

Smoke-impacted samples ([CO] >176 ppb) from Hewlett and High Park wildfires were used to determine a temperature dependent relationship between n_{INP} and n_{500nm}, based on methods used to develop D10,

$$n_{INP} = (n_{500nm})^{0.15} 10^{(0.11(273.15-T_K)-1.6)} \quad \text{Eq. 3.3}$$

where T is the processing temperature of the CFDC in degrees kelvin and n_{INP} and n_{500nm} are in units of L^{-1} and cm^{-3}, respectively. This parameterization is shown in Figure 3.14 for T_{CFDC} of -30, -26, and -22 °C.

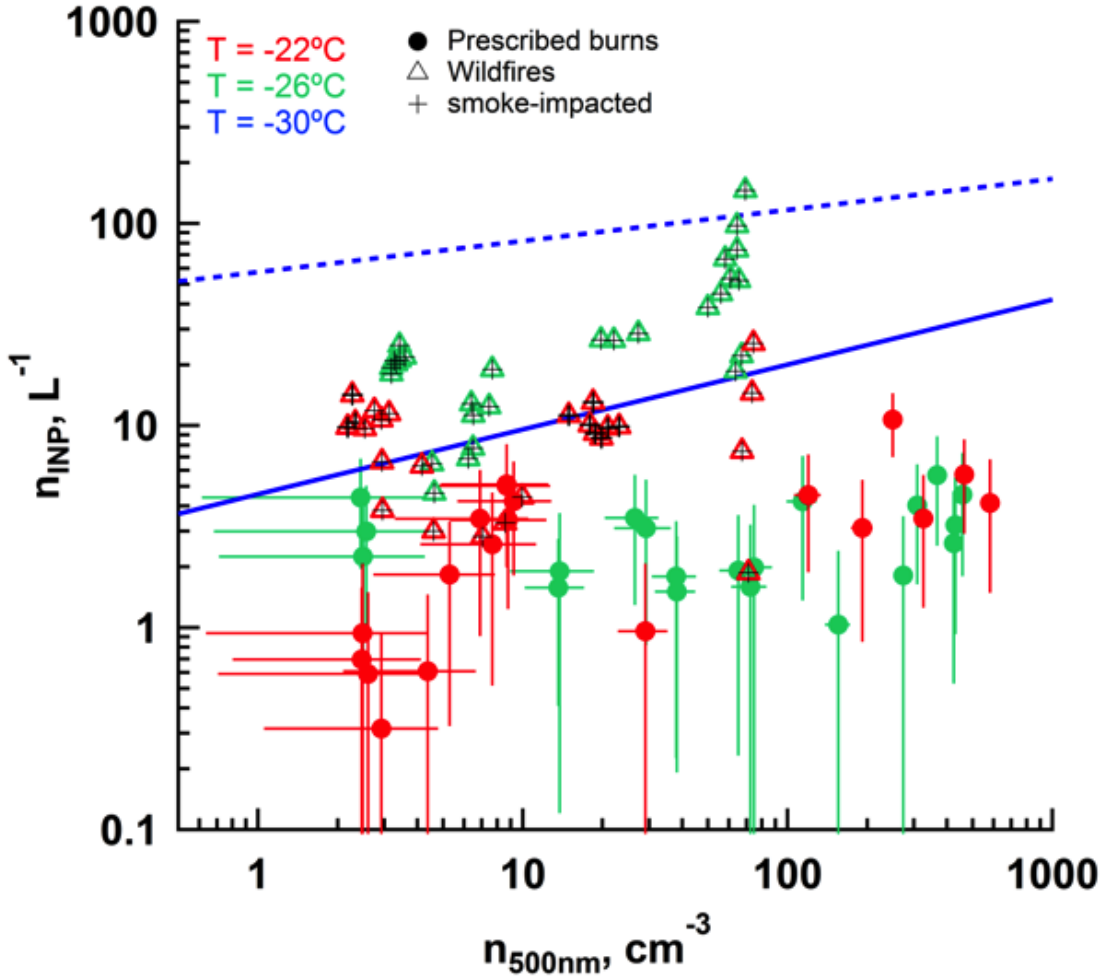

Figure 3.13. Relationship between n_{INP} and n_{500nm} for CFDC temperatures of -26 and -22 ºC during the prescribed burns (circles) and wildfires (triangles). Power law regression fits are also shown corresponding to wildfire (dashed) and prescribed (solid) lines of fit for -30 ºC processing temperature. Black crosses indicate smoke-impacted periods

Comparison between predicted INP from the new wildfire parameterization and observed INP is shown in Figure 3.15 for the smoke-impacted periods of the Hewlett and High Park wildfires. The new wildfire-specific INP parameterization predicts over 86% of the points within a factor

of 2 of the observed concentration (Figure 3.15). Overall, the wildfire smoke-impacted periods are better described by Equation 3.3 than by D10.

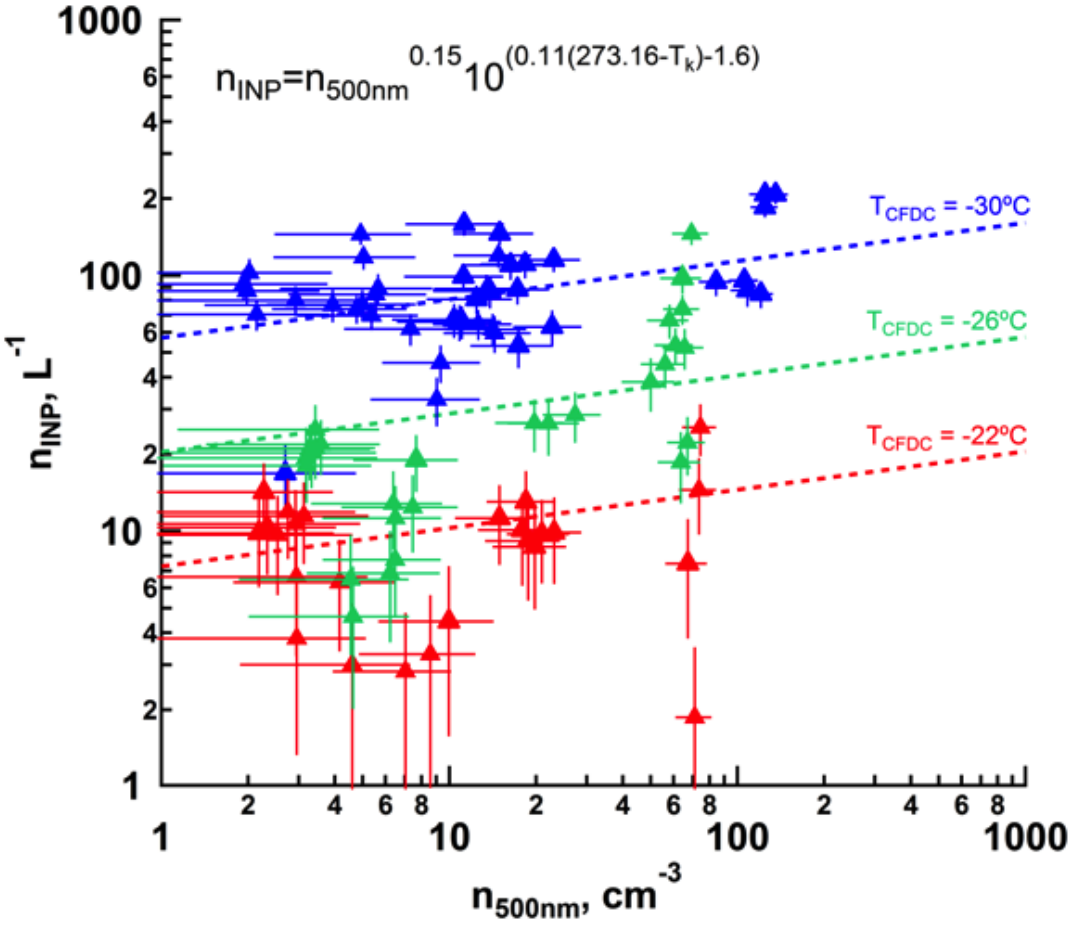

Figure 3.14. New parameterization, described in Equation 3.3, developed from the smoke-impacted data collected during the Hewlett and High Park wildfires. Data and fitted lines for -22 (red), -26 (green), and -30 (blue) °C are shown.

Unfortunately, due to the low volume sampling rate of the CFDC and lower n_{INP} at modestly supercooled temperatures, many measurements conducted at warmer temperatures have large uncertainties, resulting in weak relationships between n_{500nm} and n_{INP}, shown in Figure 3.16. Although the statistics are poor, these data propose a temperature dependent relationship between n_{500nm} and n_{INP} does exist for smoke aerosol emitted from the prescribed burns, with

lower n_{INP} at -22°C and -26°C compared to -30°C, and should be considered for further clarification during future measurements of smoke aerosol. Recent studies have utilized an aerosol particle concentrator upstream of the CFDC, which greatly reduced uncertainty in the measurements of low INP concentrations [Prenni et al., 2013] and should also be considered in future projects.

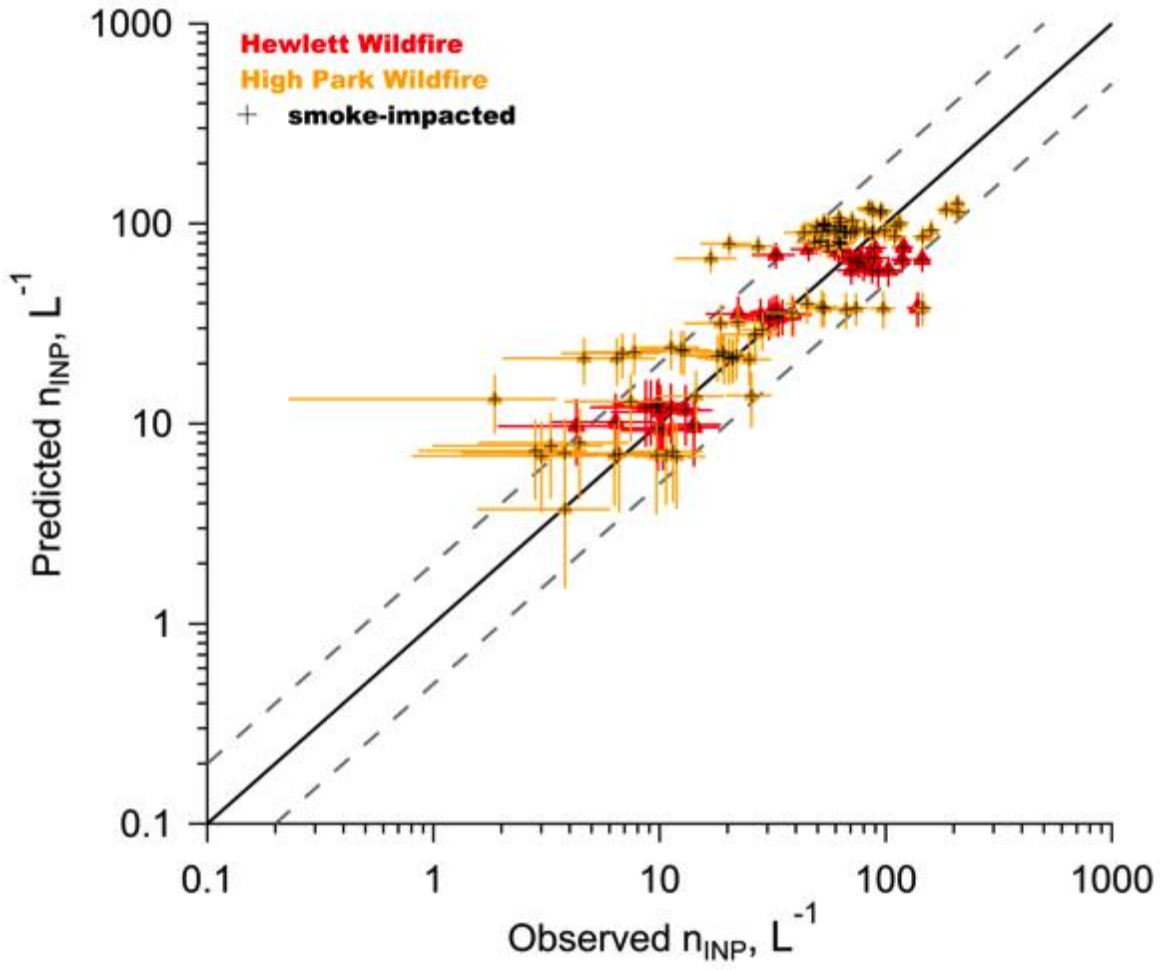

Figure 3.15. Observed and predicted n_{INP} (using Eq 3.3) for the Hewlett wildfire (red) and High Park wildfire (orange). Solid line is the 1:1 line with a factor of 2 outlined with dashed lines.

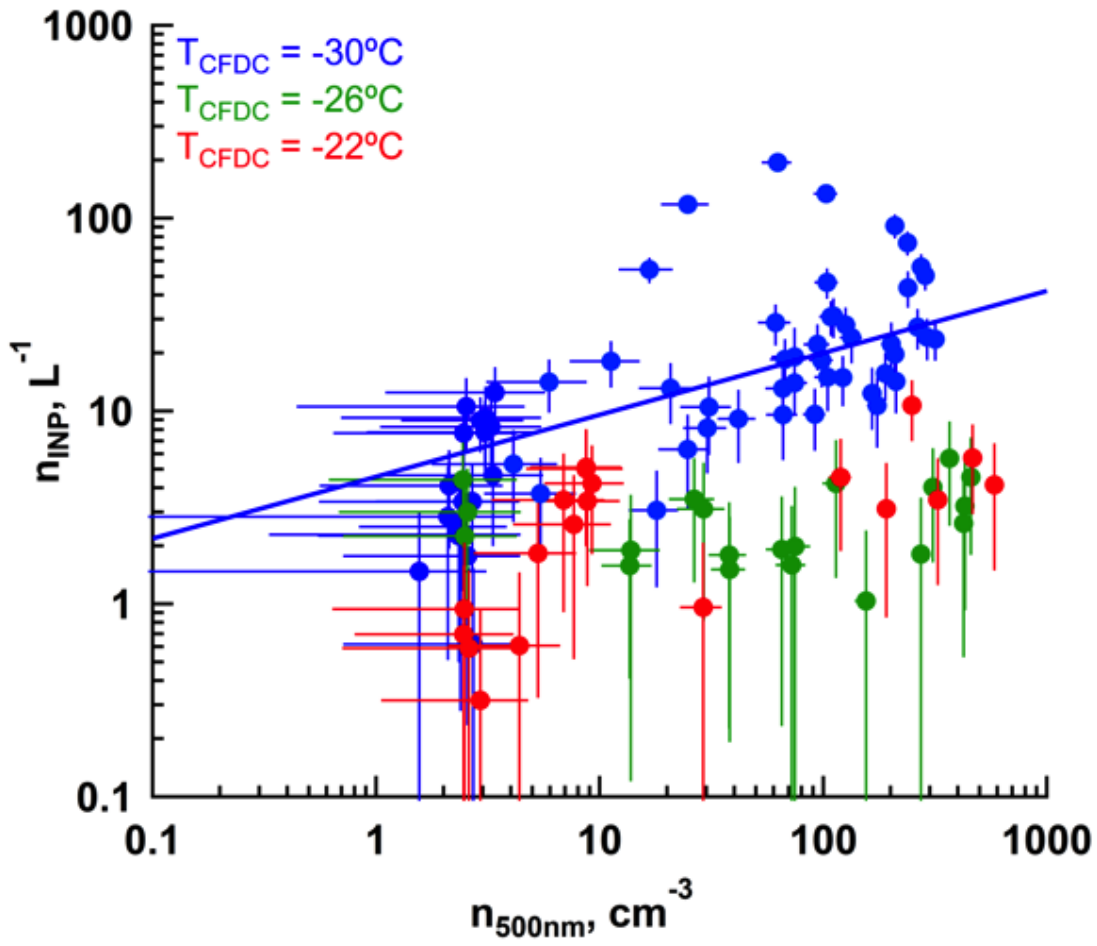

Figure 3.16. n_{500nm} vs n_{INP} for data collected at -22, -26, and -30 °C during the Georgia prescribed burns. Error bars show the Poisson counting uncertainty.

3.2.5. The influence of non-carbonaceous coarse aerosol on INP during wildfires

As discussed in Section 3.2.3, the relationship between n_{INP} and n_{500nm} was different for the Colorado wildfires compared to the other fire types in this study. Our analyses suggest that these differences may be attributed to the presence of coarse-mode soil or dust aerosol during these fire periods. These particles may have been lofted by the vigorous convection generated by wildfires and then emitted with the smoke plume, as suggested by Chalbot et al. (2013), or coarse aerosol may have been regionally enhanced due to long-range transport of mineral dust. It is also possible dust and biological particles could be lofted in areas surrounding the wildfires,

due to the outflow created by the fires. Enhanced concentrations of these dust and soil particles are likely important contributors to the INP population and may therefore elevate the concentrations of INP measured by the CFDC.

Ambient measurements of CO and mass concentrations of $PM_{2.5}$ and were used to assess the presence of coarse-mode particles associated with smoke emissions detected during the High Park wildfire, shown in Figure 3.17. For typical smoke aerosol, the particle size distribution is dominated by fine mode particles [Capes et al., 2008] and thus the majority of the aerosol mass concentration is accounted for by $PM_{2.5}$. This was the case for the plumes that intersected the sampling site on June 10, 11, and 12. However, the plumes detected on June 13 and 14 had PM_{coarse} mass concentrations up to 60 μg/m^3, accounting for nearly 50% of the aerosol mass. The PM_{coarse} detected during these plumes followed the trend of CO concentrations, indicating that the coarse aerosol was associated with wildfire smoke emissions. Although the CFDC is limited to particles less than 2.4 μm, the enhanced PM_{coarse} mass concentrations indicates the aerosol associated with the fire emissions was influenced by additional aerosol not typical of smoke aerosol.

Long range transport of Asian mineral dust, a known source of INP, typically occurs in late spring [VanCuren and Cahill, 2002]. This particularly potent INP source was important to consider for these data. Ambient PM_{coarse} mass concentrations collected from 2002 to 2012 at the Mount Zirkel Wilderness (MZW) IMPROVE site, a high-elevation site often influenced by long-range transport of Asian dust, are shown in Figure 3.18. Samples corresponding to fine soil mass concentrations above 1 μg/m^3, signifying dust influence, are highlighted. These measurements indicate that PM_{coarse} mass concentrations associated with long-range transport rarely exceed 10 μg/m^3 at these high elevation sites. Because the excursions of PM_{coarse}

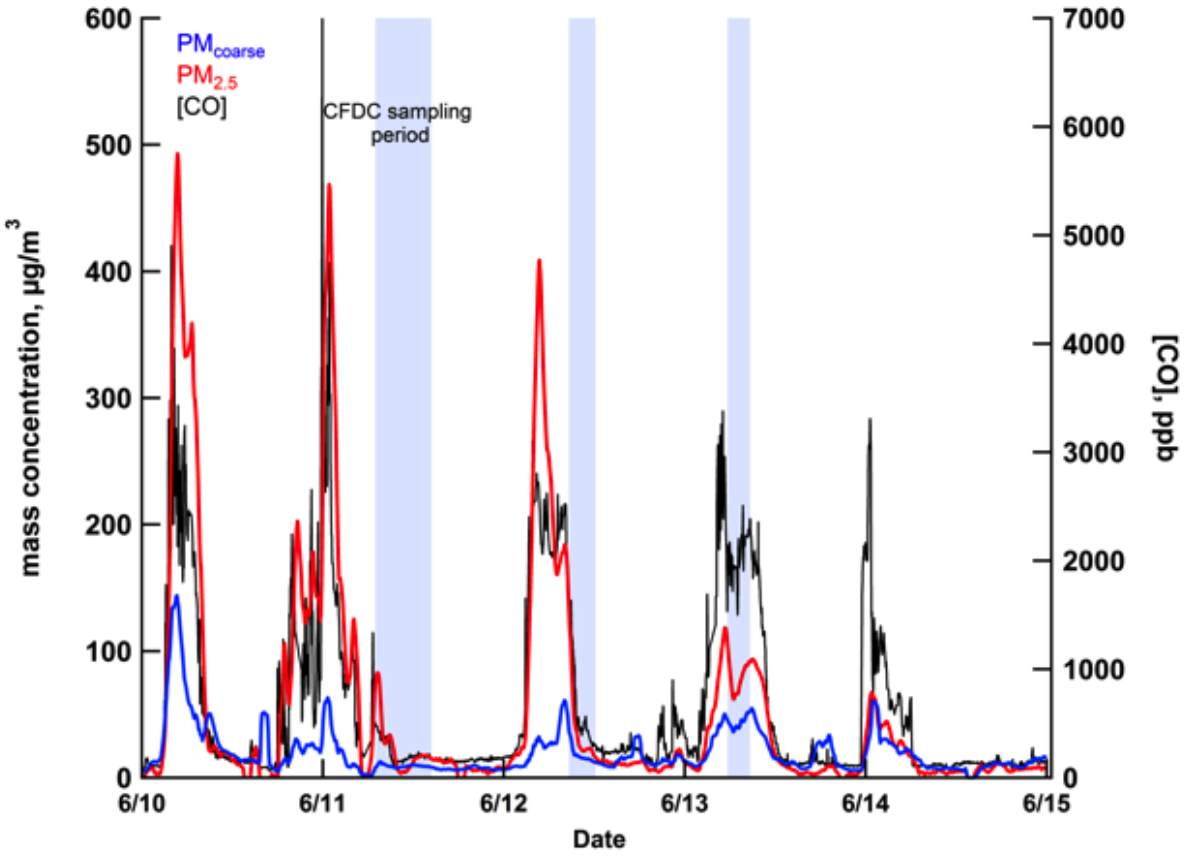

Figure 3.17. Time line of carbon monoxide (black), PM_{coarse}(blue), and $PM_{2.5}$(red) during the High Park wildfire. Grey shaded regions correspond to periods measured with the CFDC.

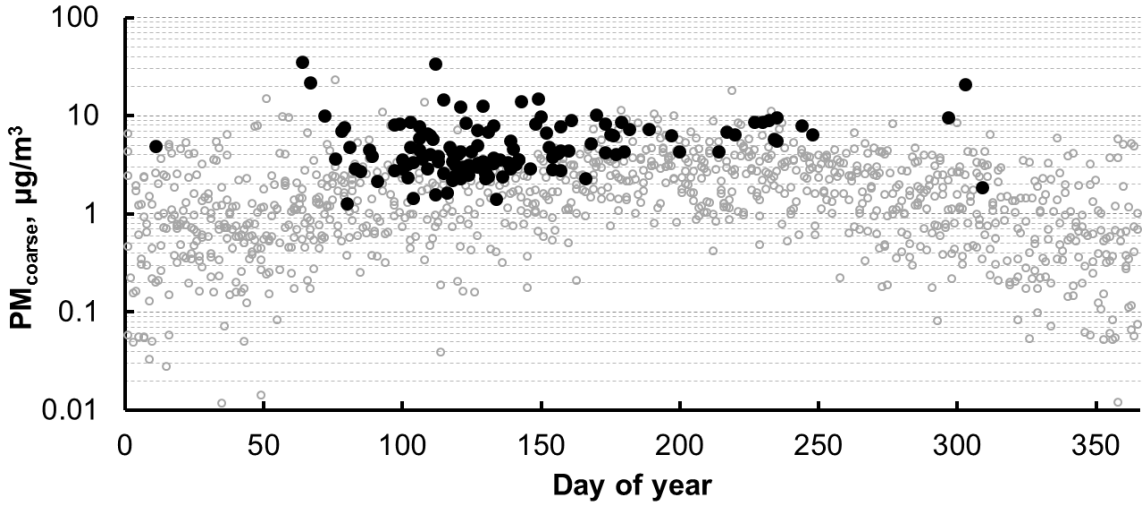

Figure 3.18. Mass concentration of coarse aerosol determined at the IMPROVE Mount Zirkel wilderness site from 2002 to 2012. Samples corresponding to fine soil mass concentrations greater than 1 µg/m^3 (black points) are highlighted as likely events of long-range dust transport.

measured at the sampling location during the High Park wildfire were 3 times higher than the largest PM_{coarse} mass concentrations measured over a 10 year period at a long-range transport susceptible site, it is unlikely that the PM_{coarse} peaks detected on June 13 and June 14 were due to long-range dust transport alone. These analyses indicate that the High Park wildfire emitted an anomalously high concentration of larger particles, which was not the case in the laboratory or prescribed burning studies. These larger particles appear to have important implications on the INP population, demonstrated by the greater number of INP observed for a given number of particles greater than 500 nm.

Particle mass concentrations were not monitored during the Hewlett Gulch wildfire, so the National Aerosol Analysis and Prediction System (NAAPS) model was used to investigate the presence of coarse aerosol in the sampling area, specifically in the form of dust. Dust is of specific interest due to possible long-range transport, mentioned previously, and due to elevated Ca/TC ratios observed on HiVol filters collected during the wildfires (Figure 3.5). A timeline of the predicted PM_{10} dust mass concentrations is shown in Figure 3.19 for the Fort Collins area

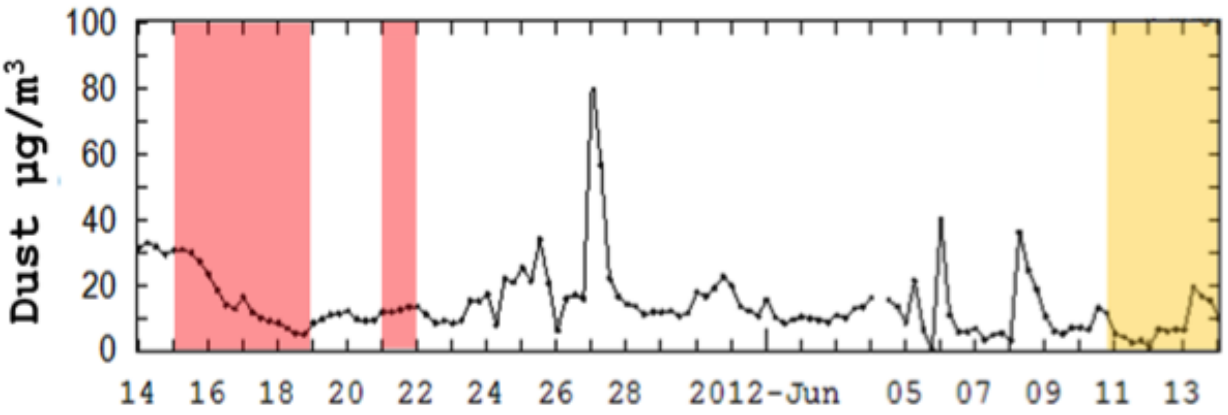

Figure 3.19. NAAPS model output from May 14 to June 14, 2012 of PM_{10} dust concentrations at 40.5º latitude and -104.5º longitude (near Fort Collins, Colorado). The Hewlett (red) and High Park (orange) wildfire measurement days are highlighted.

(40.5 ºN, 104.5 ºW) from May 14 to June 14, 2012. The NAAPS model predicted PM_{10} dust concentrations that exceeded 20 µg/m^3 from May 14-16, which was the beginning of the Hewlett wildfire. The NAAPS model also predicted elevated dust concentrations on June 13 during the High Park wildfire. However, Figure 3.17 shows that the PM_{10} mass concentration measured at the sampling site on June 13 reached 130 µg/m^3, indicating dust may have contributed but was not the sole source of coarse mode aerosol.

An additional measure of long-range transport of dust during the wildfires is soil concentrations observed at high elevation sites west of Fort Collins. Two IMPROVE network sites, located at the Rocky Mountain National Park (RMNP) and the MZW site were used to evaluate the presence of high regional dust concentrations. The locations of these sites are shown in Figure 3.20. Timelines of fine soil mass concentrations are shown in Figure 3.21 and Figure 3.22 for the RMNP and MZW sites, respectively, from 2002 to 2012.

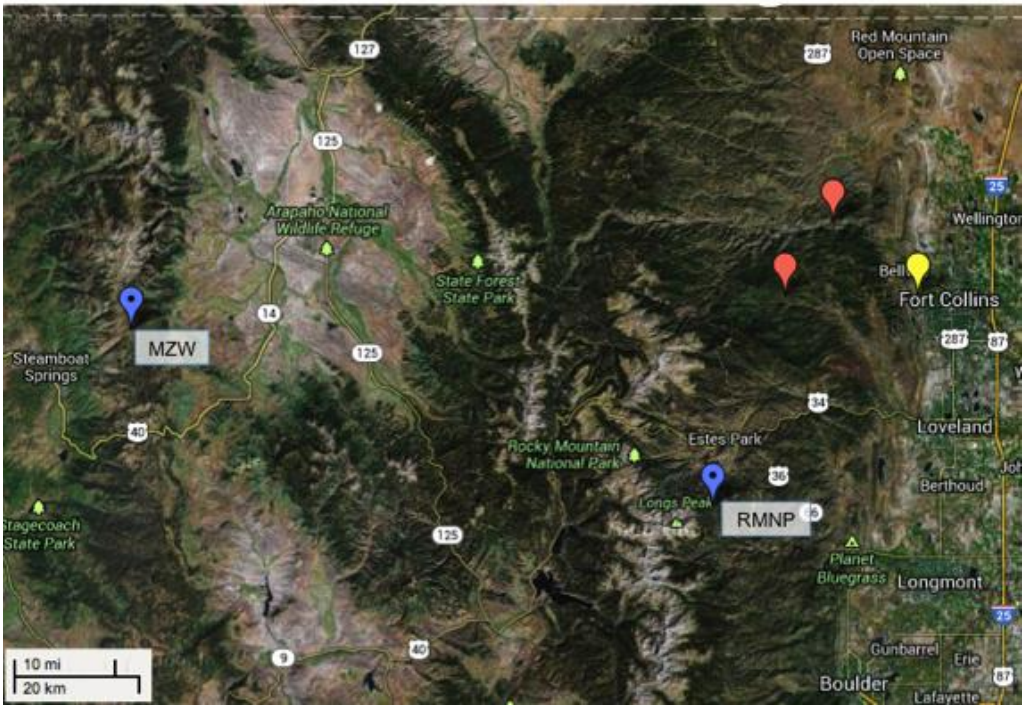

Figure 3.20. Map of IMPROVE sites, the Rocky Mountain National Park and Mount Zirkel wilderness sites. Red markers show locations of the Hewlett (most north) and High Park wildfires and the CSU foothills campus.

Mass concentrations of fine soil on May 15 and May 18 were greater than 1 μg/m^3 at both locations and the fine soil mass concentration estimated on June 14 was also greater than 1 μg/m^3 at the RMNP site. Although these concentrations were lower than soil mass concentrations associated with large dust transport events (> 5 μg/m^3), these data suggest regional dust was present during the wildfire measurements, particularly during the Hewlett wildfire, and may have severed to enhance n_{INP}.

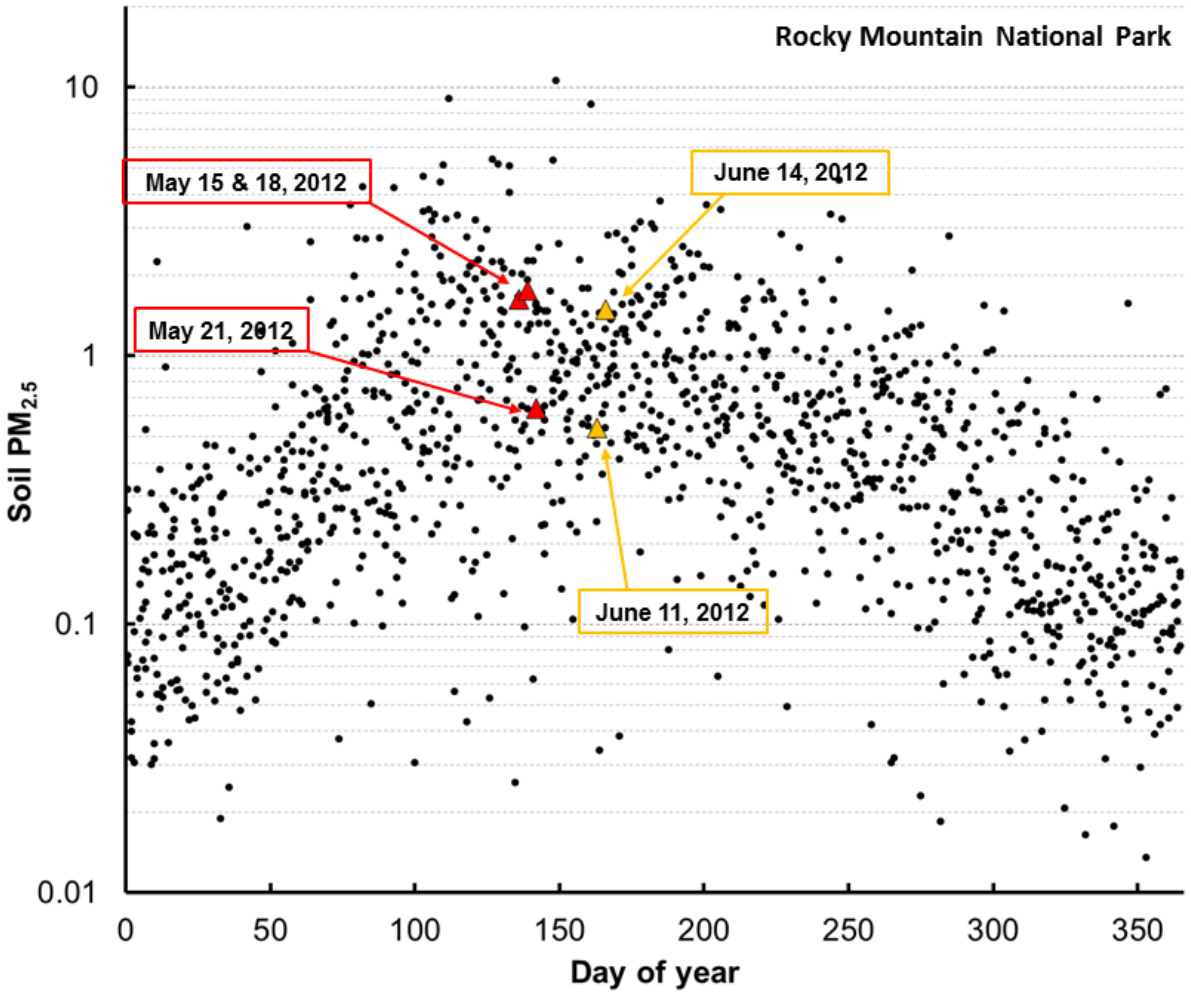

Figure 3.21. Fine soil mass concentrations measured at the Rocky Mountain National Park IMPROVE site from 2002 to 2012. Days from the Hewlett (red) and High Park (yellow) wildfire fires are indicated.

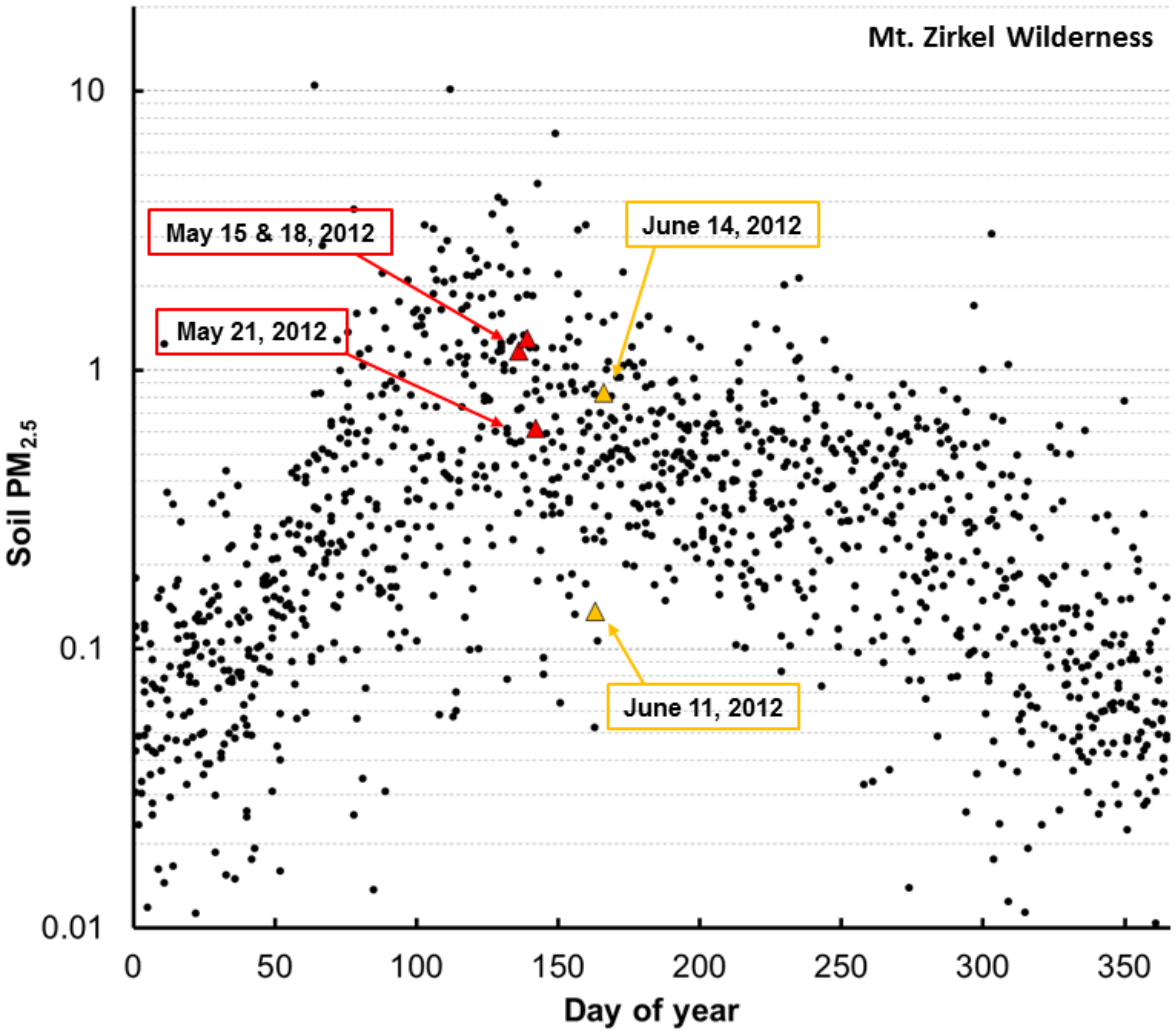

Figure 3.22. Fine soil mass concentrations measured at the Mount Zirkel wilderness IMPROVE site from 2002 to 2012. Days from the Hewlett (red) and High Park (yellow) wildfire fires are indicated.

Finally, a parameterization that is used to predict INP specifically from desert mineral sources (D13), developed in the same manner as D10, was used for comparison to these data, shown in Figure 3.23 [DeMott et al., 2013]. The parameterization is defined by:

$$n_{INP,T_k} = (n_{a>0.5\mu m})^{1.25} \exp(0.46(273.16 - T_k) - 11.46) \qquad \text{Eq 3.4}$$

where n_{INP} is in number of INP per standard liter and n_{500nm} is the number of particles with diameters greater than 500 nm per standard cm^3. Interestingly, the non-impacted samples collected during the Hewlett wildfire period appear to have a similar slope to the dust-specific

parameterization, consistent with presence of mineral dusts and soils supported by the IMPROVE and NAAPS model analyses. However, the mineral dust specific parameterization under predicts the INP observed during the wildfire non-impacted periods. The smoke-impacted samples collected during the wildfires, although more dust-like than the prescribed and laboratory fires, have a much weaker slope compared to D13, suggesting the INP source is more complex than mineral dust particles alone.

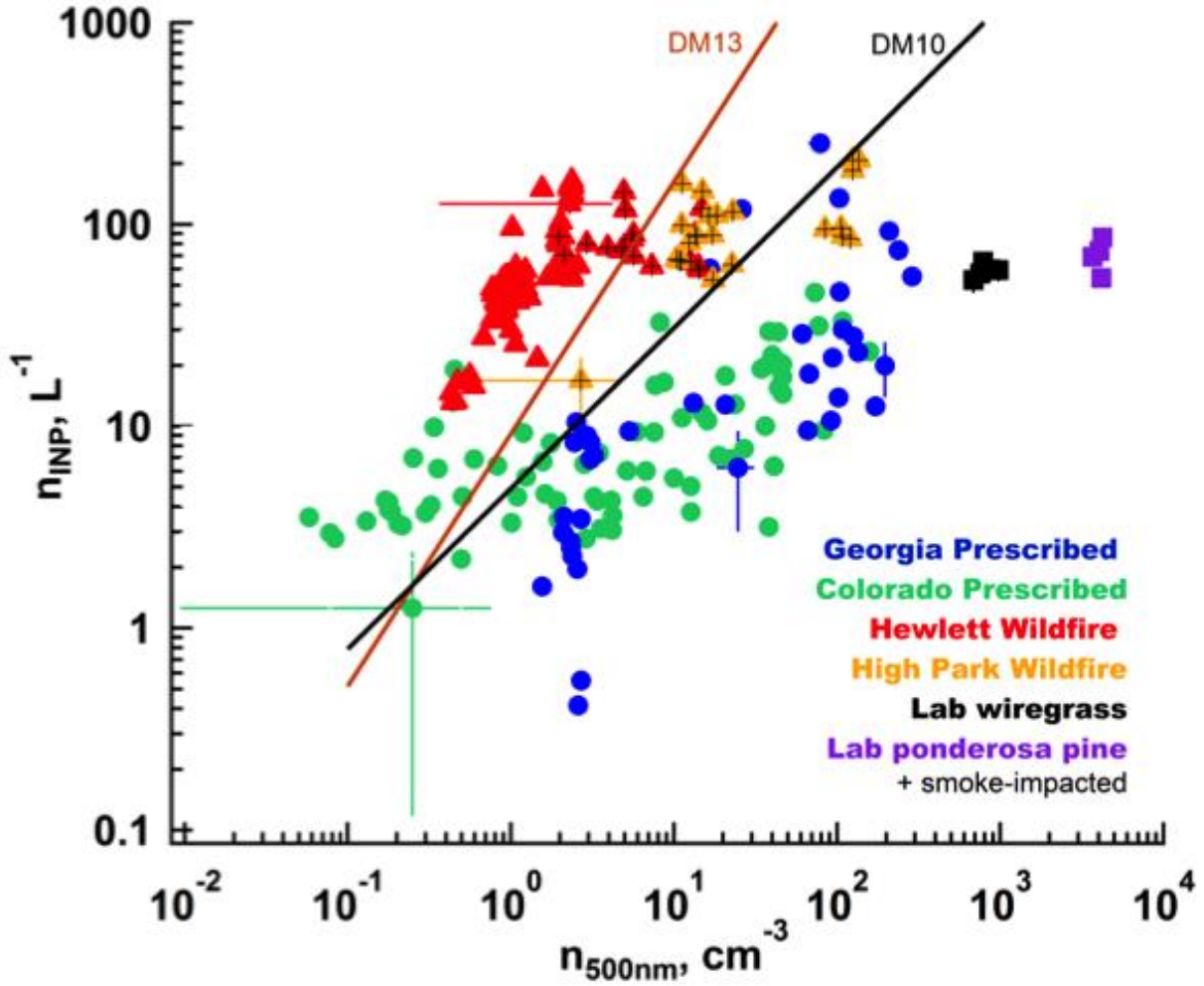

Figure 3.23. The relationship of n_{500nm} to n_{INP} at -30 °C for wildfires (triangles) and prescribed fires (circles) and the D13 and D10 prediction of INP based on dust and "global" aerosol data sets, respectively. Black crosses indicate smoky periods.

To explore the sensitivity of the slope of the smoke-impacted data to the smoke-impacted CO concentration threshold, Figure 3.24 is the same as Figure 3.25 for CO concentration thresholds of 115, 125, 150, and 200 ppb. The slope for smoke-impacted samples does not steepen until the CO condition was relaxed from 176 to 115 ppb, indicating the complex mixture is truly specific to samples influenced by smoke and the steep slope, resembling mineral dust, is specifically observed in the non-impacted samples.

The preceding analyses provide evidence that coarse particles, potentially in the form of dust, were present during the measurements made of the wildfire emissions and likely served to increase the concentrations of INP emitted from these wildfires compared to the laboratory/prescribed fires. The NAAPS model and IMPROVE observations provide support for long-range transported dust during the Hewlett wildfire. Although the IMPROVE observations provide evidence for dust influence due to long-range transport at the end of the High Park measurement period (June 13), the $PM_{2.5}$ and PM_{coarse} mass concentrations observed at the CSU Foothill campus show that it was more likely that coarse aerosol was directly emitted from the High Park wildfire. It is important to emphasize that aerosol emitted from all wildfires may not have this apparent dust influence and these results are specifically for the Hewlett and High Park wildfires. However, wildfires typically occur in arid regions, similar to Colorado, and the dust transport season coincides with the wildfires season in the Western US. These data are likely a realistic representation of the Western US and can be used for comparison of future wildfires.

3.3. Particle types serving as INP

As discussed in Section 3.2.5, INP observed during our sampling of wildfire emissions may have been influenced by non-carbonaceous aerosol, possibly of different origin than the burn, and thus single particle compositional analyses of the actual particles that activated as INP

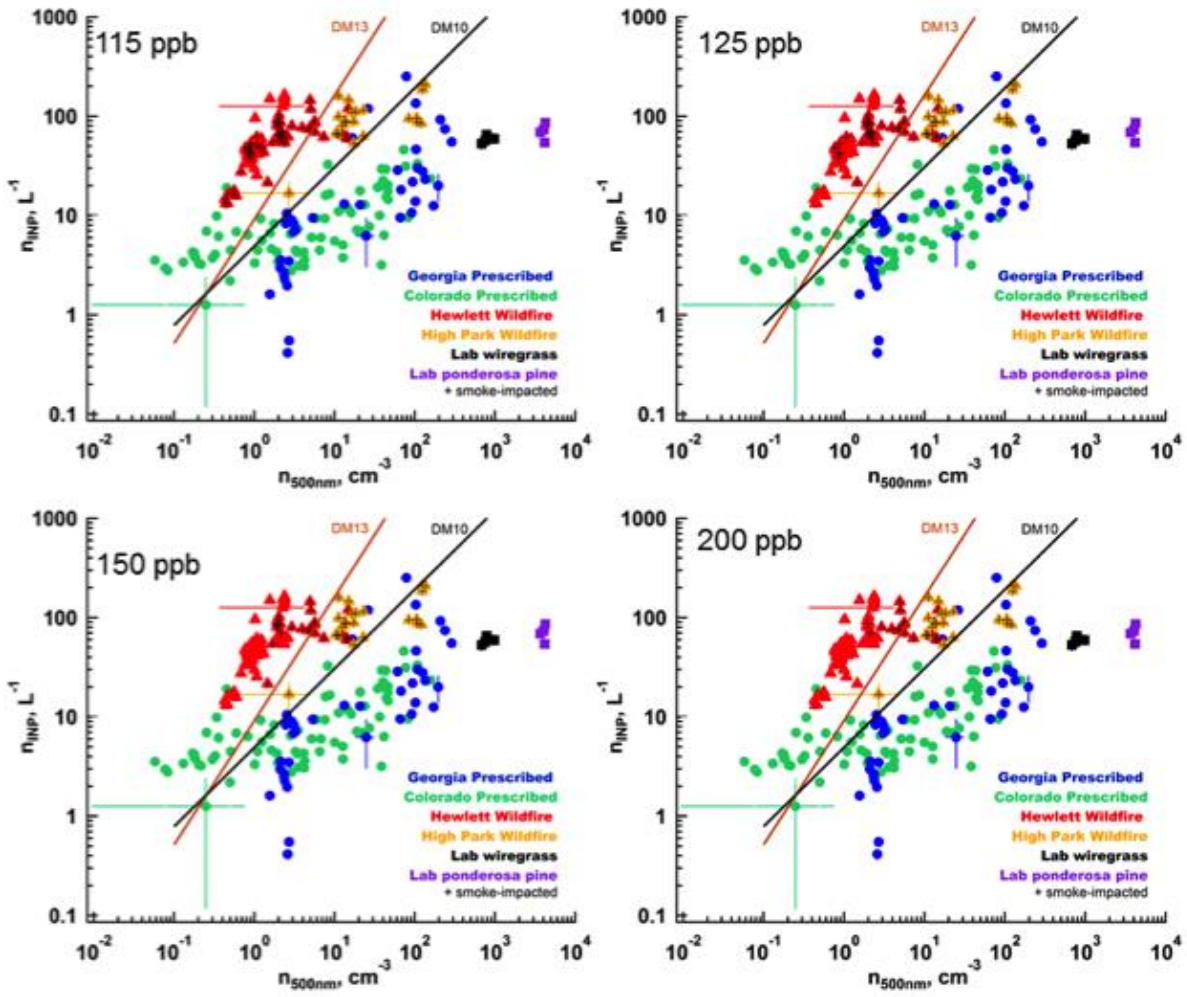

Figure 3.24. Same as Figure 3.23 for different CO concentration thresholds for defining smoke-impacted samples.

are of interest. Even for INP definitively originating from the fire emissions, it is of interest to understand which of the complex particle types present in smoke may represent the dominant INP sources. Section 3.3.1 describes the single particle categorization results from grids collected during the Georgia prescribed burns and both wildfires. The role of refractory black carbon (rBC) was also explored in the FLAME IV laboratory burn studies, using the SP2-CFDC set up, and results are discussed in Section 3.3.2.

3.3.1. Single particle analysis of residual INP

TEM grids were used to collect the residual ice crystals at the base of the CFDC via impaction, as discussed in Chapter 2, and analyzed for elemental composition; images were saved for each particle studied. Approximately 50-60 particles were analyzed on each grid and then categorized into six different particle types. Ten grids were collected during the Georgia prescribed burns and one grid was collected during each wildfire. Each grid is labeled in the format "date_sample#" (e.g. "030811_B" is the second grid collected on March 08, 2011), and collection periods are show in Figures B. 1-12 (Appendix B). Contributions of particle types active as INP and the T_{CFDC} range during grid collection are summarized in Figure 3.25.

Although the single particle analyses provide detailed information on the types of particles active as INP in the samples from these biomass burning events, uncertainties and limitations are associated with these analyses. Each grid was loaded with at minimum 5,000 INP, and only about 1% of the particles were randomly selected for detailed analysis due to the time consuming nature of the analyses. However, the goal of this analysis was to gain a general sense of the types of particles active as INP and examine whether obvious differences in the types of particles acting as INP existed among the grids.

The majority (70-95 %) of the residual ice crystals collected during the Georgia prescribed burns between March 11 and March 15 were classified as carbonaceous particles, with the exception of grid 031111_B. Of those carbonaceous particles, 30-70% of them were soot particles, indicating soot was an important type of INP emitted from the Georgia prescribed burns. To our knowledge, this is the first confirmation of a clear association of INP with soot from biomass burning.

Grids collected during the Georgia prescribed burns on March 08 contained less than 50% carbonaceous INP and less than 1% were soot particles. C/Min-mix and Min/Ox mix

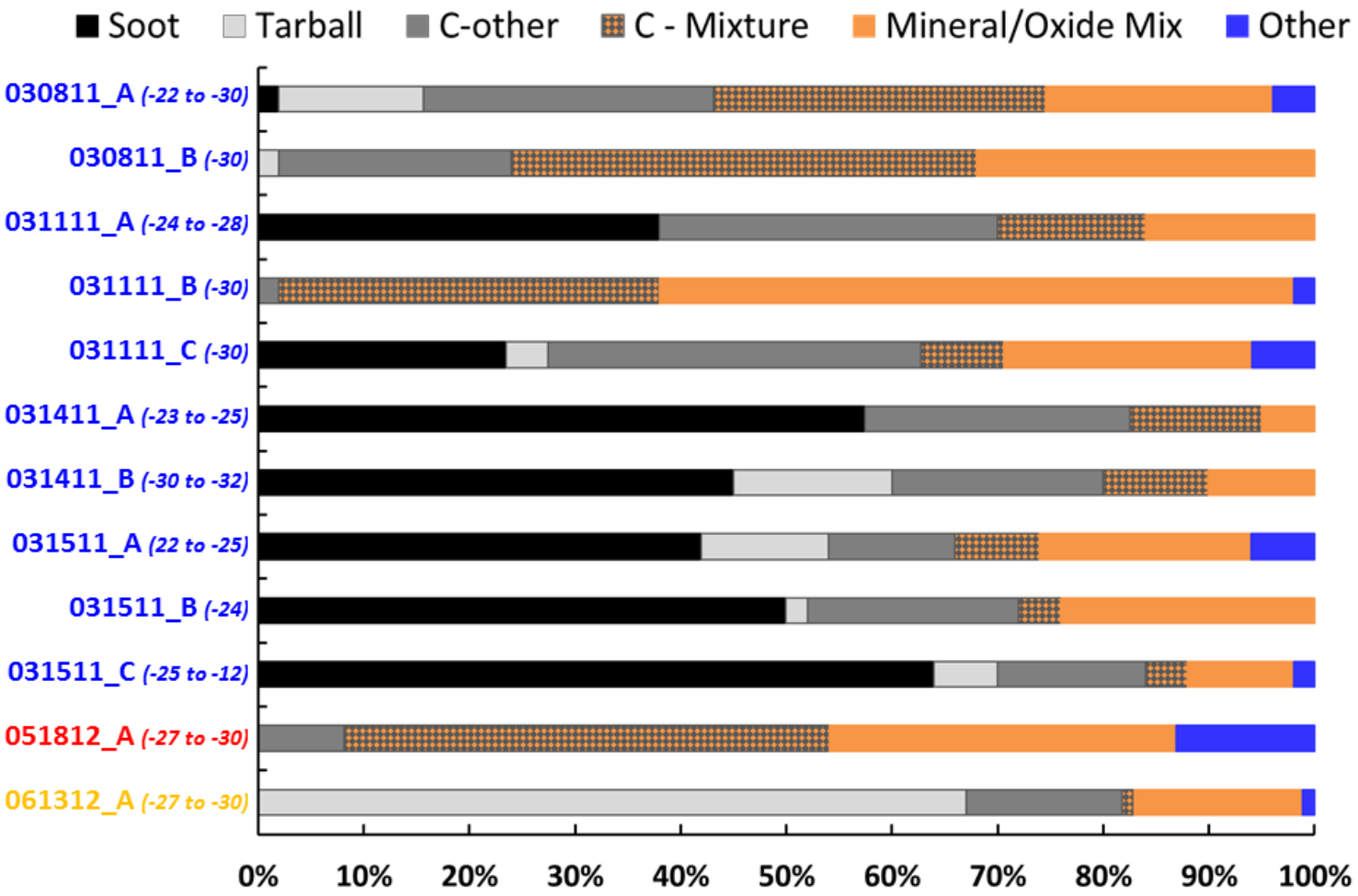

Figure 3.25. IN particle categorization of grids collected during the Georgia prescribed burns (blue, Hewlett wildfire (red) and High Park wildfire (orange) are ordered chronologically; the CFDC processing temperature during the grid collection is shown in parentheses. Particle categories included soot (black), tarballs (light grey), carbonaceous-other (grey), carbonaceous-mineral/metal oxide mixture (grey and orange textured), mineral/metal oxide (orange) and other (blue). Particle types are discussed further in Section 2.2.

particles dominated the particle types analyzed on the March 08 grids. Measurements were made further away from the fire on March 08, suggesting a change in the type of particle active as INP in slightly aged smoke. However, an important difference on March 08, compared with the other days from the prescribed burn study, was that the sampling inlet was not sampling fire emissions during the entire sampling period (as shown in the n_{CN} timeline in Appendix B and discussed further in Section 3.1.1) and thus other sources of INP may have contributed to these grids. Indeed, grid 030811_B was collected after the main smoke plume was sampled, indicated by the relatively low n_{CN}. Differences in the land cover on March 08 compared to the other burn day may also have an impact on INP particle types, with less loamy sand (sand contained more organic material) and different forest cover. However, the impact of these different burn areas on n_{INP} is unknown.

Interestingly, the only grid collected during a period when flaming phase and flying ash were reported nearby (031111_B) contained over 50% Min/Ox mix particles, over 35% C/Min-mix particles and no soot particles. Grid 031111_C, the succeeding grid collected for the same processing T_{CFDC}, contained over 60% carbon-dominated particles and therefore this difference does not appear to be a feature of variations in T_{CFDC}. These single particle data suggest mineral/oxide materials played an increasing role in the INP population with flaming phase combustion, possibly attributed to ash, dust or other coarse particles being kicked up by the vigorous nature of flaming phase combustion. Flaming phase combustion may represent a scenario where the most abundant INP is determined by a competition between particles lofted as dust/soils and carbonaceous particles, with dust/soil particles appearing to be more favored.

Results from grids collected during the Hewlett (051812_A) and High Park (061312_A) wildfires are also presented in Figure 3.20. These grids were collected during periods of carbon monoxide concentrations above background concentrations (136 ±20 ppb): 150-500 ppb during

the Hewlett grid and 1800-2000 ppb during the High Park grid, and thus are expected to represent the INP present in the fire emissions. Both wildfire grids contained no active soot particles and were strikingly different. The Hewlett grid most closely resembled the 031111_B grid from the Georgia prescribed fires, with the majority (>75%) of the INP containing mineral and metal oxide characteristics.

Mineral/metal oxide particles on the Hewlett grid support the hypothesis that the INP population was influenced by soils or dust, the evidence for which was discussed previously. A lower fraction of mineral/metal oxide particle types were observed on the High Park grid and were compensated for by more carbonaceous particles, particularly tar ball types that are indicative of processed fire emissions. The high fraction of tarball type particles and the early morning collection period of the High Park fire grid suggests the smoke measured during this period was more representative of a smoke that was mixed to the surface the previous evening and remained in a stagnant environment until the thickening of the boundary layer in the morning. Although photochemical processing would not be significant, the production of secondary carbonaceous particles was likely in the thick smoke plume. It is clear these particles are an important piece of the population of INP in night processed smoke.

3.3.2. The role of refractory black carbon particles as biomass burning INP

During the FLAME IV experiment, an SP2 was essentially used as a filter for rBC upstream of the CFDC during two room burns of fuels relevant to this study: wiregrass and ponderosa pine. This experiment was done as part of a systematic NASA-funded study to use this procedure to identify the role of rBC in atmospheric ice nucleation. The SP2 laser, which acts to remove rBC from the aerosol, was switched on and off while n_{INP} was monitored using the CFDC. The laser-on-laser-off cycle was repeated twice and the impact of the laser on INP

was quantified by the fractional change in the number concentrations of INP, f_{INP}, described by Equation 3.4.

$$f_{INP}=1-\frac{n_{INP,OFF}-n_{INP,ON}}{n_{INP,OFF}} \qquad \text{Eq 3.4}$$

where $n_{INP,OFF}$ and $n_{INP,ON}$ are the number concentrations of INP determined while the laser was off and on, respectively, such that f_{INP} of 0 would indicate rBC does not contribute to the INP population and f_{INP} of -1 would indicate all INP contain rBC. The fractional change in n_{500nm} ,f_{500nm}, was also determined by Equation 3.4 using $n_{500nm,OFF}$ and $n_{500nm,ON}$. f_{500nm} provides information on the amount of rBC in the aerosol, since some fires may produce little BC (Levin et al., 2010; Figure1.3). Dilution of the smoke sampled during the SP2 experiments was accounted for by determining a linear fit of n_{500nm} with time. The uncertainty of f_{INP} and f_{500nm} describes the variability of the dilution linear fit.

Fractional changes in n_{INP} and n_{500nm} are shown in Figure 3.26. These results demonstrate that the effect of the removal of rBC is variable between the two fuel types. INP number concentrations produced from burning ponderosa pine were not as affected by the laser as the n_{INP} emitted from wiregrass combustion, as f_{INP} was more negative for smoke emitted from the burning of wiregrass than that from ponderosa pine. This reduction is a feature of not only the presence of soot particles emitted from biomass burning serving as INP, but also the abundance of rBC containing particles in the burning emissions, which is described by f_{500nm}. n_{500nm} emitted from the combustion of ponderosa pine was only reduced by 20% (f_{500nm} = -0.2) after passing through the SP2 laser, indicating that aerosol emitted from ponderosa pine combustion contained approximately 20% rBC, whereas smoke from the burning wiregrass contained approximately 50% rBC (f_{500nm} = -0.5). f_{INP} was not clearly different from zero for the smoke emitted from the ponderosa pine burn and n_{INP} was reduced by10-80% after rBC was

removed from the smoke emitted from the wiregrass burn. These results are consistent with the single particle TEM analyses, where INP collected during prescribed burns of wiregrass consisted of up to 60% soot particles and no soot particles were identified on the grids collected during the wildfires, for which the dominate fuel was ponderosa pine.

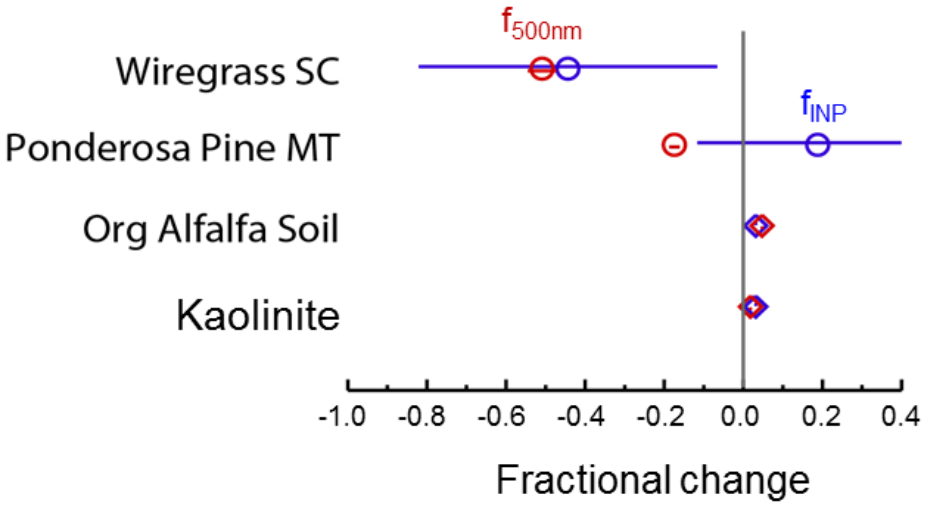

Figure 3.26. Fractional change in INP (blue) and larger (red) particle number concentrations due to the removal of refractory black carbon by an SP2 laser during the FLAME IV room burn experiments (figure courtesy of Ezra Levin)

Also shown in Figure 3.26 is the f_{500nm} and f_{INP} observed from laboratory tests on known IN active mineral dust aerosol. These results indicate little impact of the SP2 laser on the nucleation ability of these non-rBC particles, suggesting the SP2 processing is selective in removing only the INP with compositions dominated by rBC. Additional laboratory studies are underway to further prove the concept of this SP2-CFDC technique, and confirm the selectivity for soot INP, as discussed in Section 2.2.7.

4. Summary and recommendations

Measurements describing the number concentrations of INP (n_{INP}), particles greater than 500nm (n_{500nm}), and condensation nuclei (n_{CN}), bulk aerosol chemical composition, carbon monoxide concentration and types of particles acting as INP were made during five biomass burning events. The fuel type, combustion efficiency, plume histories, and burning conditions were diverse amongst these events, which included prescribed burning, wildfires and laboratory burns. Therefore, these data provided a valuable data set for assessing variations in INP emitted from diverse fire conditions.

The prescribed burns included measurements made of smoke emitted from prescribed burns in Colorado in July of 2009, presented previously by Prenni et al. (2012), and a series of prescribed burns that took place in Georgia in March of 2011. Measurements were also made during two Colorado wildfires in the summer of 2012: the Hewlett wildfire and the High Park wildfire. The laboratory burns discussed in this study were part of FLAME IV and included two room burns: wiregrass, resembling the fuel burned in the Georgia prescribed burns, and ponderosa pine, the dominant fuel for the Colorado prescribed burns and wildfires.

Bulk aerosol chemical composition analyses revealed elevated total carbon and levoglucosan concentrations on days in which the CFDC was deployed during the Georgia prescribed burns and Colorado wildfires. Daily levels of n_{CN} suggest higher particle numbers were present during the Georgia prescribed burns than during the Colorado wildfires. We attributed this difference to the impact of transport and aging; the wildfires were measured from at least 10 times the distance as the prescribed fires, allowing for dilution, particle volatilization, and coagulation to decrease $n_{CN.}$

Smoke-impacted samples were identified as samples with CO concentrations above two standard deviations above the mean concentration observed during fire-free periods (176 ppb). However, we were faced with the challenge of identifying smoke plumes on measurement days without CO measurements available. It was determined that n_{CN} serves as a reliable indicator of smoke for measurements made near the source, but n_{CN} is too vulnerable to plume processing to use as a smoke marker for measurements made at further distances, such as the measurements of the wildfire plumes.

The vulnerability of CN was further evident in our efforts towards describing relationships between INP emissions and other emission parameters. The statistically significant relationships between n_{INP} and n_{CN} observed in younger smokes appeared to be consistent with one another, including the Georgia and Colorado prescribed burns and laboratory burns. However, the wildfire n_{INP} to n_{CN} relationship was not consistent with the relationship found in the other fires, and the relationship was statistically less significant. We suggest that total particle number concentrations are a poor descriptor for comparing INP emitted from biomass burning events with different transport distances and plume histories. It is strongly encouraged for future measurements of biomass burning events to include measurements of CO and CO_2 in order to compare emission factors. The lack of CO and CO_2 measurements during the prescribed burns and some of the sampling periods of the wildfires limited the ability to confidently identify periods when the sampling location was smoke-impacted.

Because the impact of aging is so great for n_{CN}, and obtaining measurements of wildfires near the emission stage is not easily accomplished, less plume-processing-vulnerable particles (d_p>500nm) were considered for describing the amount of INP associated with the fires. Emissions of INP and their relation to n_{500nm} revealed strong differences between the wildfires

and prescribed/laboratory fires. For a given value of n_{500nm} the wildfires were associated with a higher concentration of INP compared to observation from prescribed and laboratory fires; a factor of 10 enhancement in n_{INP} was observed at -30ºC. A parameterization previously developed by DeMott et al., (2010) for "global" well-mixed INP sources was used to compare the emissions of INP from these biomass burning events. The parameterization over-predicted INP emitted from the prescribed fires and under-predicted INP emitted from the wildfires evaluated in this study. A difference in the relationship between n_{500nm} and n_{INP} was clear between the wildfires and the prescribed/laboratory fires; fuel type, combustion efficiency, transport distance and the potential influence of dust were considered for explaining this variability.

Fuel type and modified combustion efficiency were eliminated as reasons for this variability by comparing the relationship between n_{500nm} and n_{INP} between biomass burning events of contrasting fuel type and MCE. The n_{INP} emitted from the Georgia prescribed (wiregrass) and Colorado prescribed (ponderosa pine) fires were both over-predicted by D10 and related to n_{500nm} similarly, regardless of fuel type. Burns with contrasting MCE, the laboratory room burn of wiregrass (MCE=0.97) and the prescribed burn of wiregrass in Georgia, reported to be a mixture of smoldering and flaming, were both over predicted by D10. Also, based on bulk potassium to total carbon mass concentrations rations, the combustion efficiency of the wildfires was not considerably different from the Georgia prescribed burns. Fuel type and MCE were not important reasons for the differences observed during the wildfires.

Dissimilarities in transport time were unable to explain the observations because 1) dilution would act to reduce both n_{500nm} and n_{INP}, 2) previous studies [e.g., Hobbs et al., 2003] of aged smoke plumes show the number of >500 nm particles are not typically impacted by

coagulation or other aging processes, and 3) deactivation by covered nucleating sites due to coagulation, although never been confirmed, would have the reverse effect on this relationship than what was observed.

The influence of non-carbonaceous aerosol, such as dust or soils, originating from the fire itself or long-range transport was found to be the main reason for the elevated n_{INP} observed during the wildfires compared to the prescribed/laboratory fires. $PM_{2.5}$ and PM_{coarse} mass concentrations revealed the plumes emitted from the High Park fire on June 13 and 14 contained anomalously high contributions of coarse aerosol to the total aerosol mass. Long range transport was considered as a possible reason for the high coarse aerosol, but the NAAPS model and IMPROVE observations indicate that PM_{coarse} rarely exceeds 10 $\mu g/m^3$ and would only explain a fraction of the PM_{coarse} mass concentrations observed. These results indicate that soils were likely emitted during the wildfires and thereby increased concentrations of INP.

Predicted PM_{10} dust mass concentrations from the NAAPS model and $PM_{2.5}$ soil mass concentrations observed at high elevation IMPROVE sites provide sufficient evidence for long-range transport of dust to the region during the measurement of the Hewlett wildfire. This explained the high n_{INP} observed during periods that were clearly not impacted by smoke. A mineral dust-specific INP parameterization also supported a strong dust influence and still under-predicted INP associated with the Hewlett wildfire non-impacted periods. These analyses, in addition to elevated bulk calcium to total carbon ratios, indicate the INP population measured during the Hewlett wildfire periods was clearly influenced by long-range transport of dust and the High Park wildfire was influence by dusts/soils emitted by the fire itself and at times by long-range transport.

Measurements from these biomass burning events provided evidence for the existence of a temperature dependent relationship between n_{500nm} and n_{INP} for smoke aerosol, where lower n_{INP} was observed at warmer temperatures. However, consistent with observations at -30 ºC, this relationship was different between the wildfires and prescribed/laboratory fires at warmer temperatures, such that one parameterization could not describe all biomass burning events. A new parameterization was developed for the wildfires, but the low concentrations measured at warmer temperatures during the Georgia prescribed fires prevented a parameterization from being developed for the remaining data. Future studies should take advantage of recently deployed methods for detecting low n_{INP} by using a particle concentrator upstream of the CFDC.

This study provides a close look at the individual particles responsible for immersion/condensation freezing heterogeneous ice nucleation within smoke plumes. Soot particles were most common in plumes emitted from the Georgia prescribed burns, contributing up to 60% of the collected INP. To our knowledge, these are the first confirmations of soot active as INP from biomass burning. A new instrumental setup, using an SP2 as a rBC filter upstream of the CFDC, was deployed during FLAME IV to evaluate the impact of removing rBC from the aerosol on INP concentrations. Reductions of 50 (±30)% in n_{INP} were observed for smoke emitted from a room burn of wiregrass and minimal change was observed during the ponderosa pine room burn.

The single particle analyses indicate potential importance of mineral/metal oxide particles during highly flaming combustion. Greater contributions of particles containing mineral species were observed on the grid collected during the Hewlett wildfire, consistent with the apparent presence of enhanced regional dust concentrations. Ambiguity still exists due to the clear contributions of C-mix particles during the Hewlett sampling period. Although the grid collected

on June 13 during the High Park wildfire was during a period with higher concentrations of coarse mode particles than typical smoke, the majority (> 80%) of the residual INP were carbon-dominated particles in the form of Tarball, indicative of plume processing that may have occurred overnight. There were also many carbon-dominated particles that were unidentified, suggesting a highly active carbonaceous soil may have also been responsible for the elevated n_{INP} and higher coarse aerosol mass concentrations.

Based on the results of this study, it would be beneficial to continue evaluating biomass burning as a source of INP, particularly emissions from wildfires since they appear to produce more INP. Although relevant, the presence of dust during these biomass burning events created challenges for assessing the true background n_{INP} and therefore the ability to attribute all of the INP to carbonaceous smoke aerosol. However, n_{INP} was elevated for each smoke-impacted measurement and these wildfires appeared to be important sources of INP that are not present in the prescribed or laboratory burns. The influence of dust during the wildfires provided a demonstration of the importance for gaining knowledge on the types of particles emitted from specific aerosol sources, how they compete with other potent INP sources, and therefore how INP populations are impacted near the emission of a biomass burning plume versus downstream of the fire when the plume interacts with other sources, such as dust.

References

Andreae, M.O., 1983. Soot Carbon and Excess Fine Potassium: Long-Range Transport of Combustion-Derived Aerosols. Science 220, 1148–1151.

Archuleta, C.M., DeMott, P.J., Kreidenweis, S.M., 2005. Ice nucleation by surrogates for atmospheric mineral dust and mineral dust/sulfate particles at cirrus temperatures. Atmos. Chem. Phys 5, 2617–2634.

Banta, R.M., Olivier, L.D., Holloway, E.T., Kropfli, R.A., Bartram, B.W., Cupp, R.E., Post, M.J., 1992. Smoke-Column Observations from Two Forest Fires Using Doppler Lidar and Doppler Radar. Journal of Applied Meteorology 31, 1328–1349.

Cantrell, W., Heymsfield, A., 2005. Production of Ice in Tropospheric Clouds: A Review. Bulletin of the American Meteorological Society 86, 795–807.

Capes, G., Johnson, B., McFiggans, G., Williams, P.I., Haywood, J., Coe, H., 2008. Aging of biomass burning aerosols over West Africa: Aircraft measurements of chemical composition, microphysical properties, and emission ratios. Journal of Geophysical Research: Atmospheres 113, n/a–n/a.

Chalbot, M.-C., Nikolich, G., Etyemezian, V., Dubois, D. W., King, J., Shafer, D., Gamboa da Costa, G., Hinton, J. F., Kavouras, I. G., 2013. Soil humic-like organic compounds in prescribed fire emission using nuclear magnetic resonance spectroscopy. Environmental Pollution 181, 167-171.

Clements, C. B., Zhong, S., Bian, X., Heilman W. E., Byun, D. W., 2008. First observations of turbulence generated by grass fires. Journal of Geophysical Research 113.

de Boer, G., Morrison, H., Shupe, M. D., Hildner, R., 2011. Evidence of liquid dependent ice nucleation in high-latitude stratiform clouds from surface remote sensors. Geophysical Research Letters 38.

DeMott, P.J., Sassen, K., Poellot, M.R., Baumgardner, D., Rogers, D.C., Brooks, S.D., Prenni, A.J., Kreidenweis, S.M., 2003. African dust aerosols as atmospheric ice nuclei. Geophys. Res. Lett. 30, 1732.

DeMott, P.J., Prenni, A.J., Liu, X., Kreidenweis, S.M., Petters, M.D., Twohy, C.H., Richardson, M.S., Eidhammer, T., Rogers, D.C., 2010. Predicting global atmospheric ice nuclei distributions and their impacts on climate. Proceedings of the National Academy of Sciences 107, 11217.

DeMott, P. J., A. J. Prenni, C. S. McCluskey, G. R. McMeeking, Y. Tobo, R. C. Sullivan, M. D. Petters, M. Niemand, and O. Möhler, 2013: A simplified parameterization of freezing

nucleation by mineral dust particles. In preparation for submission to Atmos. Chem. Phys. Disc.

DeMott, P.J., Möhler, O., Stetzer, O., Vali, G., Levin, Z., Petters, M.D., Murakami, M., Leisner, T., Bundke, U., Klein, H., Kanji, Z.A., Cotton, R., Jones, H., Benz, S., Brinkmann, M., Rzesanke, D., Saathoff, H., Nicolet, M., Saito, A., Nillius, B., Bingemer, H., Abbatt, J., Ardon, K., Ganor, E., Georgakopoulos, D.G., Saunders, C., 2011. Resurgence in Ice Nuclei Measurement Research. Bulletin of the American Meteorological Society 92, 1623–1635.

Georgii H., 1963. Investigations of the deactivation of inorganic and organic freezing-nuclei. S Angew Math Phys 14, 503-510.

Haywood, J., Boucher, O., 2000. Estimates of the direct and indirect radiative forcing due to tropospheric aerosols: A review. Reviews of Geophysics 38, 513–543.

Hobbs, P.V., Sinha, P., Yokelson, R.J., Christian, T.J., Blake, D.R., Gao, S., Kirchstetter, T.W., Novakov, T., Pilewskie, P., 2003. Evolution of gases and particles from a savanna fire in South Africa. J. Geophys. Res. 108, 8485.

Hoose, C., Möhler, O., 2012. Heterogeneous ice nucleation on atmospheric aerosols: a review of results from laboratory experiements

Janhäll, S., Andreae, M.O., Pöschl, U., 2010. Biomass burning aerosol emissions from vegetation fires: particle number and mass emission factors and size distributions. Atmos. Chem. Phys. 10, 1427–1439.

Koppmann, R., Von Czapiewski, K., Reid, J.S., others, 2005. A review of biomass burning emissions, part I: gaseous emissions of carbon monoxide, methane, volatile organic compounds, and nitrogen containing compounds. Atmospheric Chemistry and Physics Discussions 5, 10455–10516.

Lamb D., Verlinde, J., 2011: *Physics and Chemistry of Clouds.* Cambridge University Press, New York.

Levin, E. J. T., McMeeking, G. R., Carrico, C. M., Mack, L. E., Kreidenweis, S. M., Wold, C. E., Moosmüller, H., Arnott, W. P., Hao, W. M., Collet Jr., J. L., 2010. Biomass burning smoke aerosol properties measured during Fire Laboratory at Missoula Experiments (FLAME). J. Geophys. Res. 115, D18310.

Levin, Z., Teller, A., Ganor, E., Yin, Y., 2005. On the interactions of mineral dust, sea-salt particles, and clouds: A measurement and modeling study from the Mediterranean Israeli Dust Experiment campaign. J. Geophys. Res. 110, D20202.

Liousse, C., Devaux, C., Dulac, F., Cachier, H., 1995. Aging of savanna biomass burning aerosols: Consequences on their optical properties. J Atmos Chem 22, 1–17.

Lohmann, U., 2002. A glaciation indirect aerosol effect caused by soot aerosols. Geophysical Research Letters 29, 11–1–11–4.

Lohmann, U., Feichter, J., 2005. Global indirect aerosol effects: a review. Atmos. Chem. Phys. 5, 715–737.

McMeeking, G.R., Kreidenweis, S.M., Baker, S., Carrico, C.M., Chow, J.C., Jr, J.L.C., Hao, W.M., Holden, A.S., Kirchstetter, T.W., Malm, W.C., Moosmüller, H., Sullivan, A.P., Wold, C.E., 2009. Emissions of trace gases and aerosols during the open combustion of biomass in the laboratory. J. Geophys. Res. 114, D19210.

Park, R.J., Jacob, D.J., Logan, J.A., 2007. Fire and biofuel contributions to annual mean aerosol mass concentrations in the United States. Atmospheric Environment 41, 7389–7400.

Petters, M.D., Parsons, M.T., Prenni, A.J., DeMott, P.J., Kreidenweis, S.M., Carrico, C.M., Sullivan, A.P., McMeeking, G.R., Levin, E., Wold, C.E., Collett, J.L., Moosmüller, H., 2009. Ice nuclei emissions from biomass burning. Journal of Geophysical Research 114.

Pósfai, M., Gelencsér, A., Simonics, R., Arató, K., Li, J., Hobbs, P.V., Buseck, P.R., 2004. Atmospheric tar balls: Particles from biomass and biofuel burning. J. Geophys. Res. 109, D06213.

Pósfai, M., Simonics, R., Li, J., Hobbs, P.V., Buseck, P.R., 2003. Individual aerosol particles from biomass burning in southern Africa: 1. Compositions and size distributions of carbonaceous particles. J. Geophys. Res. 108, 8483.

Pratt, K.A., DeMott, P.J., French, J.R., Wang, Z., Westphal, D.L., Heymsfield, A.J., Twohy, C.H., Prenni, A.J., Prather, K.A., 2009. In situ detection of biological particles in cloud ice-crystals. Nature Geosci 2, 398–401.

Pratt, K.A., Murphy, S.M., Subramanian, R., DeMott, P.J., Kok, G.L., Campos, T., Rogers, D.C., Prenni, A.J., Heymsfield, A.J., Seinfeld, J.H., Prather, K.A., 2011. Flight-based chemical characterization of biomass burning aerosols within two prescribed burn smoke plumes. Atmos. Chem. Phys. 11, 12549–12565.

Prenni, A.J., DeMott, P.J., Sullivan, A.P., Sullivan, R.C., Kreidenweis, S.M., Rogers, D.C., 2012. Biomass burning as a potential source for atmospheric ice nuclei: Western wildfires and prescribed burns. Geophys. Res. Lett. 39, L11805.

Prenni, A.J., Petters, M.D., Kreidenweis, S.M., Heald, C.L., Martin, S.T., Artaxo, P., Garland, R.M., Wollny, A.G., P|[ouml]|schl, U., 2009. Relative roles of biogenic emissions and Saharan dust as ice nuclei in the Amazon basin. Nature Geoscience 2, 402–405.

Prenni, A.J., Tobo, Y., Garcia, E., DeMott, P.J., Huffman, J.A., McCluskey, C.S., Kreidenweis, S.M., Prenni, J.E., Pöhlker, C., Pöschl, U., 2013. The impact of rain on ice nuclei populations at a forested site in Colorado. Geophysical Research Letters 40, 227–231.

Pruppacher, H.R., Klett J.D., 1997: *Microphysics of clouds and precipitation.* Kluwer Academic Publishers, London

Reid, J.S., Koppmann, R., Eck, T.F., Eleuterio, D.P., 2005. A review of biomass burning emissions part II: intensive physical properties of biomass burning particles. Atmos. Chem. Phys. 5, 799–825.

Richardson, M.S., DeMott, P.J., Kreidenweis, S.M., Cziczo, D.J., Dunlea, E.J., Jimenez, J.L., Thomson, D.S., Ashbaugh, L.L., Borys, R.D., Westphal, D.L., Casuccio, G.S., Lersch, T.L., 2007. Measurements of heterogeneous ice nuclei in the western United States in springtime and their relation to aerosol characteristics. Journal of Geophysical Research 112.

Rogers, D.C., 1994. Detecting Ice Nuclei with a Continuous—Flow Diffusion Chamber-Some Exploratory Tests of Instrument Response. Journal of Atmospheric and Oceanic Technology 11, 1042–1047.

Rogers, D.C., DeMott, P.J., Kreidenweis, S.M., Chen, Y., 2001. A continuous-flow diffusion chamber for airborne measurements of ice nuclei. Journal of Atmospheric and Oceanic Technology 18, 725–741.

Rosenfeld, D., Yu, Y., Liu, G., Xu, X., Zhu, Y., Yue, Z., Dai, J., Dong, Z., Dong Y., Peng, Y., 2011. Glaciation temperatures of convective clouds ingesting dester dust, air pollution and smoke from forest fires. Geophysical Research Letters 38.

Sassen, K., Khvorostyanov, V.I., 2008. Cloud effects from boreal forest fire smoke: evidence for ice nucleation from polarization lidar data and cloud model simulations. Environmental Research Letters 3, 025006.

Seigel, R.B., van den Heever, S.C., Saleeby, S.M., 2013. Mineral dust indirect effects and cloud radiative feedbacks of a simulated idealized nocturnal squall line. Atmos. Chem. Phys. 13, 4467–4485.

Seinfeld, J.H., Pandis, S.N., 2006. Atmospheric Chemistry and Physics: From Air Pollution to Climate Change. Wiley, Hoboken, NJ.

Simoneit, B.R.T., Schauer, J.J., Nolte, C.G., Oros, D.R., Elias, V.O., Fraser, M.P., Rogge, W.F., Cass, G.R., 1999. Levoglucosan, a tracer for cellulose in biomass burning and atmospheric particles. Atmospheric Environment 33, 173–182.

Spracklen, D.V., Mickley, L.J., Logan, J.A., Hudman, R.C., Yevich, R., Flannigan, M.D., Westerling, A.L., 2009. Impacts of climate change from 2000 to 2050 on wildfire activity and carbonaceous aerosol concentrations in the western United States. Journal of Geophysical Research: Atmospheres 114, n/a–n/a.

Sullivan, A.P., Frank, N., Kenski, D.M., Collett, J.L., 2011. Application of high-performance anion-exchange chromatography–pulsed amperometric detection for measuring carbohydrates in routine daily filter samples collected by a national network: 2. Examination of sugar alcohols/polyols, sugars, and anhydrosugars in the upper Midwest. Journal of Geophysical Research 116.

Taylor, J.R.,1997: *An introduction to Error Analysis: The Study of Uncertainties in Physical Measurements*, 49 pp.

Twohy, C.H., DeMott, P.J., Pratt, K.A., Subramanian, R., Kok, G.L., Murphy, S.M., Lersch, T., Heymsfield, A.J., Wang, Z., Prather, K.A., Seinfeld, J.H., 2010. Relationships of Biomass-Burning Aerosols to Ice in Orographic Wave Clouds. Journal of the Atmospheric Sciences 67, 2437–2450.

Twomey, S., 1977. The Influence of Pollution on the Shortwave Albedo of Clouds. Journal of the Atmospheric Sciences 34, 1149–1152.

VanCuren, R.A., Cahill, T.A., 2002. Asian aerosols in North America: Frequency and concentration of fine dust. Journal of Geophysical Research 107.

Wang, C., Prinn, R.G., 1999. Impact of emissions, chemistry and climate on atmospheric carbon monoxide: 100-yr predictions from a global chemistry–climate model. Chemosphere - Global Change Science 1, 73–81.

Ward, D.E., Radke, L.F., 1993. Emissions measurements from vegetation fires: A comparative evaluation of methods and results. Fire in the Environment: The Ecological, Atmospheric and Climatic Importance of Vegetation Fires 13, 53–76.

Westerling, A.L., Hidalgo, H.G., Cayan, D.R., Swetnam, T.W., 2006. Warming and Earlier Spring Increase Western U.S. Forest Wildfire Activity. Science 313, 940–943.

Yokelson, R.J., Griffith, D.W.T., Ward, D.E., 1996. Open-path Fourier transform infrared studies of large-scale laboratory biomass fires. Journal of Geophysical Research: Atmospheres 101, 21067–21080.

APPENDIX A. OPC CALIBRATIONS

The optical particle counter (OPC), used to detect particles exiting the continuous-flow diffusion chamber, was calibrated using polystyrene latex (PSL) sphere of four sizes: 500nm, 1μm, 1.5μm and 2μm. PSL was aerosolized using high purity nitrogen and glass nebulizer fill with PSL solution (2 drops of PSL to approximately 5 mL of water). A dryer was located between the aerosol generator and the OPC inlet.

Aerosol was generated and sampled for 13 to 30 minutes. Average counts were calculated for each MCA channel (1-256) over 3 minute periods, shown in Figure A.1. Calibrations using 500nm, 1μm, and 1.5μm particles were fairly consistent during each trial and there was greater variability for the 2μm PSL. The greater variability for the larger sizes can be attributed to contaminations in the nebulizer or poor aerosol generation.

The MCA channel corresponding to the average maximum signal is considered the channel representing the size of the tested PSL size; these are labeled in Figure A.1. For MCA channel representative of 500nm particles is channel 6. Therefore, channel 6 was used as the cutoff for accumulating particles greater than 500nm for calculating n_{500nm} from the CFDC data.

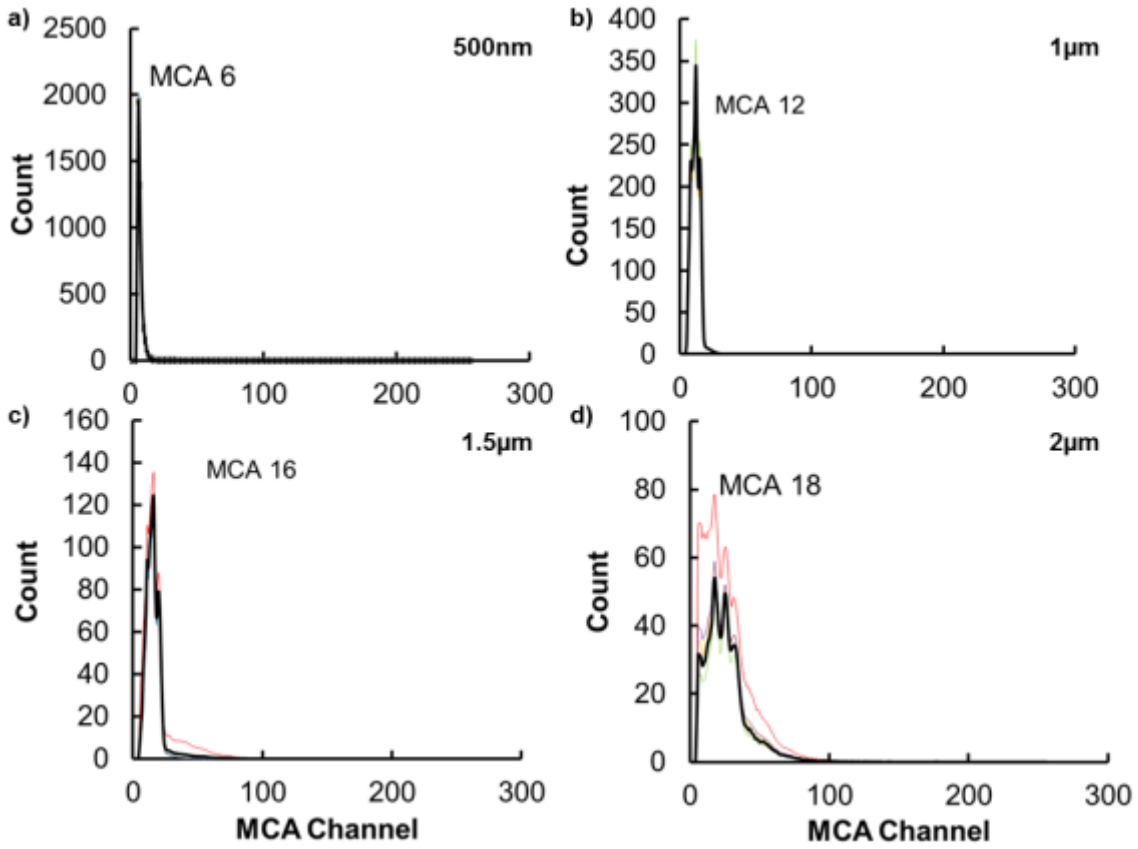

Figure A.1. Calibration results of the OPC using a) 500nm, b) 1µm, c) 1.5µm and d) 2.5µm PSL particles. Channels with maximum signal are labeled.

APPENDIX B. DAILY TIMELINES

Figures B.1-13are timelines of total particle number concentrations, number concentrations of ice nucleating particles and particles greater than 500 nm, carbon monoxide concentrations and the operating temperature and water supersaturation of the continuous flow diffusion chamber. Periods when transmission electron microscopy grids were collected are also shown. Figures B.14-21 show the wind direction and wind speed measured at the Christman Field weather station, located near the Foothills Campus during the wildfire measurement periods.

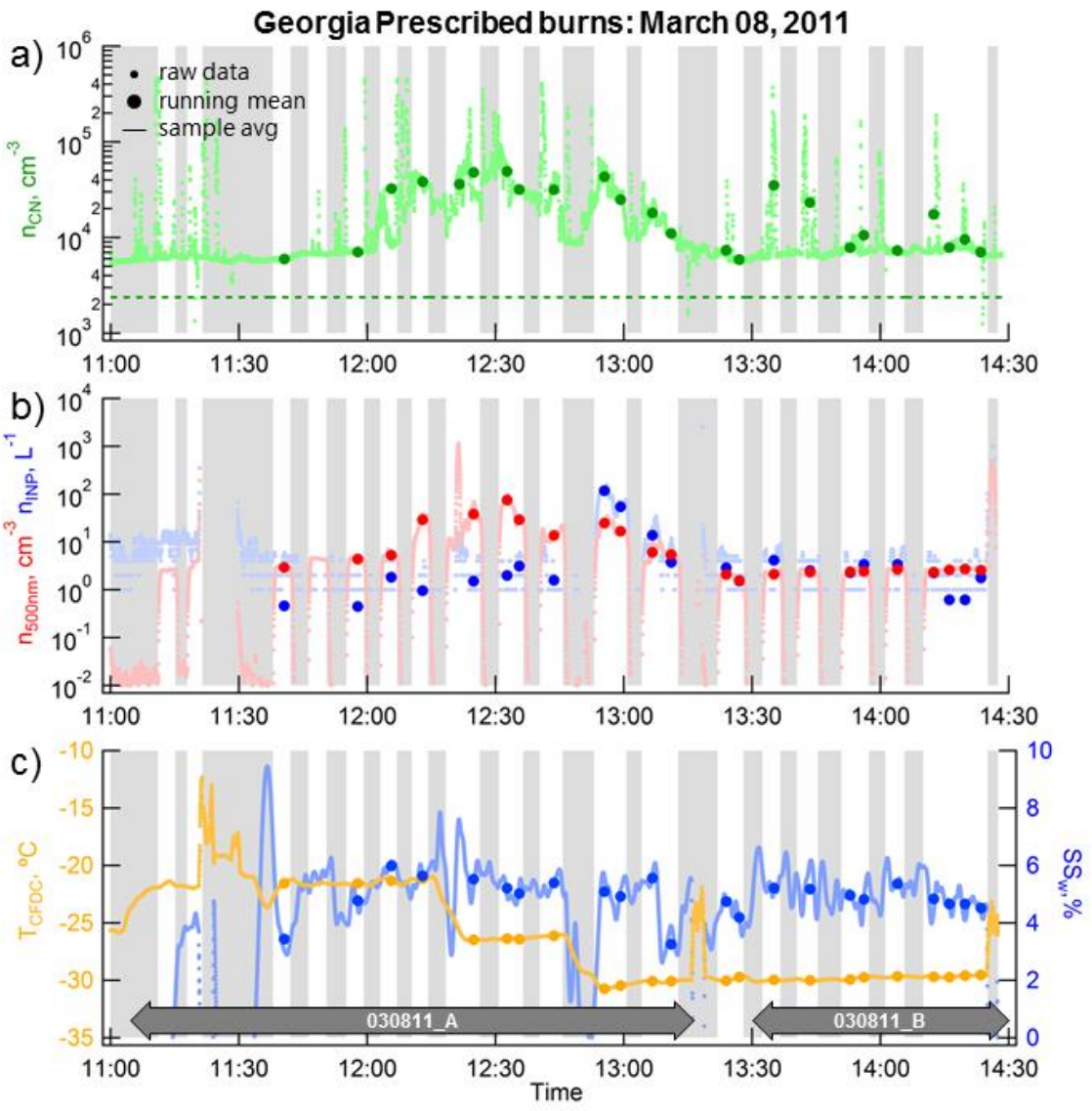

Figure B.1. Timelines of a) raw (light green) and sample-averaged (dark green) total particle number concentrations; background median n_{CN} is indicated (dashed line), b) raw (light red and light blue) and sample-averaged(red and blue) number concentrations of particles with diameters greater than 500nm and INP, respectively, and c) 30 second running meant (light orange and light blue) and sample-average(orange and blue) CFDC processing temperature and water supersaturation, respective, measure on March 08, 2011during the Georgia prescribed burns. Grey bars show the collection periods for the TEM grids, named accordingly.

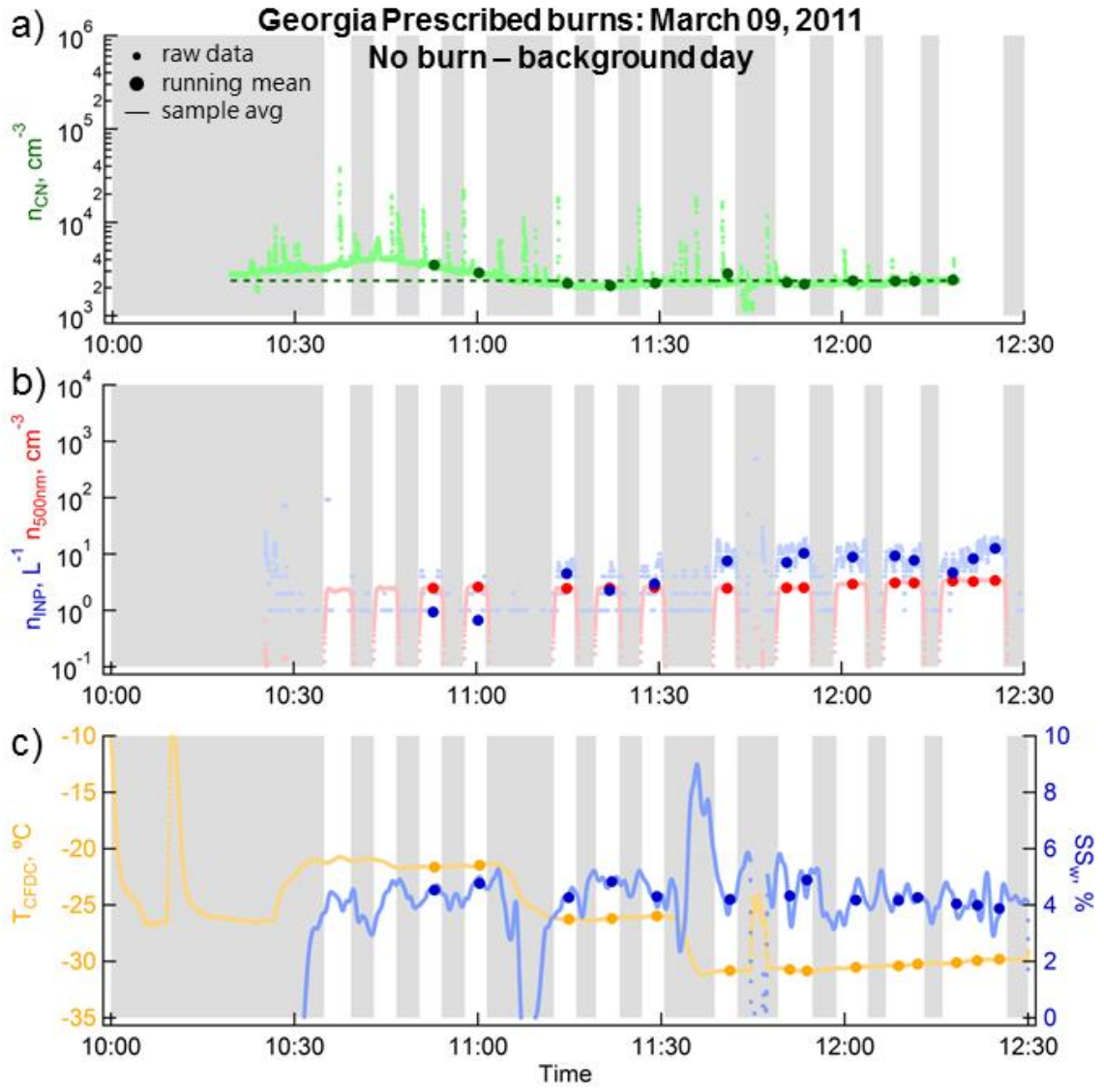

Figure B.2. Same as Figure B.1 for March 09, 2011 during the Georgia prescribed burns.

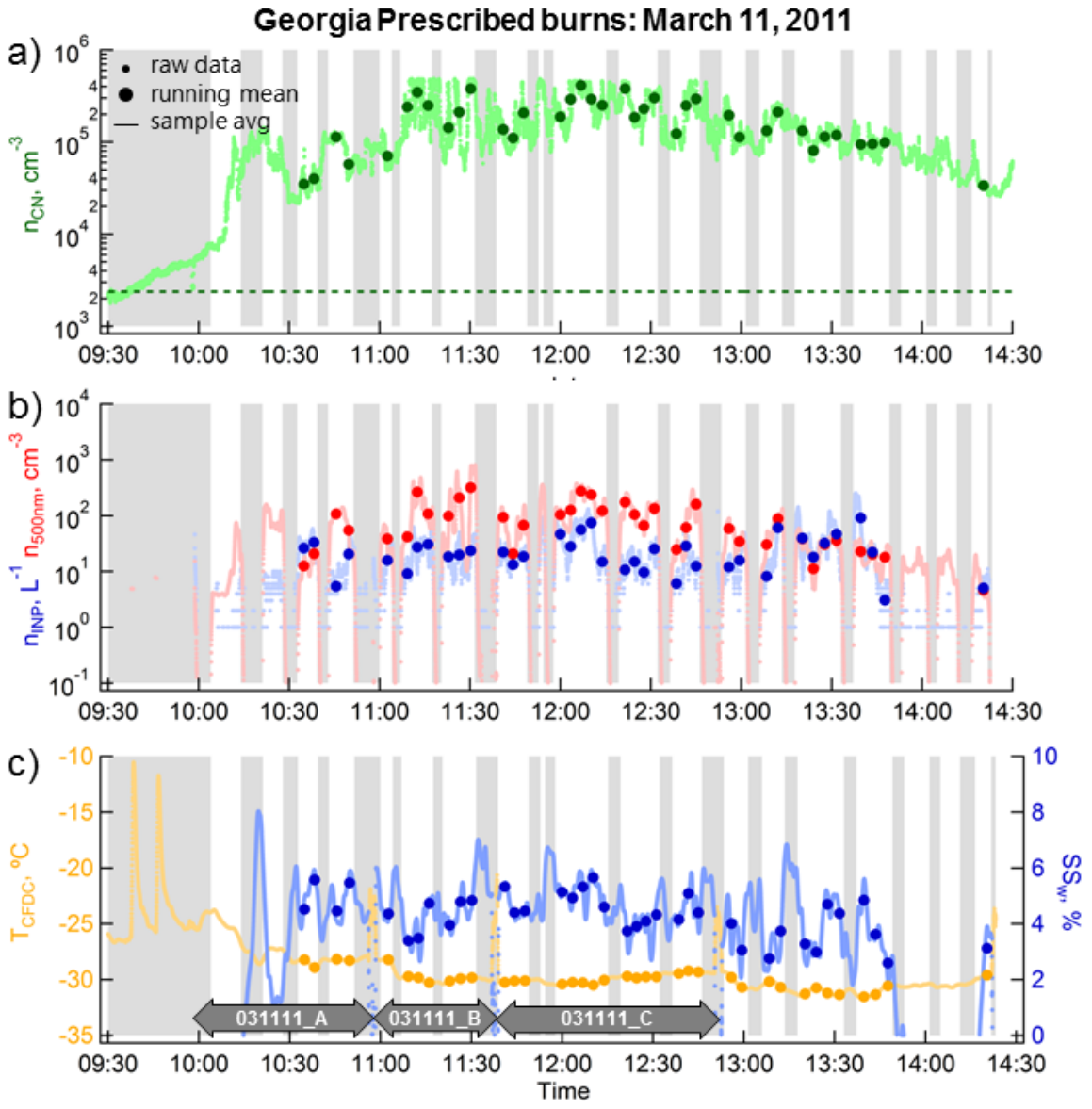

Figure B.3. Same as Figure B.1 for March 11, 2011 during the Georgia prescribed burns.

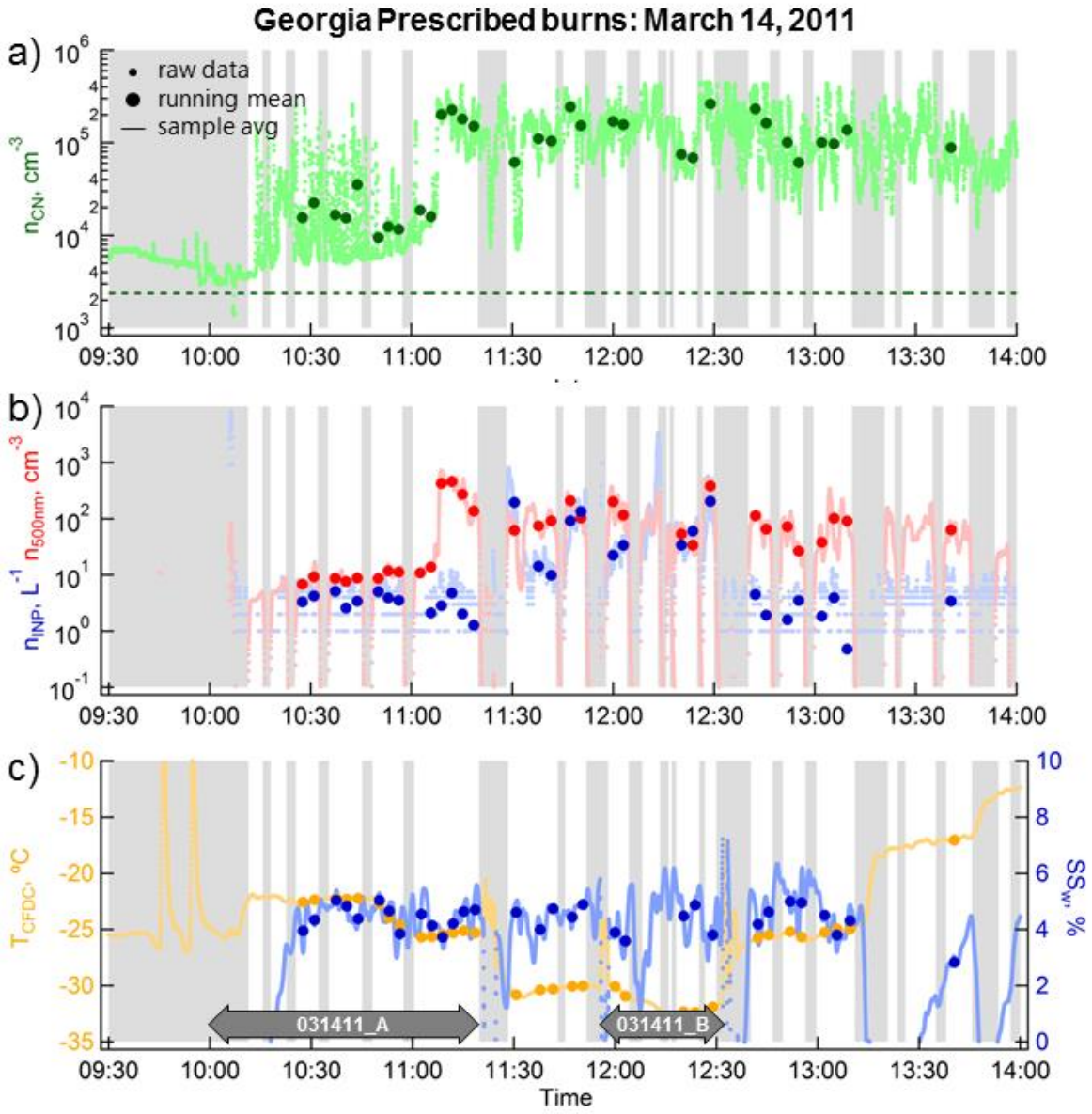

Figure B.4. Same as Figure B.1 for March 14, 2011 during the Georgia prescribed burns.

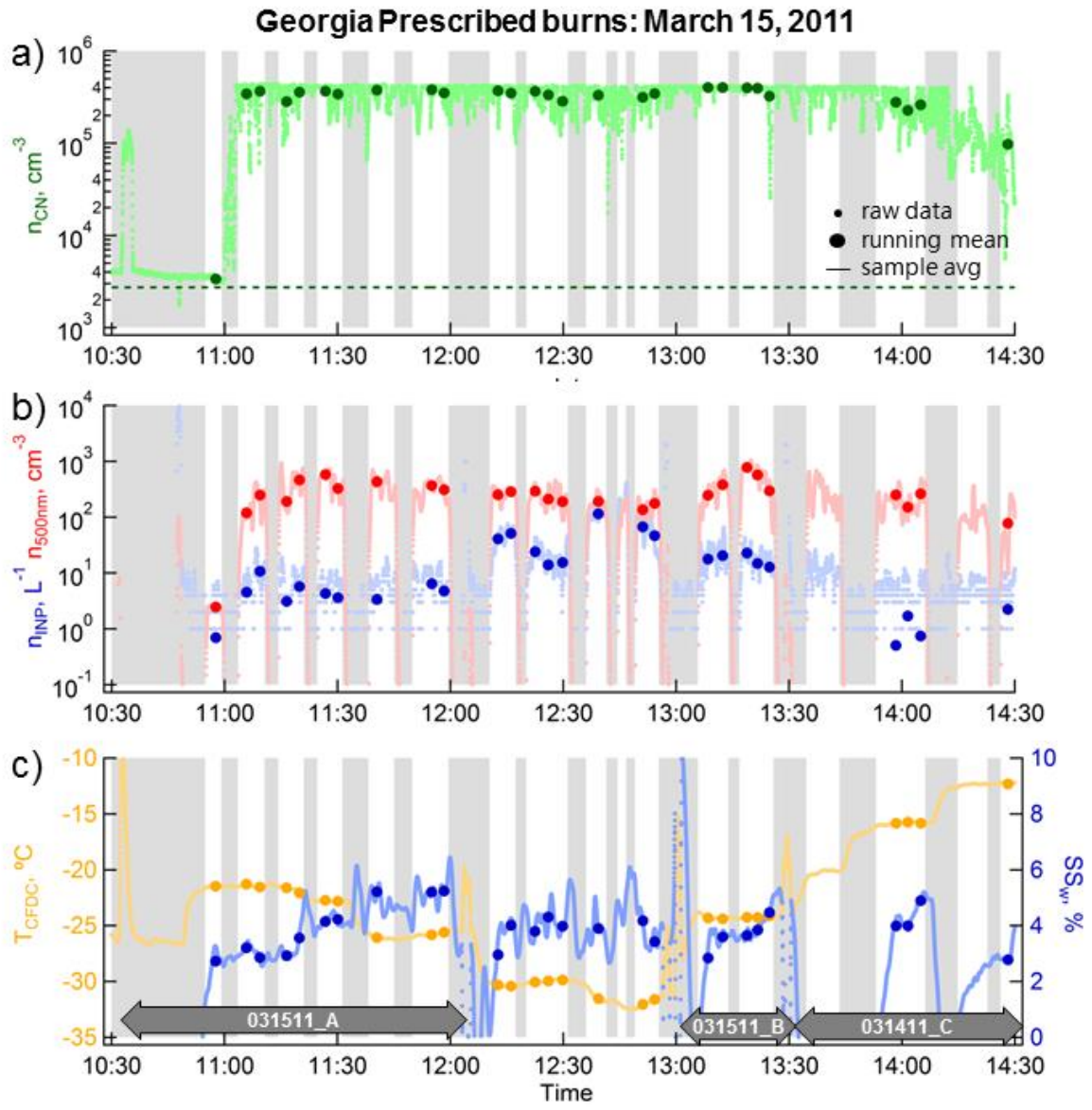

Figure B.5. Same as Figure B.1 for March 15, 2011 during the Georgia prescribed burns.

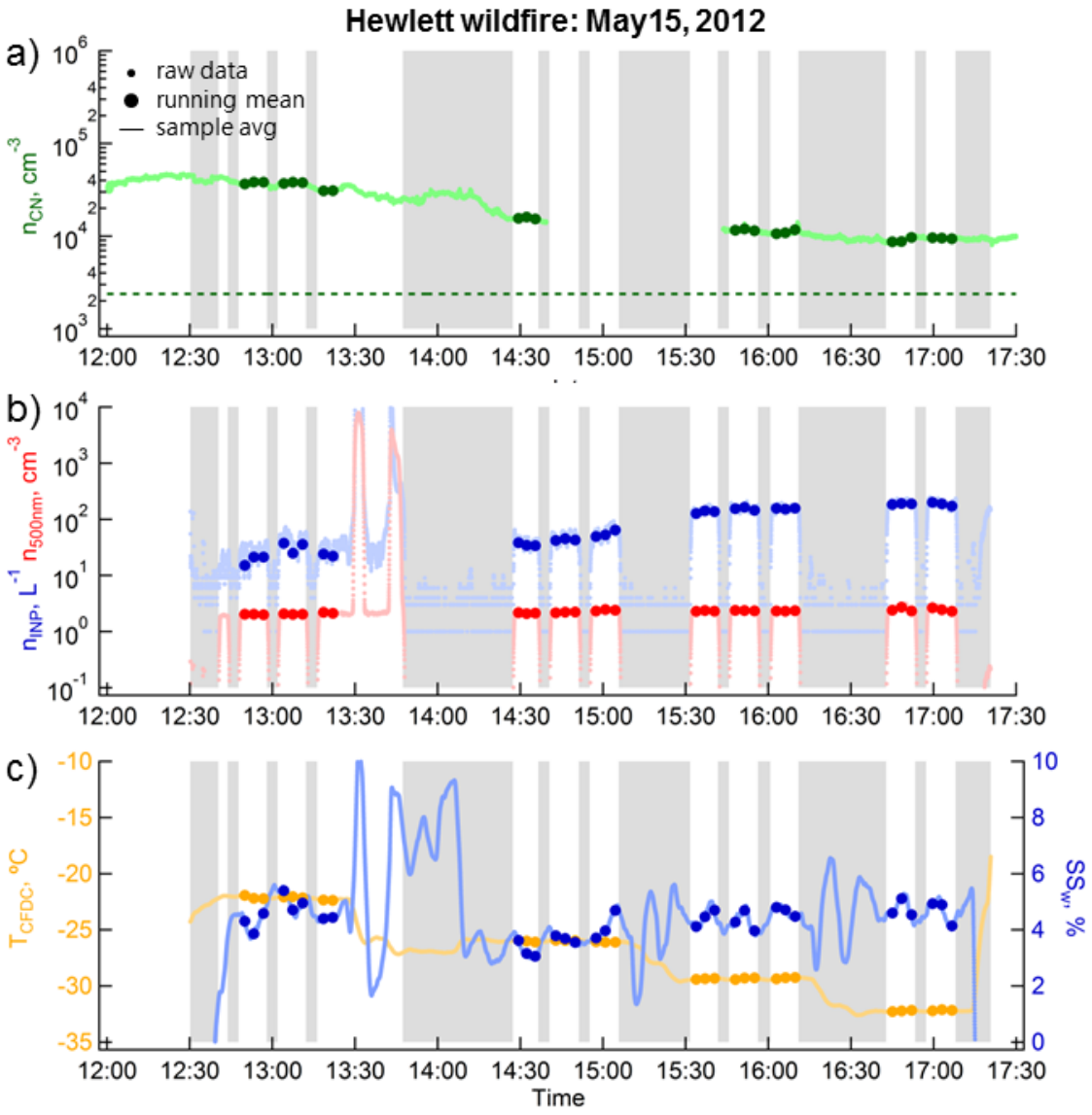

Figure B.6. Same as Figure B.1 for May 15, 2012 during the Hewlett wildfire.

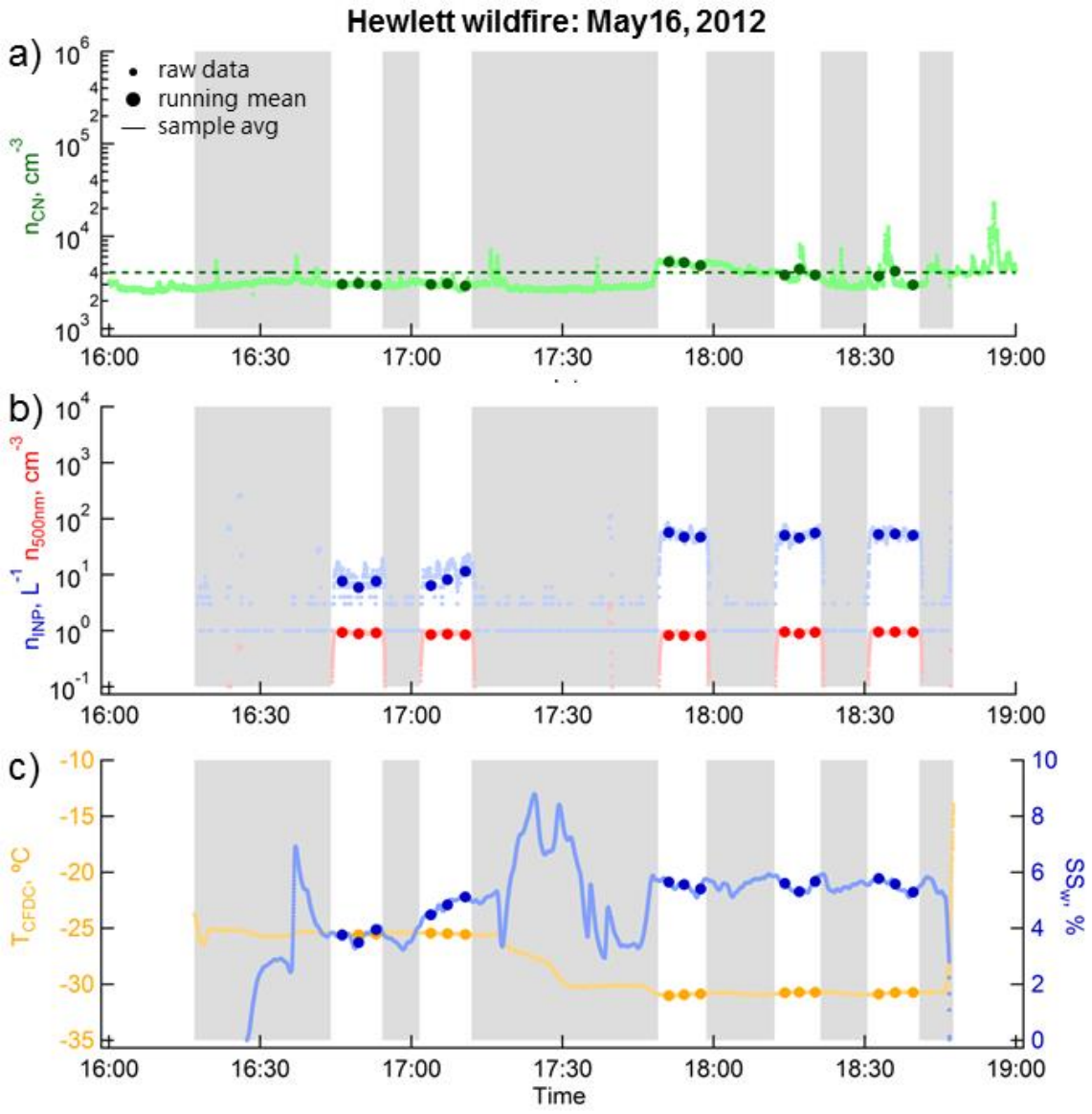

Figure B.7. Same as Figure B.1 for May 16, 2012 during the Hewlett wildfire.

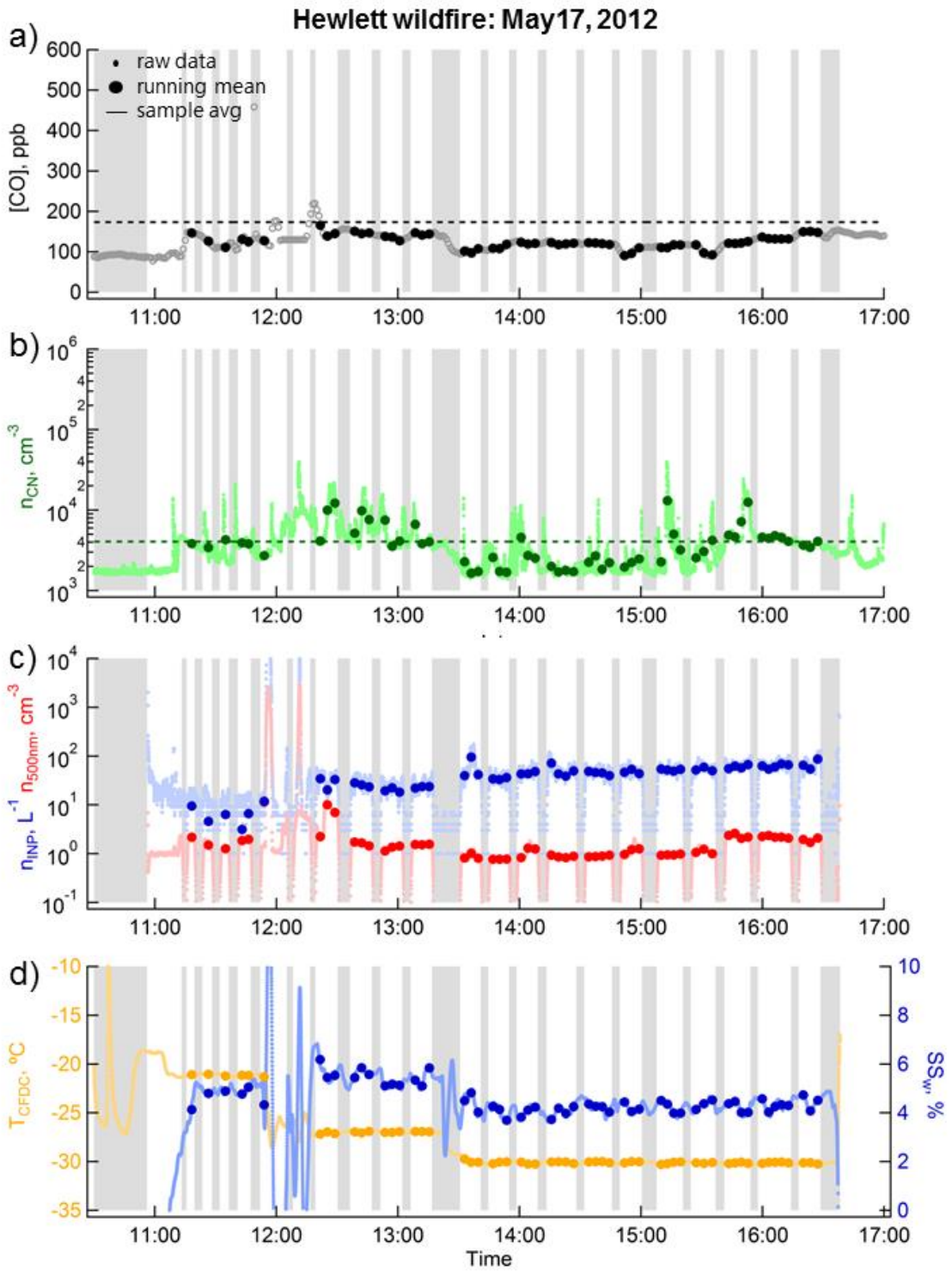

Figure B.8. a) raw (grey) and sample-averaged concentrations of carbon monoxide, background carbon monoxide plus two standard deviations is indicated (dashed line). b, c, and d are the same as Figure B.1 for May 17, 2012 during the Hewlett wildfire.

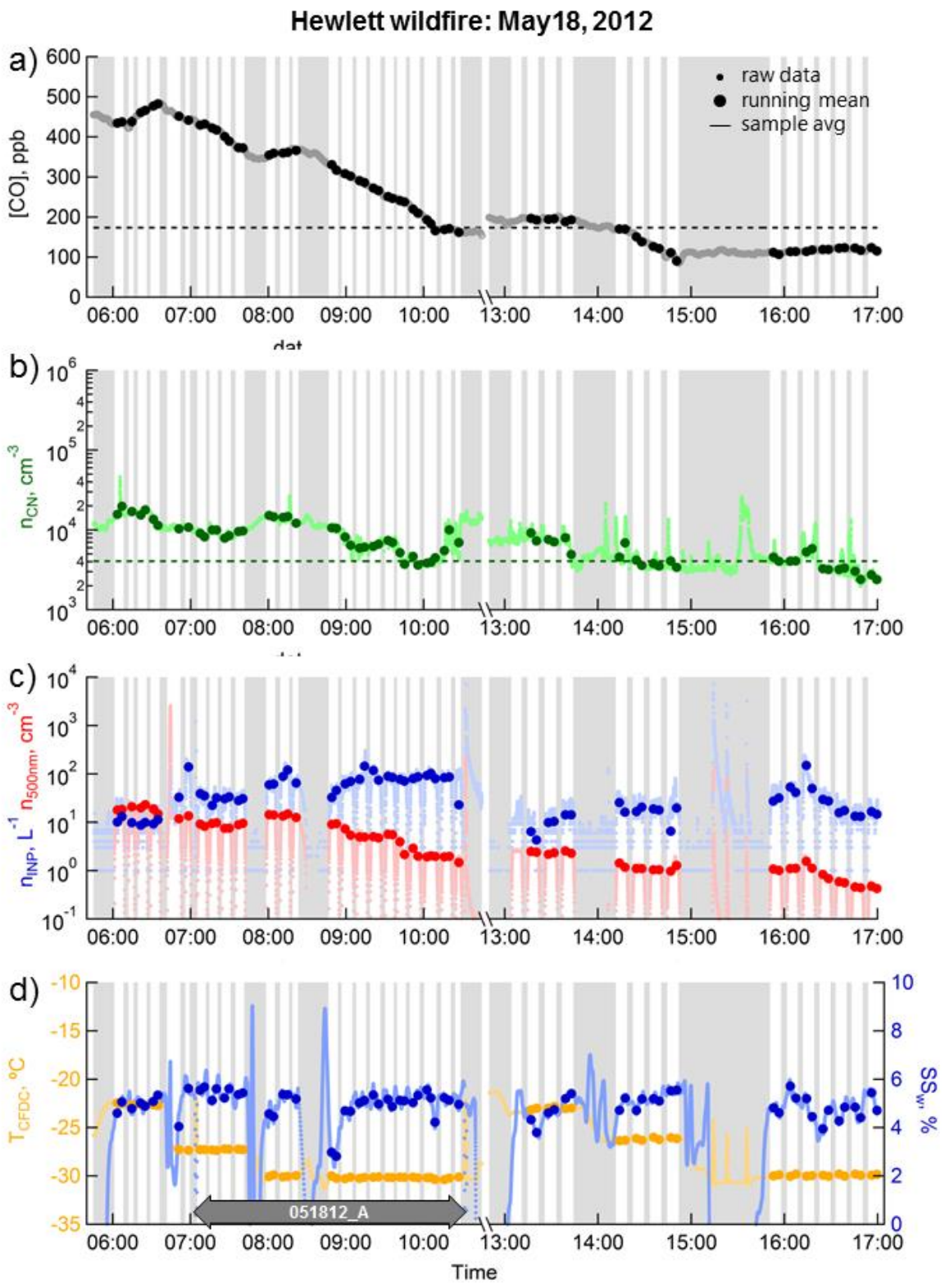

Figure B.9. Same as B.8 for May18, 2012 during the Hewlett wildfire periods

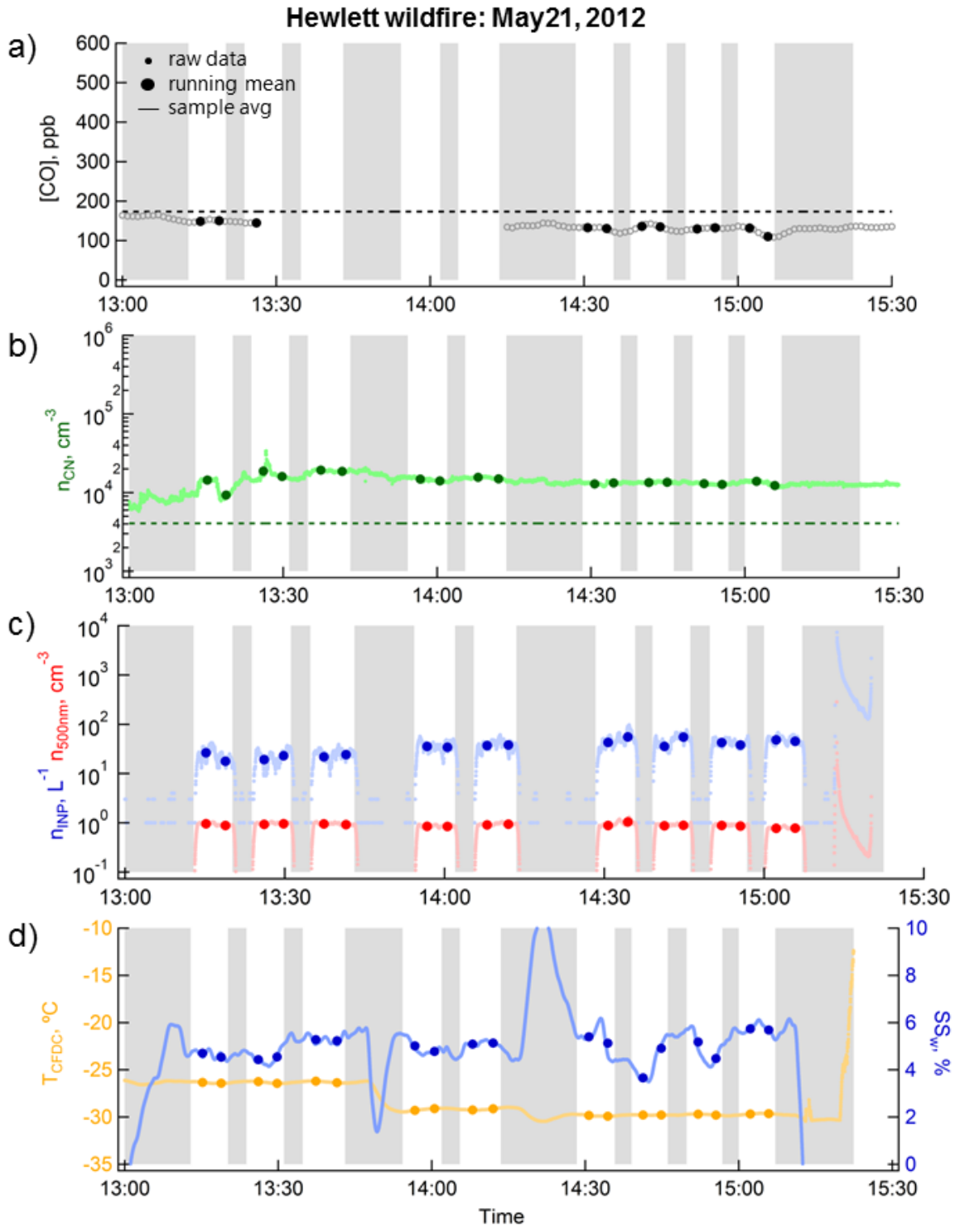

Figure B.10. Same as Figure B.8 for May 21, 2012 during the Hewlett wildfire period.

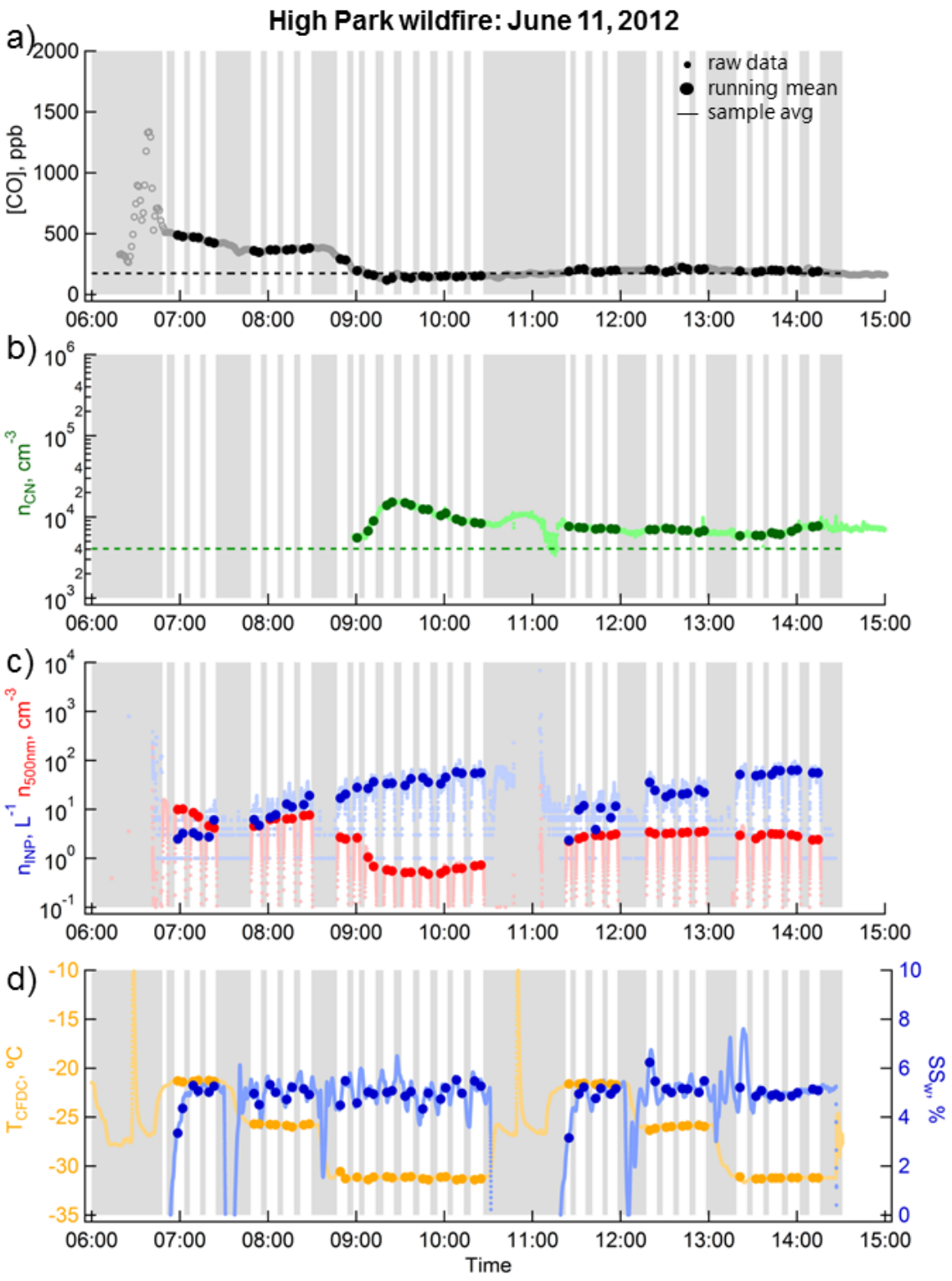

Figure B.11. Same as Figure B.8 for June 11, 2012 during the High Park wildfire period.

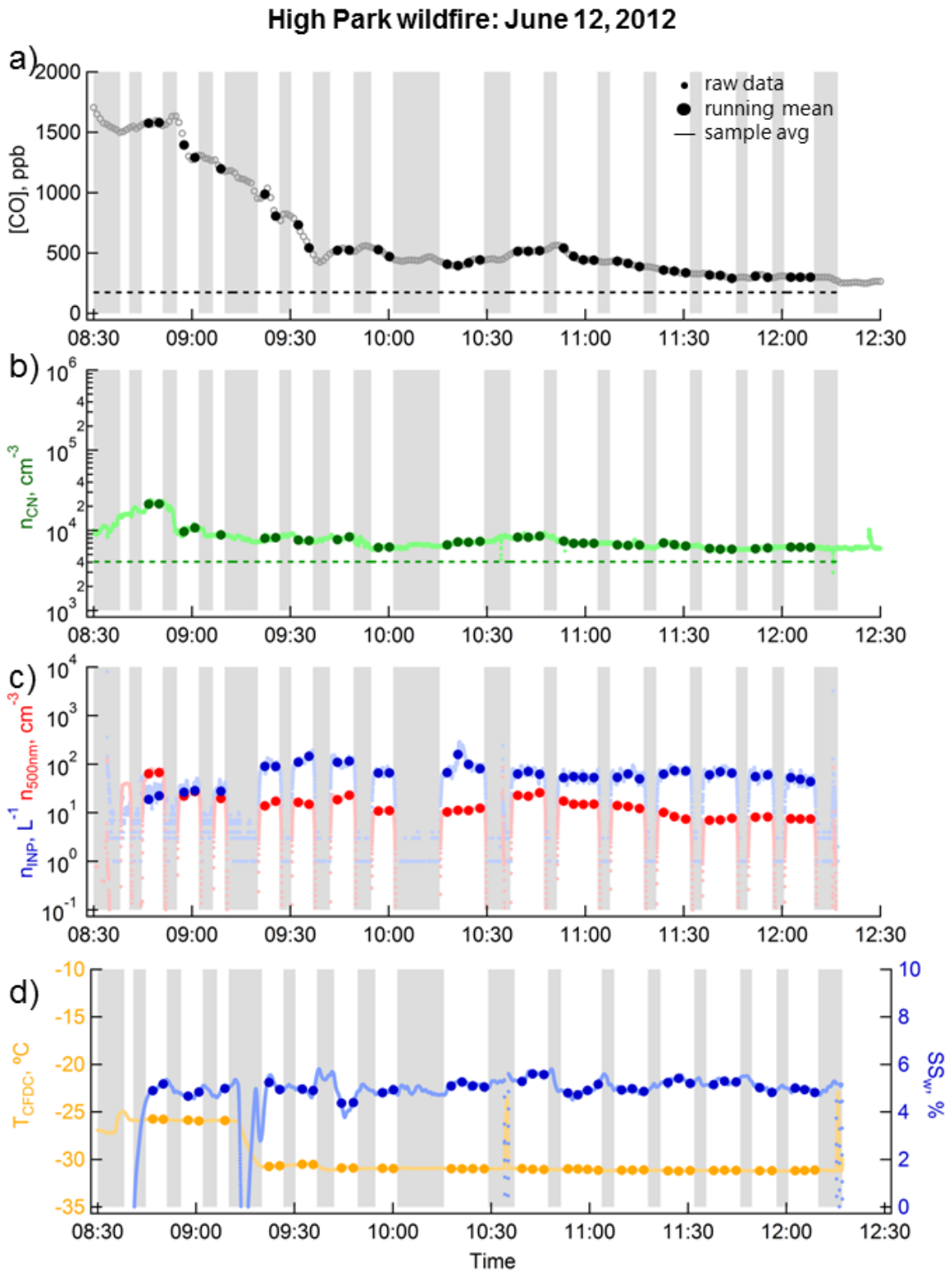

Figure B.12. Same as Figure B.8 for June 12, 2012 during the High Park wildfire period.

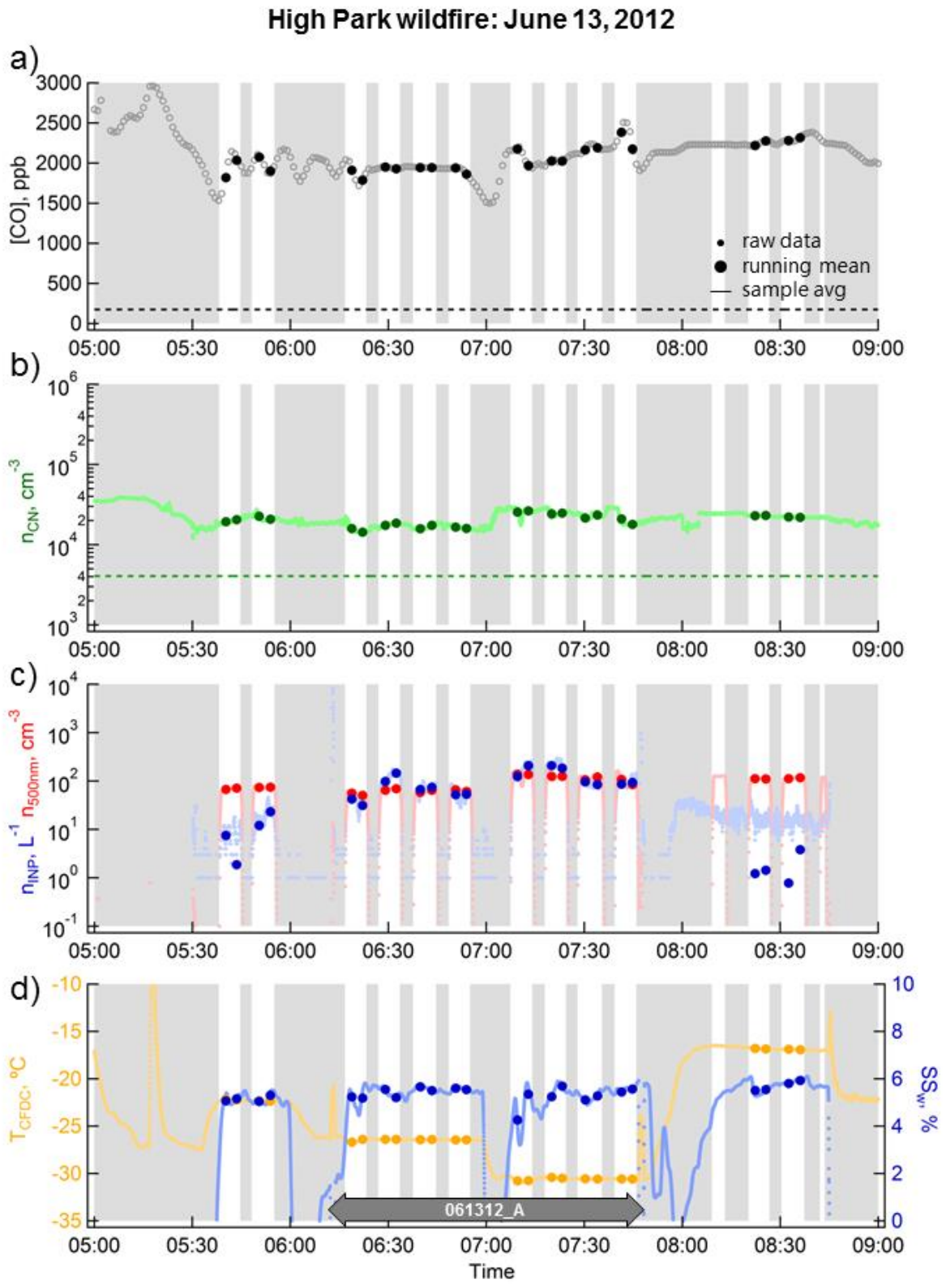

Figure B.13. Same as Figure B.8 for June 12, 2012 during the High Park wildfire period.

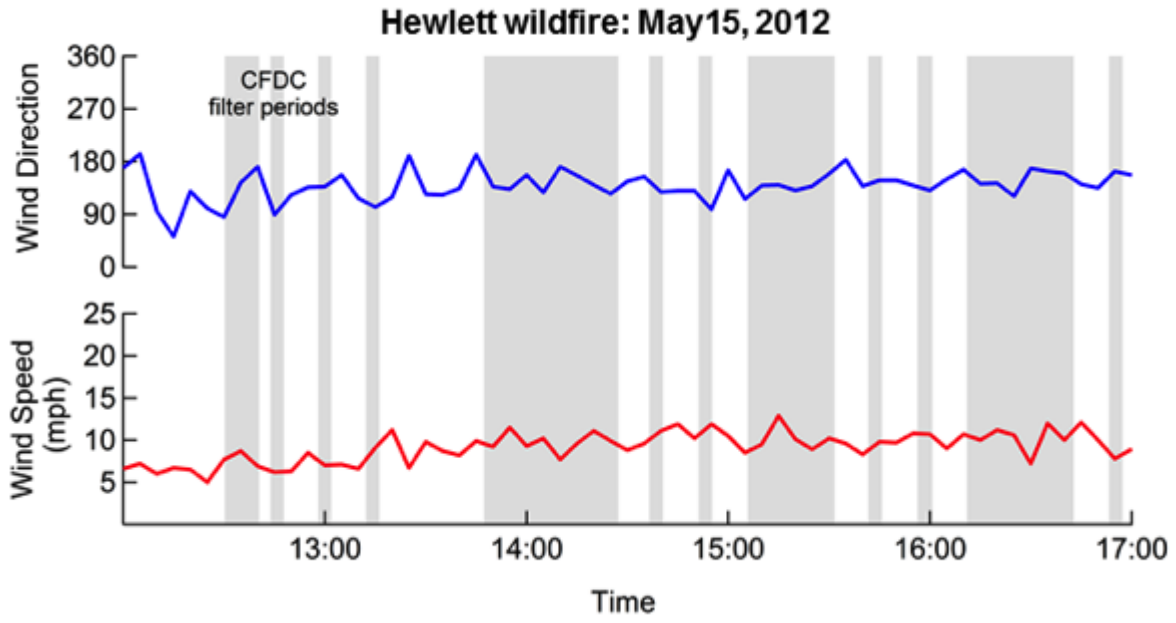

Figure B.14. Timelines of wind direction (top, blue) and wind speed (bottom, red) measured at the Christmas Field weather station, located near the CSU Foothills campus on May 15, 2012 during the Hewlett wildfire. CFDC filter periods are shaded by grey.

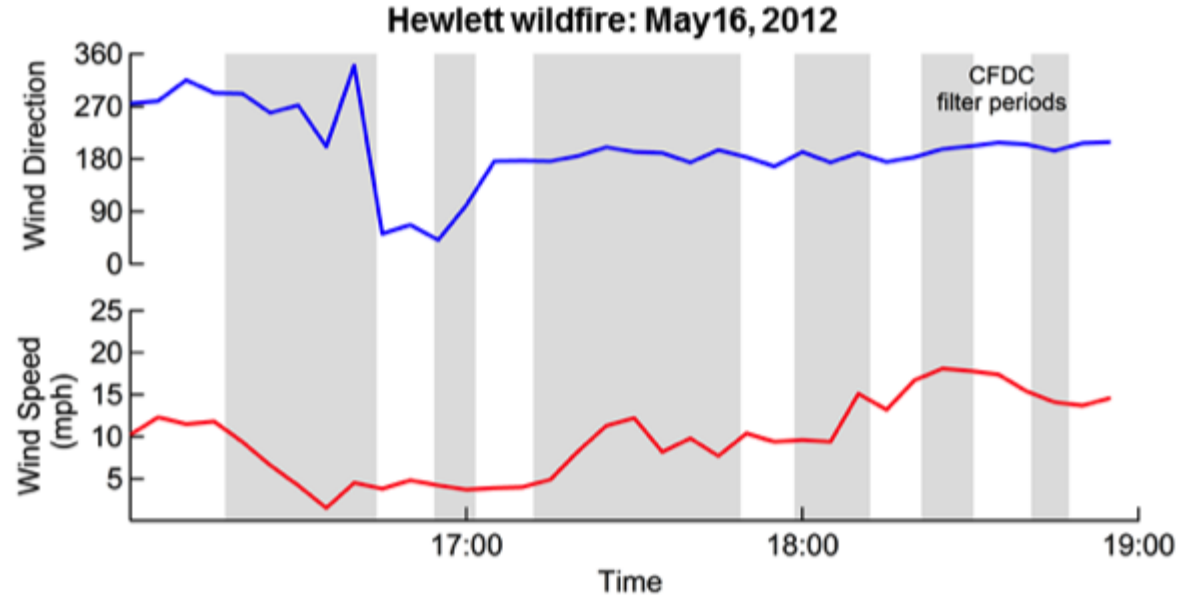

Figure B.15. Same as Figure B.14 for May 16, 2012 during the Hewlett wildfire.

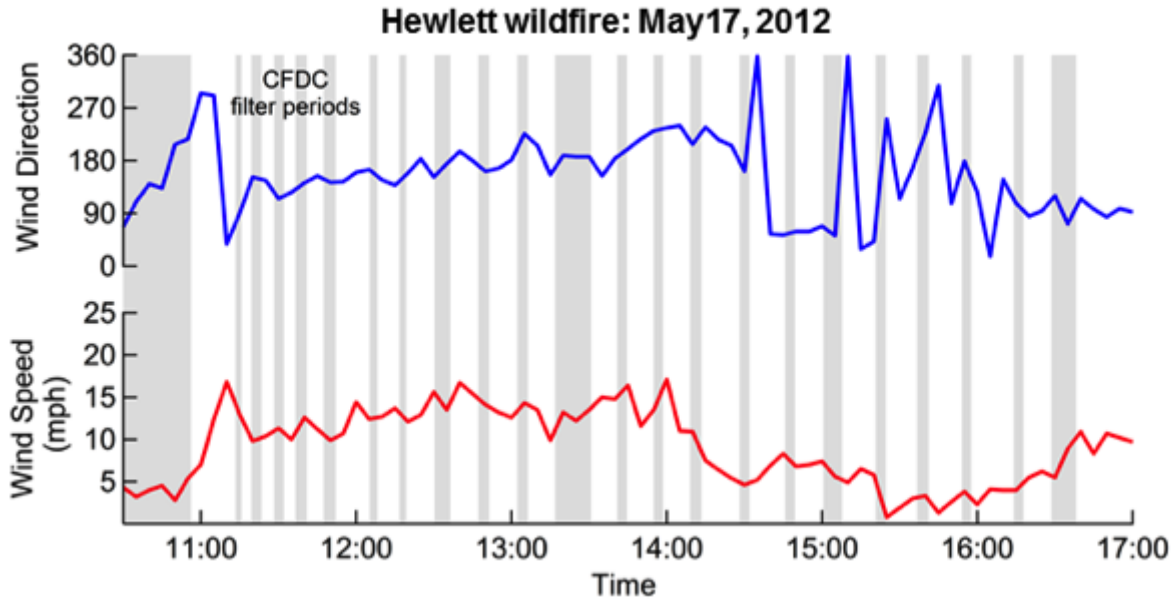

Figure B.16. Same as Figure B.14 for May 17, 2012 during the Hewlett wildfire.

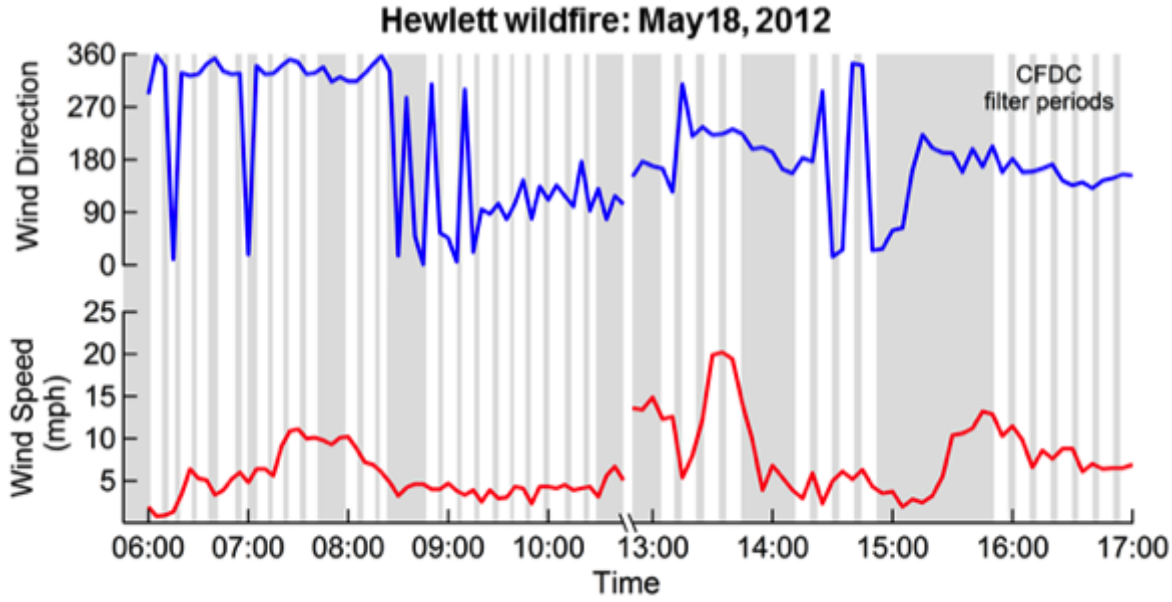

Figure B.17. Same as Figure B.14 for May 18, 2012 during the Hewlett wildfire.

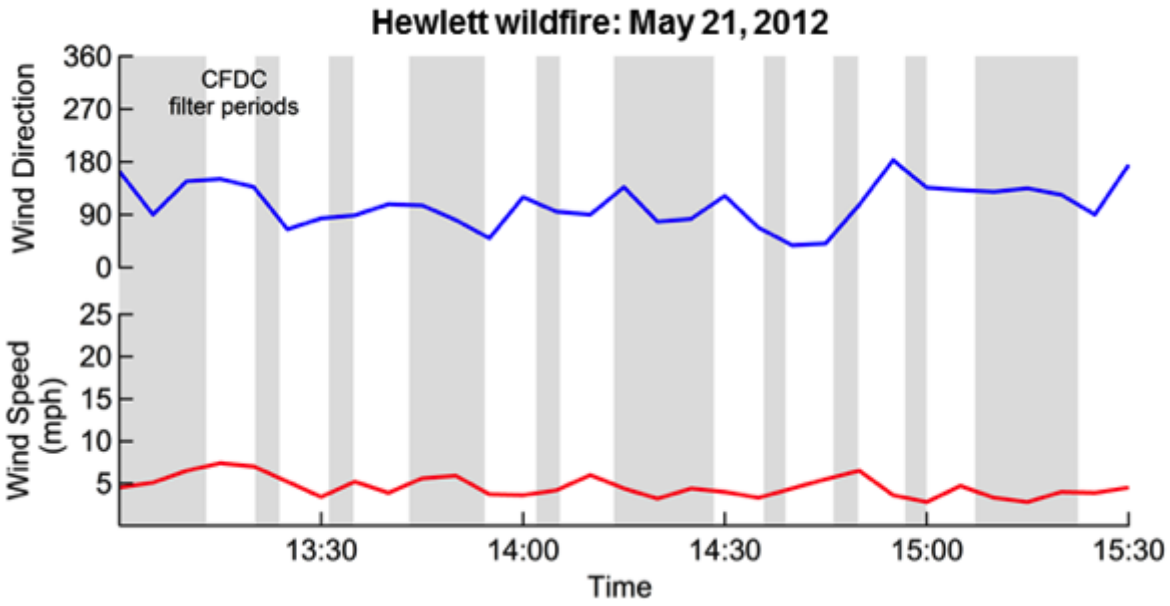

Figure B.18. Same as Figure B.14 for May 21, 2012 during the Hewlett wildfire.

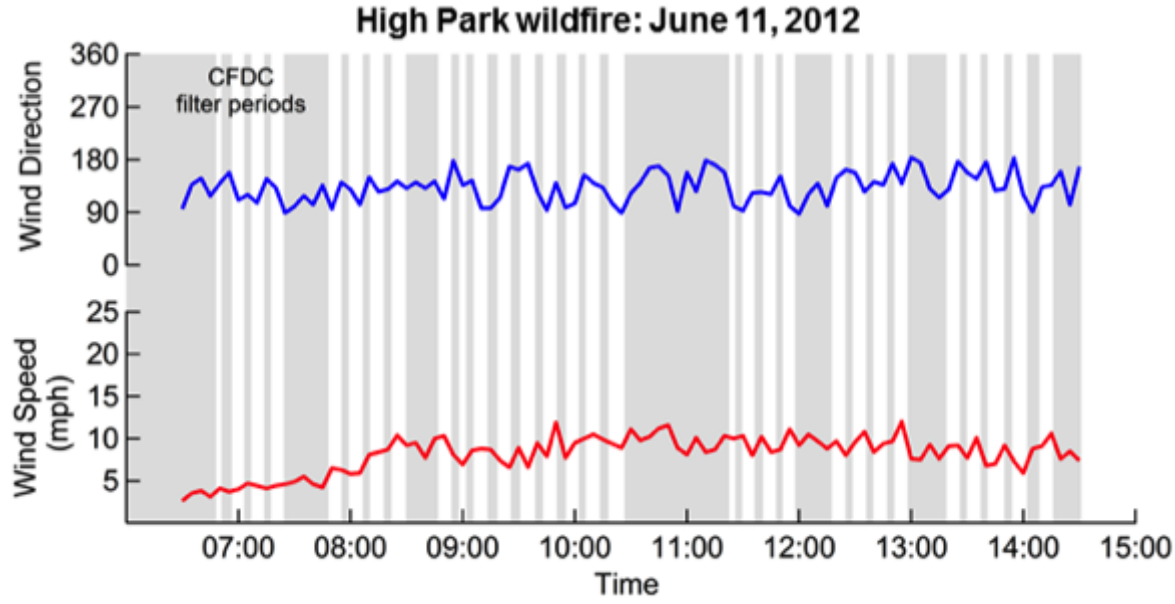

Figure B.19. Same as Figure B.14 for June 11, 2012 during the High Park wildfire.

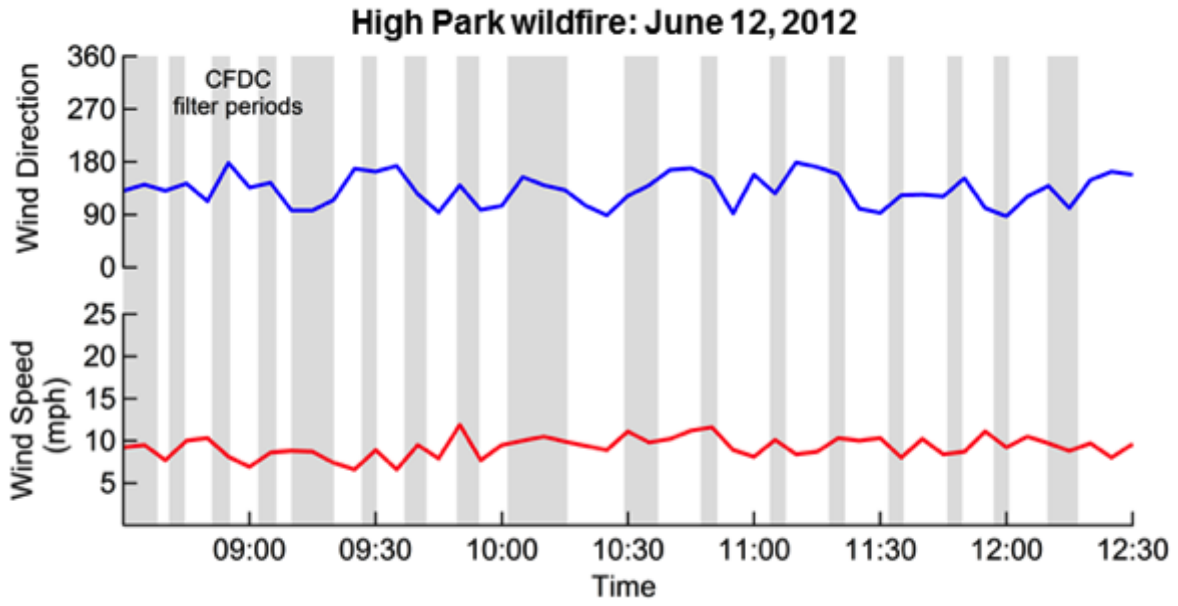

Figure B.20. Same as Figure B.14 for June 12, 2012 during the High Park wildfire.

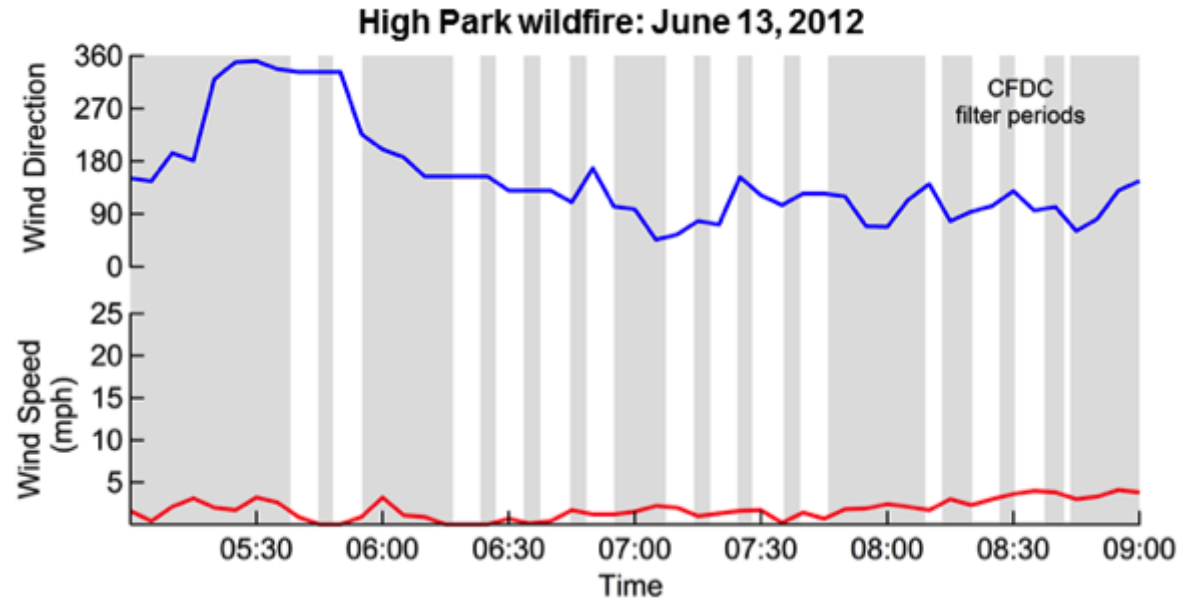

Figure B.21. Same as Figure B.14 for June 13, 2012 during the High Park wildfire.

LIST OF SYMBOLS AND ABBREVIATIONS

C/Min-mix	carbonaceous-mineral mixture
CCN	cloud condensation nuclei
CFDC	continuous flow diffusion chamber
CN	condensation nuclei
CO	carbon monoxide
C-other	carbonaceous other particle category
CPC	condensation particle counter
D10	DeMott et al., 2010 n_{INP} parameterization
EDX	energy dispersive x-ray
f_{500nm}	fractional change in n_{500nm}
f_{INP}	fractional change in n_{INP}
FLAME	fire laboratory at Missoula experiments
FMPS	fast mobility particle sizer
IMPROVE	interagency monitoring of protected visual environments
INP	ice nucleating particles
MCA	multi-channel analyzer
MCE	modified combustion efficiency
Min/Ox mix	mineral/metal oxide mixture
n_{500nm}	number concentration of particles with diameters greater than 500 nm
NAAPS	navel aerosol analysis and prediction system model
n_{CN}	number concentration of condensation nuclei (total particle concentration)
n_{INP}	number concentration of INP
OC	organic carbon
OPC	optical particle counter
PM	particulate matter
PM_{10}	mass concentration of particles with diameters less than 10 µm
$PM_{2.5}$	mass concentration of particles diameters less than 2.5 µm
PM_{coarse}	mass concentration of particles with diameters between 2.5 and 10 µm
Q_{samp}	sample flow rate of the CFDC
rBC	refractory black carbon
SP2	single particle soot photometer
SS_w	supersaturation with respect to water of the CFDC
STEM	scanning transmission electron microscope
STP	standard temperature and pressure
TC	total carbon
T_{CFDC}	CFDC temperature
TEM	transmission electron microscopy
TEOM	tapered element oscillating microbalance
t_{MCA}	MCA live time
VOCs	volatile organic compounds
V_{samp}	volume of sample air of the CFDC
ν_{500nm}	number of particles with diameters greater than than 500 nm
ν_{INP}	number of INP
σ_{500nm}	uncertainty of n_{500nm}
σ_{INP}	uncertainty of n_{INP}